Environmentally-Assisted Degradation of Structural Materials in Water Cooled Nuclear Reactors – An Introduction

Authors

F. Peter Ford
Rexford, New York, USA

Peter M. Scott
Noisy Le Roi, France

Pierre Combrade
Le Bessat, France

Claude Amzallag
Saint-Etienne, France

A.N.T. INTERNATIONAL®

Advanced Nuclear Technology International
Analysvägen 5, SE-435 33 Mölnlycke
Sweden

info@antinternational.com
www.antinternational.com

Ecolabelled printed matter, 3041 0129

Disclaimer

The information presented in this report has been compiled and analysed by Advanced Nuclear Technology International Europe AB (ANT International®) and its subcontractors. ANT International has exercised due diligence in this work, but does not warrant the accuracy or completeness of the information. ANT International does not assume any responsibility for any consequences as a result of the use of the information for any party, except a warranty for reasonable technical skill, which is limited to the amount paid for this report.

Contents

1 General introduction (Peter Ford)

This report is the sixth in a series of ANT International published reports that address the topic of environmentally-assisted degradation of structural materials in water cooled nuclear reactors. The first in the series, listed below, was published in 2006, and was an introductory treatment of the topic. This was followed by four detailed reports that analysed the behaviour of various alloys commonly used in Pressurized Water Reactors and Boiling Water Reactors (BWR).

- Ford F. P., "*Environmentally-assisted degradation of structural materials in water cooled nuclear reactors*", ANT International Stand Alone Report, 2006 [Ford, 2006].
- Ford F. P. and Scott P. M., "*Environmentally-assisted degradation of carbon and low alloy steels in water cooled nuclear reactors*" ANT International LCC4 Special Topical Report, 2008 [Ford & Scott, 2008].
- Ford F. P., Scott P. M. and Combrade P., "*Environmentally-assisted degradation of stainless steels in water cooled nuclear reactors*", ANT International Stand Alone Report, 2010 [Ford et al, 2010].
- Scott P. M., Combrade P. and Ford F. P., "*Environmentally-assisted degradation of nickel-base alloys in water cooled nuclear reactors*", ANT International Stand Alone Report, 2011 [Scott et al, 2011].
- Strasser A. and Ford F. P., "*High-strength nickel – base alloys for fuel assemblies*" ANT International Special Topical Report, 2012 [Strasser & Ford, 2012].

There are two objectives of the present report: first, to provide a second updated edition of the 2006 report cited above and, second, to provide a text-book that complements the 4-day lecture series provided by the ANT International Academy on the subject of environmentally-assisted degradation of structural materials.

The report is intended for people new to the subject, or who need a "refresher" on the essential factors behind component failures and the subsequent mitigation actions. Such a focus is critical at this time, given the ongoing retirement of experienced personnel and the loss of "corporate memory" relating to the management of materials degradation. This loss is being felt in areas of reactor license renewal, power uprates, load following, and the certification and construction of advanced designs of both BWRs and PWRs.

The degradation modes that are in-scope (Table 1-1) for this report on structural alloys are those controlled or substantially affected by the aqueous environment; that is, general and localized corrosion phenomena. Degradation modes associated with thermal or irradiation embrittlement are not addressed in detail apart from where they impact the kinetics of the environmentally-assisted degradation; an example of this is the discussion of irradiation assisted stress corrosion cracking (IASCC) where accumulating physical (e.g. embrittlement) damage due to irradiation has an impact on susceptibility to IASCC and kinetics of subcritical crack propagation. Other topics, such as "human factors" and "non-destructive examination" are certainly relevant, but are omitted from this introductory text. Topics such as analyses of the behaviour of zirconium alloys or waste storage canisters are addressed in the ANT International Zirconium Alloy Technology (ZIRAT) programme reports.

Table 1-1: Degradation modes in and out-of-scope in this report.

Degradation modes in-scope	Degradation modes out of scope
General corrosion	Thermal embrittlement (except CASS)
Boric acid corrosion	Irradiation embrittlement of low alloy and stainless steels
Flow accelerated corrosion	Human factors
Crevice corrosion	Zirconium Alloys
Pitting	Non-destructive examination
Galvanic corrosion	Mechanical and thermal-hydraulic design
Microbiologically-influenced corrosion	Radioactive waste storage
Environmentally-assisted cracking	GEN III+ and GEN IV reactors
	ANT International, 2015

1.1 Definition of the problem

Corrosion in water cooled nuclear power reactors has been a problem for many decades and has required substantial investments by the industry in research, mitigation, repair, replacement, and inspection activities.

One of the reasons for the longevity of these degradation problems is that (apart from general corrosion, fatigue in an "industrial" environment, and irradiation embrittlement of the pressure vessel) they were not considered beyond "good engineering practice" in the design-basis for the current light water reactor (LWR) fleet.

Examples of corrosion phenomena that have occurred in specific alloy/environment combinations include:

- Transgranular stress corrosion cracking (SCC) of austenitic stainless steels in chlorides at low ambient temperatures.
- Intergranular SCC of stainless steel piping in Boiling Water Reactors (BWR) and Pressurized Water Reactors (PWR).
- Irradiation-assisted SCC of stainless steel core components in BWRs and PWRs.
- Intergranular SCC of low alloy steels in low pressure (LP) stages of steam turbines.
- Transgranular SCC of carbon steel feed water piping and PWR steam generator shells.
- Intergranular SCC of nickel-base alloy vessel penetrations in PWRs and BWRs.
- Intergranular SCC of nickel-base alloys in the primary and secondary side of PWR steam generator tubing.
- Flow accelerated corrosion of carbon-steel piping in both PWRs and BWRs.
- Boric acid wastage of low-alloy PWR pressure vessel steels.

This listing of the more notable degradation modes emphasizes the domination of SCC modes that are localized at, for instance, grain boundaries.

Also of note is that there continue to be degradation issues in systems that had been thought to be "mitigated", but were not because a crucial factor had been overlooked in the specifications of the mitigation action. An example of this is SCC of unsensitised, but cold worked, L-grade stainless steels in BWRs operating in coolant that meets current water chemistry specifications for maintaining water purity and low corrosion potential. Cracking under such material and water chemistry control conditions was not expected. However, further investigations confirmed that cracking *can* occur in such "mitigated" systems due to the presence of localized strain concentrations and strain hardening associated with manufacturing operations, such as surface grinding.

The basic electrochemical thermodynamic and kinetic factors associated with *general* corrosion of the prime structural alloys are largely understood. Problems arise, however, when predicting environmentally-assisted degradation over extended periods of 60+ years when the system conditions are more complicated due to, for instance:

a) Local aqueous impurity concentrations (e.g. boric acid corrosion, crevice corrosion in oxygenated environments or on occluded heat transfer surfaces),

b) Microbiologically-influenced corrosion,

c) The effects of metallurgical micro-chemical features that lead to intergranular attack and pitting.

The situation becomes even more complicated when considering the additional role of stress, and the associated strain in the metallic structure, in initiating and propagating a crack by stress corrosion, hydrogen embrittlement or corrosion fatigue.

The interactions between the various system parameters and their effect on, for example, stress corrosion cracking is illustrated in Figure 1-1a, via a Venn diagram which indicates that SCC will occur at the intersection (depicted by the red region in the centre of the diagram) of specific conditions of "susceptible material", "environment chemistry", and "tensile stress". These factors are "conjoint"; for example, stress corrosion cracking requires that ***all three*** of these high-level system descriptors must be present for cracking to occur.

Although this information is valuable for pointing the way to a mitigation strategy, its value is limited *quantitatively* since the effectiveness of a specific mitigating action depends on the values of the other parameters such as stress, water purity and corrosion potential, (Eq. 1-1);

Eq. 1-1: $$\text{Damage} = f(X, Y, XY, XZ + \text{etc.}).\text{time}$$

where; X, Y, etc. are values of system parameters (e.g. grain boundary sensitisation, stress, water purity, cold work), and XY, XZ etc. are interactions between these parameters.

Thus, as indicated in Figure 1-1a, there are many system conditions that have to be defined in order to formulate a complete damage accumulation algorithm, with the specifics depending on the degradation mode, the reactor design, the subcomponent fabrication details, and the operating mode, (i.e. shut-down, start-up, full power, hot stand-by, etc.). This complexity leads to various degrees of uncertainty. For instance, there are (aleatory) uncertainties due to the fact that many of the degradation modes (e.g. pitting, intergranular attack) are inherently random and stochastic in nature. There are also (epistemic) uncertainties due to: (a) the completeness of the damage accumulation algorithm (Eq. 1-1), (b) the quality of the laboratory or plant data upon which the algorithm is based and, finally, (c) the accuracy of the system monitoring methods.

2 LWR designs and initial material choices (Peter Scott)

Water cooled nuclear reactors are the most widely built and exploited of all the nuclear reactor designs for electric power generation. Two basic designs originating from the United States have dominated: the Boiling Water Reactor (BWR) and the Pressurized Water Reactor (PWR), both of which are moderated and cooled by light water, i.e. H_2O. It is the compatibility of the structural materials used in these reactors in contact with their high temperature water coolants as well as external surface environments and contaminants that are the main subject of the succeeding sections. In addition, reference is sometimes made to the Russian design of PWR known by the acronym VVER (or WWER), which in concept is very similar to a PWR but with some crucial differences in choices of the main materials of construction, and to the Canadian Pressurized Heavy Water Reactor (PHWR). All these basic designs are outlined below together with the main choices of structural materials and their operating conditions.

The direct cycle BWR is perhaps the simplest of the reactor concepts and in consequence some advantages in the initial cost of construction. The basic layout is shown in Figure 2-1 where it can be seen that water is boiled directly by the nuclear fuel to generate steam that turns a turbine to generate electricity. A crucial consequence of the direct cooling cycle is that only (exceptionally) pure water must be used without any non- or poorly-volatile additives because otherwise such additives (and impurities) with steam/water distribution coefficients of <1 would concentrate in the aqueous phase and their concentrations would be impossible to control.

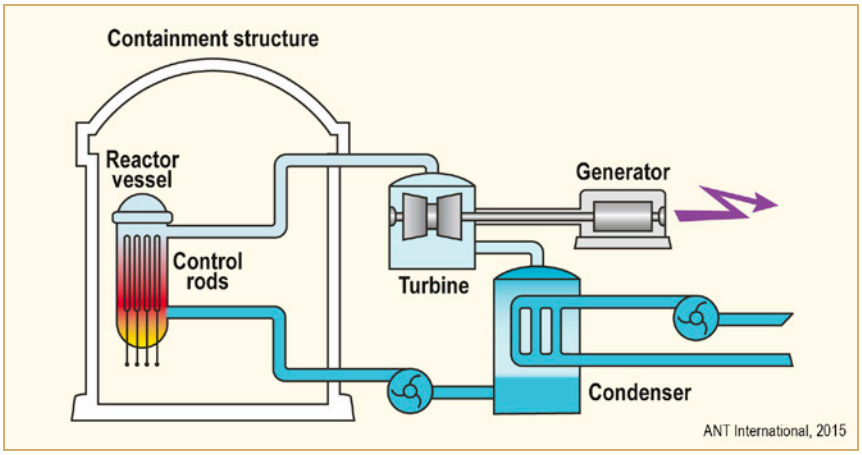

Figure 2-1: BWR general layout.

A more detailed view of the BWR pressure vessel and internals together with a list of the main generic materials of construction and their typical operating conditions are shown in Figure 2-2. The connections shown to external recirculation piping were characteristics of early models of direct cycle BWRs that were eliminated in later models by the substitution of internally mounted recirculation pumps. These recirculation pumps increase the water flow over the fuel in excess of that which would otherwise occur due to natural convection and about a quarter of the water flowing over the fuel is vaporized into steam. Since the main reactor coolant is in a direct water/steam cycle, the steam pressure is the saturated vapour pressure characteristic of the temperature of the water in contact with the fuel.

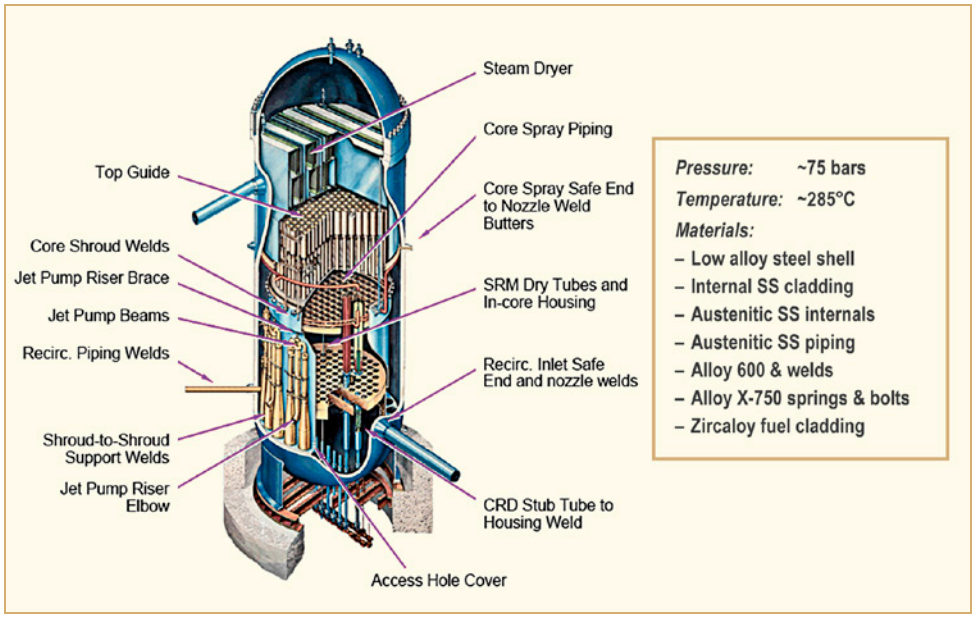

Figure 2-2: BWR Pressure Vessel and Internals, generic materials of construction, and direct cycle operating conditions.

The PWR basic design is inherently more complicated than that of direct cycle BWRs because steam generators separate the primary nuclear fuel coolant/moderator from a secondary steam raising circuit to drive a turbine and generate electricity, as shown in Figure 2-3.

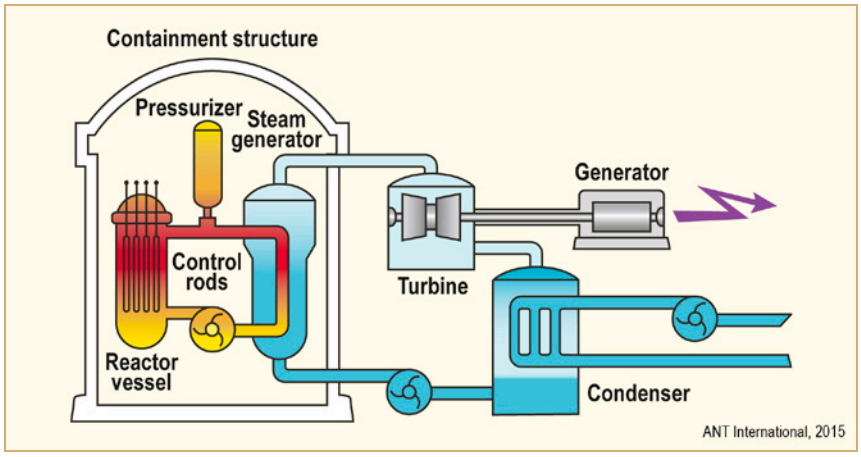

Figure 2-3: PWR general layout.

The primary recirculating coolant is sub-cooled, i.e. does not boil (except for some limited nucleate boiling on highly rated fuel elements) due to a significantly higher temperature and consequently vapour pressure being maintained by electrical heaters in the pressurizer than in the remainder of the primary circuit. A sub-cooled primary coolant allows the use of additives; hydrogen to supress the radiolytic decomposition of water, lithium hydroxide to adjust the pH to the optimum value needed to reduce general corrosion to a minimum, and boric acid that in combination with the control rods regulates the nuclear reaction rate in the core. The main generic structural materials and typical operating conditions for the primary circuit are shown in Figure 2-4 together with a more detailed cross-sectional view of the PWR pressure vessel.

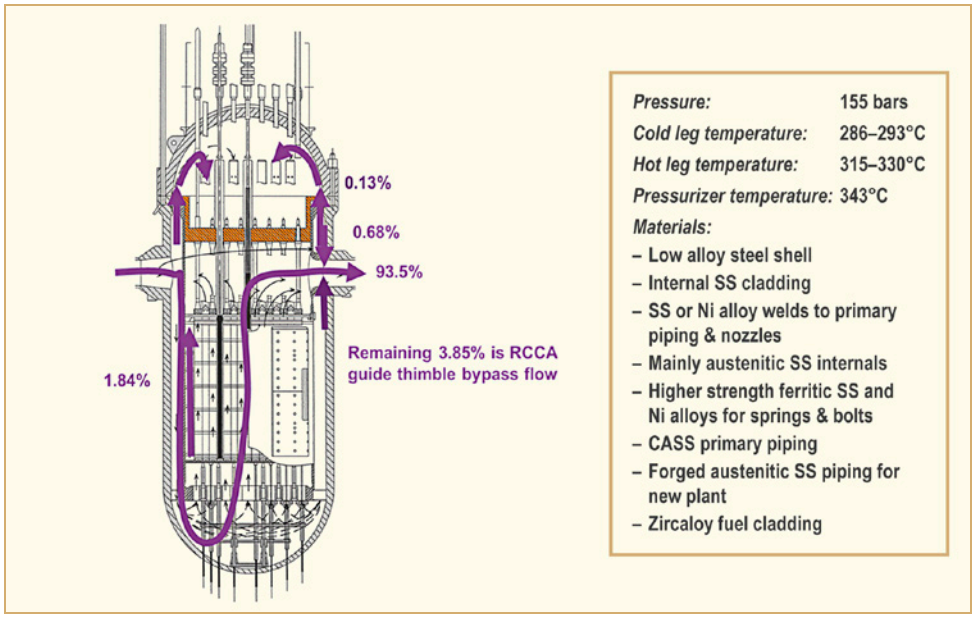

Figure 2-4: PWR pressure vessel and internals, primary circuit generic materials of construction and operating conditions.

Two main types of steam generator have been deployed in PWRs, recirculating and once through. Sketches of these basic designs are shown in Figure 2-5 together with the main generic structural material types and typical operating conditions. In the recirculating type, which is much more numerous, secondary water is boiled on the shell side by primary water flowing inside the steam generator tubes. About one quarter of the recirculating secondary water is vaporized into steam. On the other hand, in once trough steam generators, all the feed water entering the steam generator is volatilized into steam and superheated in one pass.

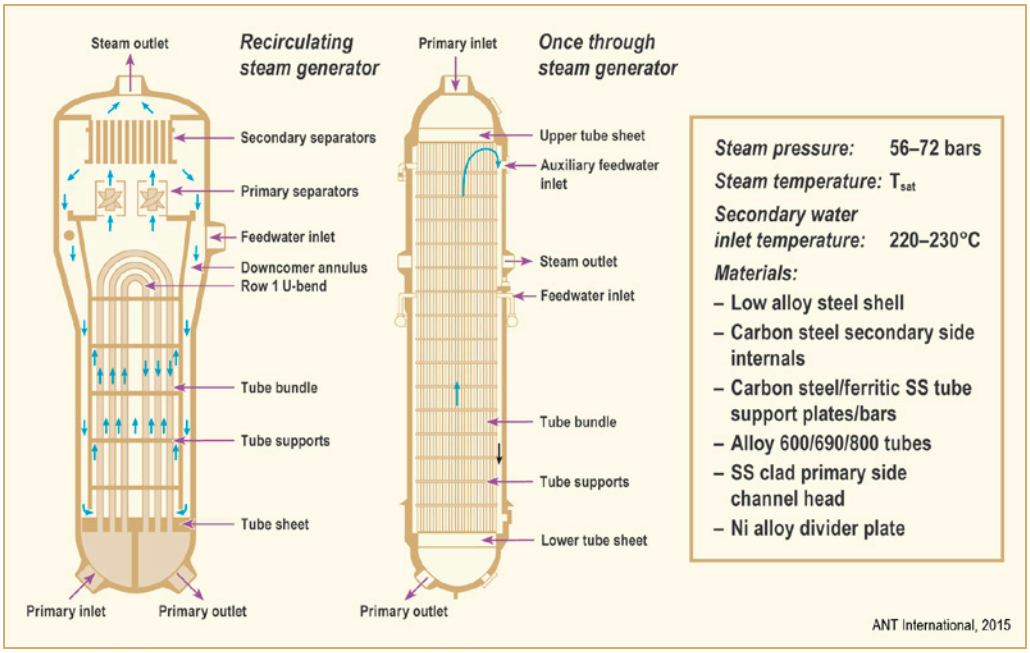

Figure 2-5: Sketches of the two main types of PWR steam generator and typical operating conditions.

3 Basic principles of physical metallurgy (Peter Ford)

The structural alloys used in water-cooled nuclear reactors cover a wide spectrum of compositions, as indicated in the ternary equilibrium phase diagram for the nickel-chromium-iron system at 400°C (Figure 3-1). The dominant stable phases, which depend on specific compositions, are ferrite and austenite, (as indicated respectively by the green and blue regions in Figure 3-1). The ferrite phase has a body centred cubic (bcc) crystal structure, whereas the austenite phase has a face-centred cubic (fcc) structure. Duplex ferrite plus austenite phase structures are possible with intermediate compositions in the yellow region.

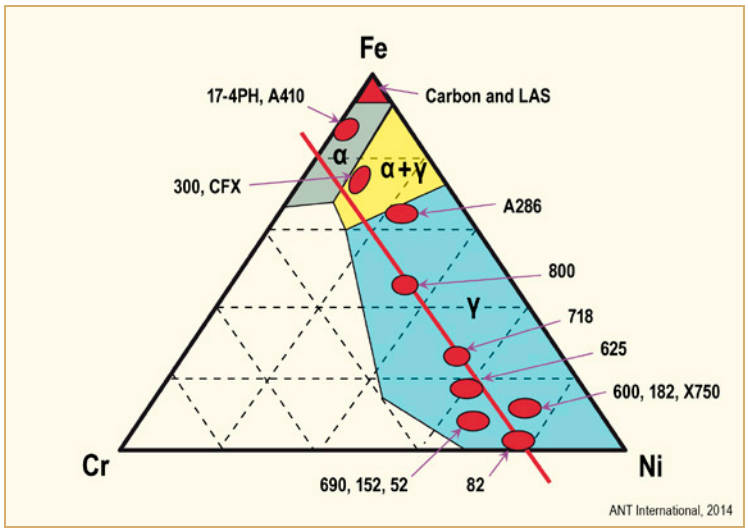

Figure 3-1: Ternary diagram for the Fe-Cr-Ni system at 400°C illustrating the compositions of the main structural alloys in water cooled reactors and the thermodynamically stable austenitic (Y) and ferritic (α) crystal structures denoted by the blue and green areas respectively. The austenite phase in the yellow region is metastable leading to a wide range of austenitic, ferritic, martensitic and duplex stainless steels. Note that the austenite phase is stable for all the nickel-base alloys, with chromium contents around 20% (denoted by the red line).

As might be expected, there is an associated spectrum of physical metallurgical phenomena, tensile properties and fracture resistance, in traversing from the iron-rich to the nickel-rich regions of this equilibrium diagram. These physical metallurgical aspects are now discussed for: (a) carbon and low alloy steels; (b) stainless steels; (c) nickel-base alloys; (d) high-strength nickel-base alloys and; (e) fabrication issues associated with brittle structures and welding.

3.1 Carbon and low-alloy steels

3.1.1 Introduction and applications

Carbon and low alloy steels are iron-based alloys with small amounts of elemental additions (carbon, chromium, nickel, etc.) that are made for reasons of strength, ductility, formability, grain refinement, weldability, etc. (Table 3-1 and Table 3-2). Note that only a sampling of the steels are shown in these tables, since the list is significantly longer when taking into account the different country code specifications. The purpose here is to illustrate the ranges in composition and the impact on the mechanical properties.

Table 3-1: ASTM Composition specifications for ferritic and bainitic carbon and low alloys. Concentrations are given in units of wt. % (Numbers in parentheses refer to the note number at the bottom of the table).

ASME/ASTM or AISI Spec	C max	Mn	P max	S max	Si	Cu max	Ni	Cr	Mo	V max	Typical user
Ferritic steels											
A105	0.035	0.6-1.05	0.035	0.04	0.1-0.35	0.4	0.4 max	0.3 max	0.12 max	0.05	Forging
						[ANL 01/09, 2000]	[ANL 01/09, 2000]	[ANL 01/09, 2000]	[ANL 01/09, 2000]		
A106 Grade B	0.3	0.29-1.06	0.035	0.035	0.10 min.	0.4	0.4 max	0.4 max	0.15 max	0.08	Seamless Piping
						(2)	(2)	(2)	(2)	(2)	
A216 Grade WCB	0.3	1.00 max	0.04	0.045	0.6 max	0.3	0.5 max	0.50 max	0.2 max	0.03	Casting
						(3)	(3)	(3)	(3)	(3)	
A302 Grade B	0.25	1.15-1.50	0.035	0.035	0.15-0.40				0.45-0.6		PV Plates
A333 Grade 6	0.3	0.29-1.06	0.035	0.035	0.1max						Feed water piping
A508 Grade 3	0.25	1.2-1.5	0.025	0.025	0.15-0.4		0.4-1.0	0.25 max	0.45-0.6	0.05	Forgings
A516 Grade 70	(4)	0.85-1.2	0.035	0.035	0.15-0.4						Plates
A533 Type A	0.25	1.15-1.5	0.035	0.035	0.15-0.4				0.45-0.6		PV Plates
			[Union Carbide Corp., 1977]	[Union Carbide Corp., 1977]		[Union Carbide Corp., 1977]				[Union Carbide Corp., 1977]	PV Plates
A533 Type B	0.25	1.15-1.5	0.035	0.035	0.15-0.4		0.40-0.7		0.45-0.6		
			[Union Carbide Corp., 1977]	[Union Carbide Corp., 1977]		[Union Carbide Corp., 1977]				[Union Carbide Corp., 1977]	PV Plates
Bainitic steels											
1Cr1Mo0.25V	0.33	0.85			0.25			1	1.25	0.25	Feed water piping
2Cr1Mo (Grade 22)	0.026	0.49	0.012	0.009	0.28	0.05		2.42	0.98		Cross around piping
NiCrMoV (A469 Cl.8)	0.28	0.6	0.015	0.018	0.15-0.3		3.25-4.0	1.25-2.0	0.3-0.6	0.15	Steam turbine
NiCrMoV (A470 Cl.8)	0.35	1.0	0.015	0.018	0.15-0.35		0.75	0.9-1.5	1.0-1.5	0.3	wheels and
NiCrMoV (A471 Cl.8)	0.28	0.7	0.015	0.015	0.15-0.35		2.0-4.0	0.7-2.0	0.2-0.7	0.05	rotors

Notes:

1. Sum of Cu Ni Cr and Mo shall be <1.00%; and sum of Cr and Mo shall not exceed 0.32%
2. Limits for V and Nb may be increased to 0.1% and o.05% respectively
3. Sum of Cr and Ni shall not exceed 0.32%
4. Carbon max. varies with thickness of plate; 0.5"-2".0.28% max.; 2"-4". 0.30% max.; 4."-8". 0.31%max.
5. For reactor beltline; Cu <0.1% max., P<0.012%max., S<0.015%max. and V <0.05%max.

ANT International, 2015

These steels are used in LWRs in a variety of forms including seamless piping, forgings, castings and plate. The specific carbon or low alloy steel/component combinations that are used for a particular reactor component vary between reactor design and manufacturer but, in general:

- Reactor pressure vessel vertical sections in both PWR's and BWR's were manufactured from rolled low alloy steel A533 Gr.B Class 1 plates that are then welded to form a right cylinder. Modern practice is to use forged cylinders of A508 Class 3 (as well as for nozzles and upper and lower heads). The cylinders are clad on the internal surface with a 5 to 7 mm layer of Type 309/308 stainless steel to confer general corrosion resistance. The structure is then given a post weld heat treatment (PWHT) at 595 to 620°C for one hour per 25 mm thickness of steel, in order to stress relieve the carbon/low alloy steel regions.

- The top and bottom heads of the pressure vessel in BWRs and PWRs are generally clad low alloy steel A508 Gr.2 or 3 Class 1 forgings, using the same cladding/heat treatment conditions as for the vertical sections, detailed above. After fabricating the vertical sections and the top and bottom heads, all subassemblies are welded together to form the primary pressure vessel, which is then given a further PWHT.

- Steam generator shells of PWRs are low alloy steel A533 Gr.A Class 1 or Class 2 plates, or latterly A508 Class 3 forgings, which, like the pressure vessel, are stress relieved. The secondary side of the steam generator is not usually clad.

- Steam generator tube sheets in PWRs may be A508 Gr.2 Class 1 or A508 Gr.2 Class 2, with cladding of stainless steel, or more usually, nickel-based alloys on the primary side bottom head.

- Steam generator channel heads in PWRs may be A216 Gr.WCC and are clad with stainless steel on the surface exposed to primary water.

- The pressurizer shell in PWRs may be low alloy steel A516 Gr.70, or A533 Gr.B plate, or A508 Grade III with cladding on the internal surface.

- Reactor coolant piping for PWR primary circuits may be austenitic stainless steel or, in some designs, seamless carbon steel clad internally with austenitic steel cladding. As will be discussed later, the recirculation piping in BWRs is usually austenitic stainless steel, although unclad A333 Gr. 6 carbon steel piping is used in the main steam and the feed water lines. In all plants the piping in the lower temperature emergency core cooling (ECCS) and auxiliary/support systems is usually seamless A105 or A106 Gr.B carbon steel, or austenitic stainless steel.

- Steam turbine discs and rotors are forged components using the low alloy steels A469, A470 and A471, with the desired mechanical properties being achieved by appropriate heat treatment and alloy composition. The microstructures are predominately bainitic as will be discussed in Section 3.1.2.4.

Table 3-2: Composition of high strength low alloy and maraging steels.

ASTM Spec	C	Mn	P Max	S Max	Si Max	Cu Max	Ni	Cr	Mo	V Max	Typical use
4340	0.38-0.43	0.6-0.8	0.035	0.04	0.15-0.35		1.65-2.0	0.7-0.9	0.2-0.3		Bolting
4140	0.38-0.43	0.75-1.0	0.035	0.04	0.15-0.35			0.8-1.1	0.15-0.25		
ANT International, 2015											

The mechanical properties of these steels (Table 3-3) are, as will be discussed later, directly related to the alloy microstructure and the phases present, and how these are controlled by the composition and processing parameters.

Table 3-3: Room temperature mechanical properties of carbon and low alloy steels (Cl-1 and Cl-2 refer to "Class 1" and "Class 2").

Grade	Yield Strength Ksi	Tensile Strength Ksi	Elongation %
A105	30	70	22
A106 Gr.B	35	60	30 (Long.): 16.5 (Trans.)
A216 Gr.WCB	36	70 (min.) – 95 (max)	22
A302 Gr.B	50	80 (min.) – 100 (max)	18
A508 Gr.2	50 (Cl-1): 65 (Cl-2)	80-105 (Cl-1): 90-115 (Cl-2)	38 (Cl-1): 35 (Cl-2)
A508 Gr.3	50	80 (min.) – 105 (max)	18
A516 Gr.70	38	70 (min.) – 90 (max)	21
A533 Gr.A	50 (Cl-1): 70 (Cl-2)	80-100 (Cl-1): 90-115 (Cl-2)	18 (Cl-1): 16 (Cl-2)
A533 Gr.B	50	80 (min.) – 100 (max)	18

ANT International, 2015

3.1.2 The phases and their effect on mechanical properties

The basic tool for understanding carbon and low alloy steel (C&LAS) microstructures and, thereby, their mechanical properties, is the binary Fe-C phase equilibrium diagram (Figure 3-2). This diagram is based on thermodynamic equilibrium conditions, and provides guidance as to the phases (e.g. austenite, ferrite, and cementite) that might be present in the microstructure when processed under iso-thermal or slow cooling conditions. The temperature-carbon content combinations where austenite is stable is shown by the yellow shaded region; similar stability regions for ferrite and cementite (Fe_3C) are shown by the blue and red regions respectively.

The carbon level in these steels used for structural components in nuclear plant is usually less than approximately 0.3 w/o (i.e. bounded by the dashed black line in Figure 3-2), since a lack of ductility and toughness with higher carbon contents limits the alloys' usefulness for structural components.

Following the behaviour of a 0.3% carbon steel (denoted by the dashed line in Figure 3-2) during cooling after solidification indicates that the carbon atoms are in solid solution in the austenite phase (denoted by yellow shading) when cooling from approximately 1500 to 800°C. Upon further slow cooling below approximately 800°C the γ phase starts to transform to body centred cubic (bcc) ferrite. This α phase (Figure 3-3a) at the austenite grain boundaries and grows as shown schematically in Figure 3-3b. Further cooling below a "eutectoid" temperature of 727°C causes the remaining austenite to transform to pearlite which is a mixture of ferrite (containing a maximum of 0.022 w/o carbon) and cementite (Fe_3C), (denoted as Cm in Figure 3-2). The morphology of pearlite is a lamellar mixture of ferrite and cementite, (Figure 3-3c).

It should be noted that Figure 3-2 does not indicate what happens when rapid cooling limits carbon atom diffusion during these transformations, and results in much harder phases such as "martensite" and "bainite". These non-equilibrium microstructures will be discussed in some detail in Sections 3.1.2.4, 3.1.2.5 and 3.1.2.6 since they play a crucial role in determining the range of mechanical properties that can be obtained, depending on the alloying elements and heat treatments applied.

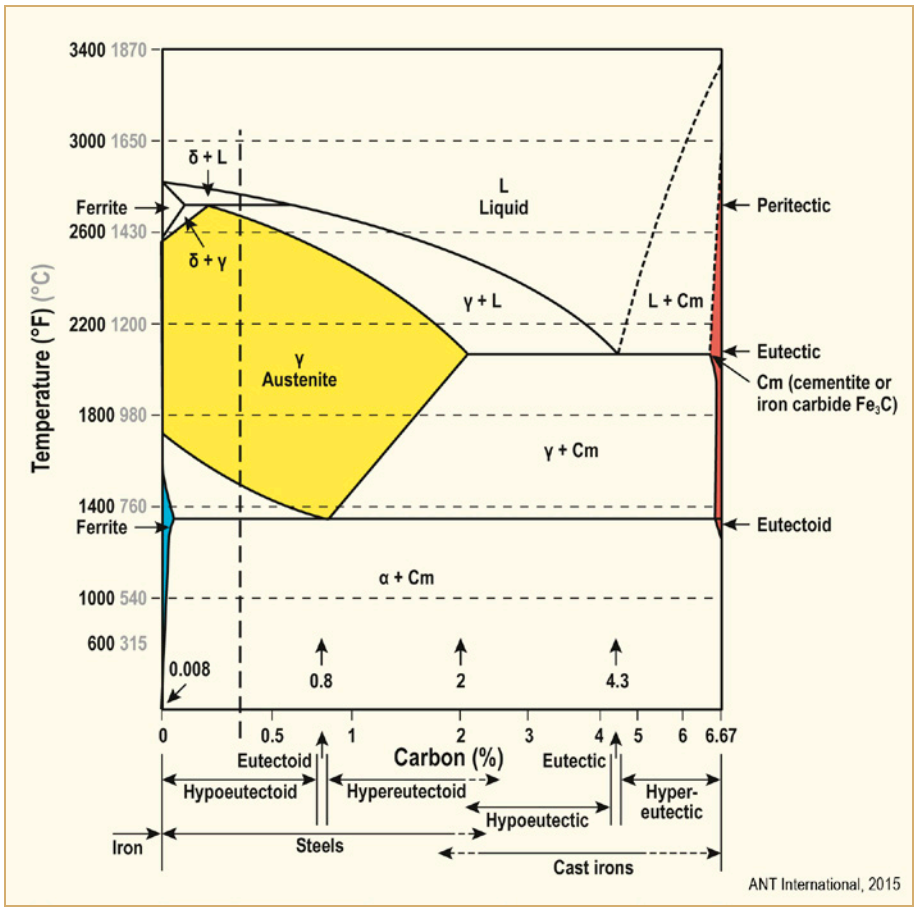

Figure 3-2: Iron-Carbon equilibrium phase diagram. Note the changes in the dominant phases as a 0.3% carbon steel is slowly cooled following solidification.

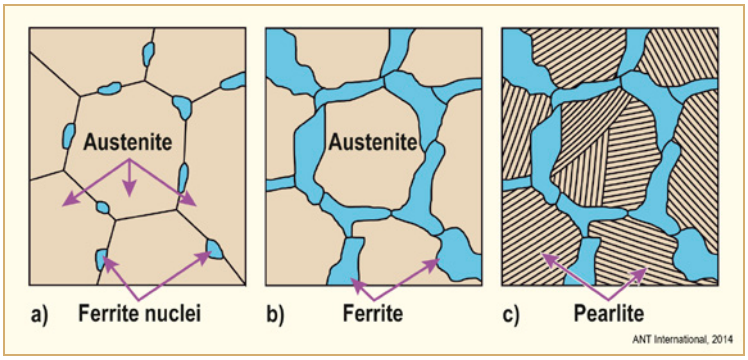

Figure 3-3: Three stages in the formation of ferrite and pearlite during slow cooling of the austenite phase of a hypo-eutectoid steel, after [Reed-Hill, 1967].

The microstructure of the various phases and their impact on the mechanical properties of the carbon and low alloy steels are now discussed.

3.1.2.1 Austenite

The face centred cubic austenite phase is stable, as seen from the yellow shaded region in Figure 3-2. Stable at elevated temperatures over a relatively wide range of temperature and carbon content. However this phase is not stable for the carbon and low alloy steels at temperatures below about 800°C. Alloying additions (e.g. nickel, chromium) alter this lower temperature limitation. For instance, significant alloying with nickel stabilizes the austenite phase at lower temperatures while, by contrast, chromium alloying stabilizes the ferrite phase at higher temperatures than 800°C. This balance between the nickel and chromium alloying determines the behaviour of a wide range of austenitic stainless steels and nickel-base alloys, as discussed in Sections 3.2 and 3.3.

Although the austenite phase is not stable at LWR operating temperatures in the carbon and low alloy steels shown in Table 3-1, the presence of "prior austenite" grain boundaries can be a site for segregation of impurity elements such as phosphorous, antinomy, tin and arsenic in quenched and tempered steels. This solute segregation, which typically occurs in the 400°C to 500°C temperature range, is retained at the lower temperatures and can give rise to temper embrittlement and IGSCC in some of the steam turbine low alloy steels. These aspects are discussed later in Section 9.6.

3.1.2.2 Ferrite

The ferrite phase is a solid solution of iron and carbon, plus one or more alloying elements such as silicon, chromium, manganese and nickel. The smaller atoms of elements such as carbon occupy interstitial sites in the body centred cubic ferrite (α) phase and can diffuse relatively rapidly compared with other larger alloying element atoms. As will be discussed later, this diffusion aspect has an impact on phase transformation kinetics and morphologies. The solubility of carbon in the ferrite phase is low, as indicated by the small blue shaded region in Figure 3-2, carbon has a maximum solubility of 0.022 w/o at the eutectoid temperature, 727°C, and decreases to below 0.005 w/o at room temperature in a binary Fe-C alloy.

In spite of this low solubility, carbon (and nitrogen and phosphorus) can have a marked effect on the yield stress of the ferrite phase, (Figure 3-4).

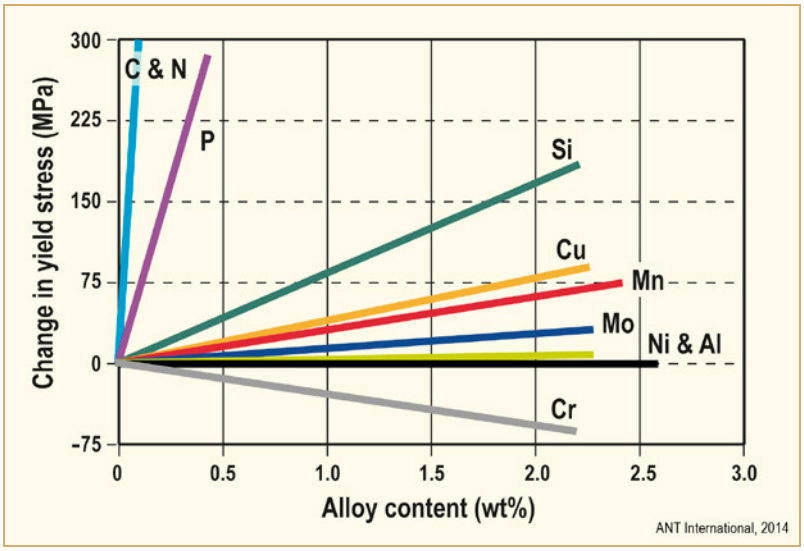

Figure 3-4: Influence of solid solution elements on the changes in yield strength of low-carbon ferritic steels, after [Finiston, 1971].

A further factor that leads to an increase in the yield stress is a decrease in the ferrite grain size, as shown in Figure 3-5. This dependency is described by the Hall-Petch relationship (Eq. 3-1) and, as will be seen later, this type of relationship between yield stress and the size of a dominant physical feature is observed in other phases and phase mixtures.

Eq. 3-1: $$\sigma_y = \sigma_0 + k_y d^{-0.5}$$

where σ_y is the yield stress, σ_0 and k_y are constants, and d is the ferrite grain size.

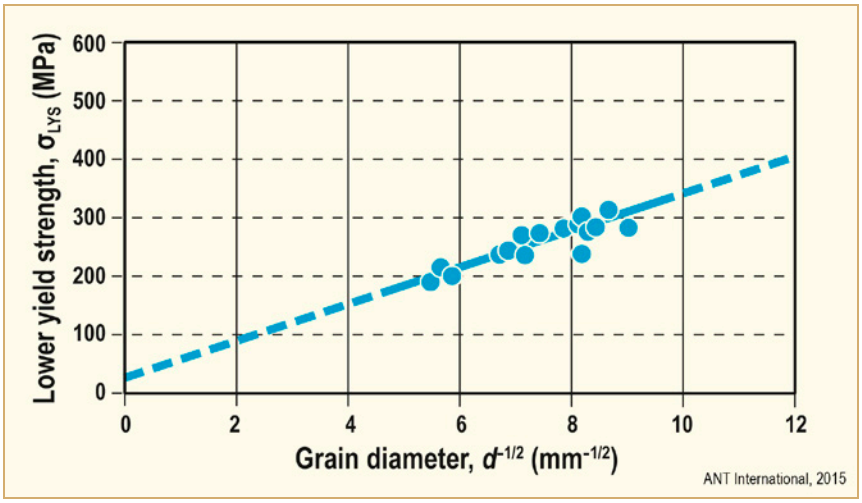

Figure 3-5: Hall-Petch relationship for yield stress as a function of grain size in low-carbon ferritic steels, after [Union Carbide Corp., 1977].

3.1.2.3 Pearlite

As indicated in Figure 3-2, and schematically in Figure 3-3, the ferrite phase nucleates at the austenite grain boundaries during slow cooling of a hypo-eutectoid steel (i.e. a steel containing less than 0.8 w/o C) below approximately 800°C. During this process the ferrite rejects carbon and the carbon content in the remaining austenite phase increases until, under equilibrium conditions, it reaches 0.8 w/o at the eutectoid temperature, 727°C, in a Fe-C alloy. Below that temperature the remaining austenite transforms (Figure 3-6) to a lamellar mixture of nearly pure Fe (the ferrite phase) and carbon-rich Fe_3C; this mixture of phases is known as pearlite. Thus, a typical slowly cooled, steel with low to medium carbon content will have a structure that is a mixture of ferrite (that formed above the eutectoid temperature) and pearlite. Increasing carbon content increases the fraction of pearlite so that the pearlite will occupy 100% of the structure for a eutectoid steel containing 0.8% carbon.

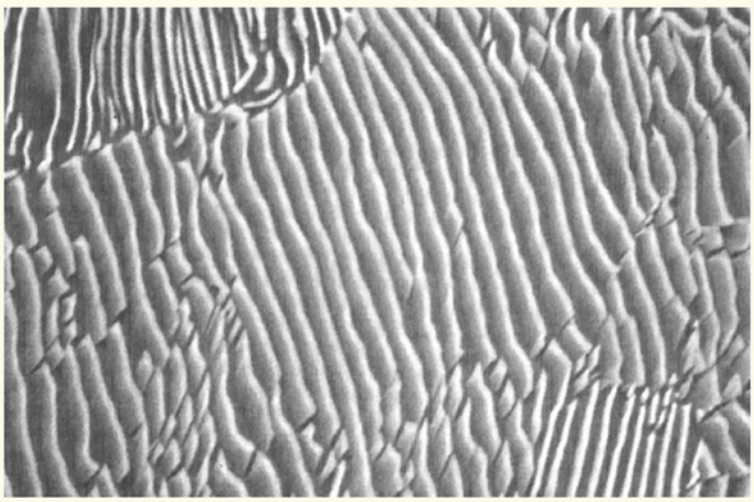

Figure 3-6: Scanning Electron Microscope (SEM) micrograph of pearlite showing cementite and ferrite lamellae (10,000×) [Vander Voort & Roosz, 1984].

These phase transformations involve nucleation and growth phenomena, which depend on temperature/time controlled diffusion processes for carbon, manganese, nickel, chromium and molybdenum alloying elements. The effect of these conditions may be illustrated on Time-Temperature-Transformation (TTT) diagrams, which quantify the extent of the transformation occurring during an iso-temperature anneal for a given time (e.g. a post weld heat treatment). Alternatively, Continuous-Cooling-Transformation (CCT) diagrams quantify the transformations that occur during the cooling process following a normalization or homogenizing heat treatment in the austenite phase stability region. The physical process for the formation of a pearlite colony in the austenite phase involves the nucleation of a Fe_3C platelet at an austenite grain boundary. This nucleation will be accompanied by carbon depletion adjacent to the platelet, which then triggers the nucleation and growth of an associated ferrite platelet.

The rates of nucleation and growth of the pearlite colonies as a function of temperature are different, with nucleation being the rate limiting process at temperatures just below the eutectoid temperature (727°C), and the growth of the pearlite colony being the rate limiting step at temperatures below 655°C, Thus, as indicated in the TTT diagram for this eutectoid steel containing 0.8% carbon (Figure 3-7), the extent of transformation from austenite to a (mixed ferrite plus Fe_3C) pearlite colony exhibits a characteristic "C-shaped" temperature–time dependency with the maximum rates of austenite transformation occurring around 550°C. This, as will be discussed further, is a consistent feature for phase nucleation and growth transformations in carbon and stainless steels, and nickel-base alloys.

4 Basics of aqueous corrosion of metals (Pierre Combrade)

4.1 Introduction

Corrosion is defined in ISO standard 8044 as a "physicochemical interaction between a metal and its environment that results in changes in the properties of the metal, and which may lead to significant impairment of the function of the metal, the environment, or the technical system, of which these form a part"[13] The standard also includes as a note: "This interaction is often of an electrochemical nature".

Corrosion in aqueous environments is due to oxidation of metal into:

- dissolved ions: in most cases M^{z+} cations, but also anions such as for example $HFeO_2^-$ in very alkaline solutions or poly-ions like "oxi-hydroxi-chloride" in very concentrated solutions. A typical dissolution reaction can be written in simplified way[14] as:

$$M \rightarrow M^{z+} + z\ e^-$$

- solid phases: oxides M_xO_y, hydroxides $M_x(OH)_y$ or more complex hydroxi-oxides. A reaction producing an oxide can be written as:

$$x\ M + y\ H_2O \rightarrow M_xO_y + 2y\ H^+ + 2\ e^-$$

The above reactions are electrochemical reactions because they involve exchanges of electrical charge between phases with different types of charge carriers, i.e. electrons in metals, ions in solution, and ionic and electronic defects in oxides.

A consequence of the above oxidation reactions is the production of an excess of positive charges in the aqueous environment and of an excess of electrons in the metal. However, electrical neutrality must be maintained in bulk phases and this implies that oxidation processes must be balanced by reduction reactions that consume excess electrons in the base metal and produce negatively charged anions or consume positively charged cations (generally H^+) in aqueous environments. The two main reduction reactions involved in corrosion processes are as follows:

- reduction of water in near neutral or alkaline environments or reduction of protons in acidic environments:

$$2\ H_2O + 2\ e^- \rightarrow H_2 + 2\ OH^-$$

$$H^+ + 2\ e^- \rightarrow H_2$$

- reduction of dissolved oxygen in aerated aqueous environments:

$$O_2 + 2\ H_2O + 4\ e^- \rightarrow 4\ OH^-$$

[13] All sentences between quotation marks are taken from definitions in the ISO 8044 standard
[14] The "simplified way" used to write reactions involving ions neglects their solvation sheaths (see Section 4.4).

However, corrosion also involves chemical reactions where the redox state of atoms may not change. These reactions are hydrolysis reactions that can lead to the formation of more complex ions or to the precipitation of solid phases. They are usually written in a simplified way as follows:

$$M^{z+} + n\ H_2O \rightarrow M(OH)_n^{(z-n)+} + n\ H^+$$

All three types of reaction described above may participate to determine the nature of the degradation and/or control the corrosion rate of a material. In particular, a reduction reaction may be the rate controlling process of corrosion, and corrosion mitigation is often obtained by inhibiting reduction rather than oxidation reactions. Hydrolysis reactions are also of major importance in promoting local changes of pH involved in localised corrosion and/or the formation of somewhat protective surface deposits.

This section will first give a short description of the main forms of corrosion and present the main parameters which may control or influence corrosion behaviour. It is considered important to emphasise the fact that a corrosion problem cannot be understood and solved without knowledge, as precise as possible, of theses parameters. Then the basics of electrochemistry and chemistry related to corrosion will be presented, including thermodynamic and kinetic aspects. Finally, different types of corrosion phenomena will be described: i.e. general corrosion, galvanic coupling, localised corrosion, microbial induced corrosion and stress corrosion cracking.

4.2 Different forms of corrosion

Most metallic materials are not thermodynamically stable in aqueous environments and tend to become oxidised, which leads to their degradation by corrosion. Their survival for engineering purposes is only possible due to slow, or very slow, oxidation kinetics.

Two main situations prevail:

- **Active dissolution**: metallic materials are not protected by any surface film and they can dissolve into the environment generally as cations (see above). In this case, corrosion rates can be limited due to:
  - very low metal solubility. This is, for example, the case of Ni or Cu in deaerated aqueous environments) and is commonly (but improperly, since solubility is never strictly zero) referred to as immunity;
  - low active dissolution rates: e.g. Ni and Mo in deaerated very acidic environments. This phenomenon is at the origin of the corrosion resistance of Ni-Mo Alloys (Hastelloy B series) with no chromium additions that are used in concentrated deaerated HCl environments, for example;
  - dissolution limited by mass transport of oxidising species and/or of corrosion products in the aqueous environment. This can be due to a slow diffusion process in a non-turbulent environment or caused by the formation on surface deposits of corrosion products or of species dissolved in the environment. This is, for example, the case of C-steel in sea water where the dissolution rate is limited by the diffusion of dissolved oxygen.
- **Passivity**: the metal surface is protected by a compact oxide film (passive film) that is spontaneously formed and repaired on contact with the corrosive environment. Dissolution is limited by solid state mass transport through the passive film. This is the case for all stainless Fe-Ni-Cr alloys, aluminium, titanium, zirconium alloys in near neutral aqueous environments.

4.2.1 General corrosion

According to ISO 8044, general corrosion is "corrosion proceeding over the whole surface of the metal exposed to the corrosive environment". A particular case is uniform corrosion which is a form of "general corrosion proceeding at almost the same rate over the whole surface".

General corrosion occurs both on active or passive metal surfaces.

4.2.2 Selective corrosion

Selective corrosion is "corrosion of an alloy whereby the components react in proportions that differ from their proportions in the alloy". This includes two particular cases:

- selective dissolution of a phase, e.g. selective corrosion of cast Ni-Al alloys in sea water where the Al-rich phase is preferentially dissolved;
- selective dissolution of an alloying element in a phase (dealloying), e.g. selective dissolution of Zn in Cu-Zn brasses.

In both cases, corrosion can occur to significant extent only if a continuous pathway is available for dissolution. In the case of dealloying, this implies a minimum concentration of alloying element is required for selective corrosion to persist and surface diffusion may play a significant role. Near room temperature, dealloying produces nano-porous surface layers, a phenomenon that is now used to produce materials with calibrated nano-porosity.

4.2.3 Galvanic corrosion

Galvanic corrosion is a form of "corrosion due to the action of a corrosion cell". In the ISO 8044 standard it is noted that "the term has often been restricted to the action of bimetallic corrosion cells, i.e. to bimetallic corrosion". In this case, contact between different metallic materials may lead to unwanted accelerated degradation of one of these materials, for example aluminium or carbon steel in contact with stainless steels or copper alloys in many environments; but it may also leads to the protection of the more "noble" material, which is extensively exploited in the so-called galvanic ("cathodic") protection of carbon steel by zinc or aluminium or magnesium, etc. to mitigate sea water or atmospheric corrosion.

4.2.4 Localised corrosion

Localised corrosion includes a series of forms of "corrosion preferentially concentrated on discrete sites of the metal surface exposed to the corrosive environment". "Localised corrosion can result in, for example, pits, cracks or grooves".

In most cases, localised corrosion occurs on passive materials due to preferential dissolution of zones with weak, defective, or no passive film.

The main forms of localised corrosion are:

- Intergranular corrosion, i.e. "corrosion in or adjacent to the grain boundaries of a metal";
- Pitting corrosion, i.e. "localised corrosion resulting in pits, i.e. cavities extending from the surface into the metal";
- Crevice corrosion, i.e. "localised corrosion associated with, and taking place in or immediately around a narrow aperture or clearance formed between the metal surface and another surface (metallic or non-metallic)". Crevice corrosion can be due to poor component design (Figure 4-1 and Figure 4-2-left), formation of deposits (Figure 4-2-right), biological fouling, etc.

Localised corrosion is not a critical problem in light water reactors, even though it is occasionally encountered on PWR steam generator tubes (as pitting) and in auxiliary cooling circuits.

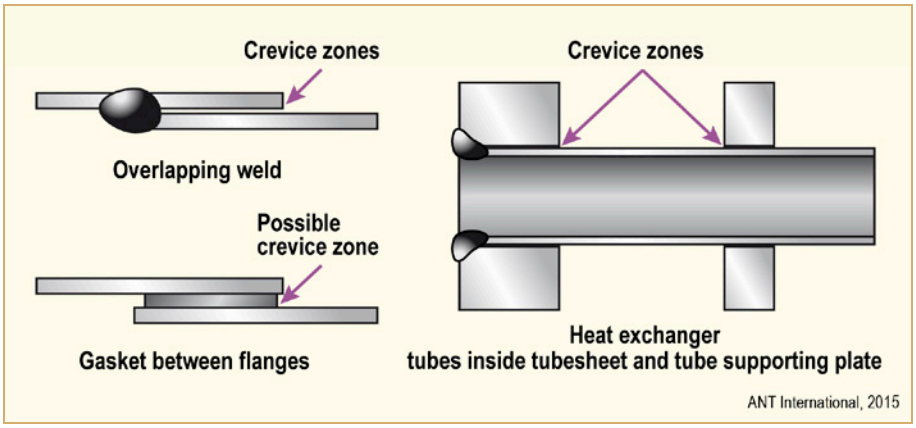

Figure 4-1: Typical crevice zones due to inadequate design.

Figure 4-2: Examples of crevice corrosion damage on Type 316 stainless steels in chloride environments: left, corrosion under a gasket in brackish water, [During, 1991] - right, corrosion under deposits in a tank washed with sea water and subsequently inadequately rinsed [Désestret, 1975].

4.2.5 Environmentally assisted cracking (EAC)

EAC is often considered as a form of localised corrosion but, in many instances it involves mechanical micro-cracking and, for this reason, the authors prefer to consider EAC as a separate type of degradation. EAC is not specifically defined by the ISO standard 8044 but its definition of stress corrosion cracking (see below) applies quite well, as follows, as a "process involving conjoint corrosion and straining of the metal due to applied or residual stress".

In aqueous environments, EAC includes several forms of degradation:

- **Stress corrosion cracking (SCC Figure 4-3),** which should be defined as a process involving the simultaneous action of a corrosive environment and an applied or residual static stress including at least one tensile component;
- **Corrosion fatigue,** which is due to cyclic loading: the presence of aqueous environment results in a decrease in resistance to fatigue;
- **Strain induced corrosion cracking,** which is due to slow straining in the plastic range;
- Some forms of **hydrogen embrittlement.**

In light water reactors, EAC, usually SCC, has been the main cause of corrosion problems, as described extensively in this book.

Figure 4-3: Example of stress corrosion cracking of a Type 316 stainless steel under thermal insulation at 50 to 60°C. Rinsing water containing 60 mg/kg of chloride and residual stresses are at the origin of cracking, [During, 1991].

4.2.6 Erosion corrosion

The standard definition of erosion corrosion is a "process involving conjoint corrosion and erosion" with a note indicating that "erosion corrosion can occur in, for example, pipes with high fluid flow velocity and pumps and pipe lines carrying fluid containing abrasive particles in suspension". This definition includes two types of degradation:

- Corrosion accelerated by the effect of flow rate on mass transport in the liquid environment, which typically results in a "scalloped" appearance of the affected surfaces;
- Corrosion accelerated by mechanical degradation of protective films, for example by abrasive particles in the flowing fluid.

In light water reactors, Flow Accelerated Corrosion (FAC) of Carbon steel belongs to the first type of degradation when occurring in liquid phase, but also involves mechanical degradation of the protective films in wet steam containing liquid water droplets (see Section 8.1).

4.2.7 Cavitation corrosion

Cavitation corrosion leads to a form of mechanical damage to the base metal, which is not the case in erosion corrosion. It creates ragged appearance to the affected surfaces with some surface cold work due to the mechanical effect of vapour bubble implosion. It occurs typically in pumps or on propellers.

4.2.8 Microbially induced corrosion (MIC)

MIC is "associated with the action of micro-organisms present in the corrosion system". It can occur both in aerobic or anaerobic conditions depending on the species of micro-organisms.

In nuclear plants, it occurs extensively on stainless steels in auxiliary cooling circuits, in stagnant conditions, and particularly on the heat tinted zones caused by welding (see section 4.7).

4.3 Main factors affecting corrosion

Corrosion is a specific phenomenon of each metal/environment system: i.e. **there is no metal intrinsically resistant to corrosion in all possible environments** (e.g. Pt may be corroded in acidic chloride solutions) **and there is no innocuous environment** (e.g. water as pure as that used in BWRs can cause cracking of stainless steels).

Thus, to solve a corrosion problem it is necessary to identify and characterise environmental parameters, material parameters, among which surface condition is of most importance, and other possible influencing parameters such as mechanical or biological parameters.

In addition, these parameters must be known for all in-service nominal conditions, for extreme fault conditions that are acceptable without shutdown, for transient conditions (e.g. plant shutdown and start-up, power transients, etc.) and for maintenance operations.

4.3.1 Environmental parameters

4.3.1.1 Bulk liquid environments versus surface films

It is important to note that most of the corrosion damage observed in the world is due to atmospheric corrosion, i.e. to aqueous surface films rather than to a bulk liquid environments.

The main differences between both types of environments are due to differences in mass transport in the liquid phase:

- In thin surface films, the diffusion of oxygen from the atmosphere to the metal surface is very fast and equilibrium between the condensed phase and atmosphere may lead to very high concentrations of species like sulphate, sulphite or chloride present as traces pollutants in the atmosphere. In addition, corrosion products, which are usually not volatile, cannot be removed into the atmosphere and therefore concentrate on the surface.

- In bulk environments, mass transport is highly dependent on hydrodynamic conditions: high flow rates favour access of oxygen to the surfaces and evacuation of corrosion products and both factors can cause significant increases in corrosion rates of materials that are protected by oxide films with non-negligible solubility in the environment, e.g. copper alloys which may be susceptible to erosion corrosion in heat exchangers or in propellers, or carbon steels which may be susceptible to FAC in steam circuits of fossil power plants and LWRs.

Another important difference is that, because thin liquid films have necessarily a high resistance to electrical (corrosion) currents flowing parallel to the surface, significant ionic currents cannot flow between zones separated by “large” distances. In other words, galvanic corrosion cannot occur over long distances.

Apart from atmospheric corrosion, thin condensate films occur in many industrial plants, e.g. in boilers and gas scrubbers where the presence of impurities in gaseous phases is responsible for the formation of very concentrated and often very acidic liquid films.

4.3.1.2 Main parameters affecting aqueous environments

At least four classes of parameters are important:

pH

pH is often determinant, mainly because the solubility of oxides that can protect metal surfaces increases when the pH becomes very acidic or very alkaline. All oxides or hydroxides exhibit a minimum of solubility as a function of pH and solubility rapidly increases exponentially when the pH departs from this minimum.

However, it must be noted that the pH for minimum oxide solubility strongly depends on the metallic element: for example, at room temperature, this pH is ~10.5 for Fe, ~9 for Cu and ~5 for Al. This is why it is difficult to optimize the pH of secondary side water in PWRs where carbon steels and copper alloys are both present. This is also why the pH of water in research reactors where aluminium alloys are extensively used is decreased to ~5 by nitric acid addition.

The effect of pH on the reduction reaction is also important. An increase in the proton reduction rate is the main reason why the active corrosion rate or iron dramatically increases as the pH becomes more acidic, even though the solubility of metallic iron does not increase.

Oxidizing species

Since degradation of metals by aqueous environments is generally due to oxidation processes, the presence of oxidising species in water is of major importance. The oxidising power characterizes the efficiency of the reduction reactions in an aqueous environment: we will see later that an environment is highly oxidising when the reduction reaction is possible over a large range of potentials and can deliver a large cathodic current.

Water can oxidise metals like Fe, Cr, Al, Zn, Mg, Ti, Zr, etc. but not significantly Ni, Cu, Ag, Pt, ... which require the presence of oxidisers more powerful than water to be significantly corroded.

Oxygen is the most widespread oxidiser present in water due to equilibrium with atmospheric oxygen: pure water in equilibrium with air at 25°C contains ~8 mg/kg of dissolved oxygen.

Other oxidising species frequently present are biocides (like chlorine, hypochlorite …), nitrates, chromates (often used as corrosion inhibitor in the past but now forbidden for environmental pollution reasons); …

In BWRs, water radiolysis produces various different oxidising species among which oxygen and hydrogen peroxide may survive throughout the whole coolant circuit, at least in the absence of added hydrogen.

The effect of oxidising power on corrosion is complex:

- On actively corroding materials, the corrosion rate increases with the oxidising potential;
- On passivating metals, passive films may be stable only in a limited range of oxidising power (potential):
  - passive films can be formed only if the oxidising power is high enough: e.g. in near-neutral environments, water is oxidising enough to passivate stainless steels but in acidic environments, a more powerful oxidiser like oxygen may be required;
  - conversely, passive films may become unstable if the environment is too oxidising: e.g. stainless steel may suffer transpassive corrosion in very oxidising acidic solutions (e.g. concentrated nitric acid) or localised corrosion in chloride-containing environments.

Temperature

Most reactions and mass transport phenomena involved in corrosion are thermally activated. Accordingly, when increasing temperature, active corrosion rates generally increase, passive films become less efficient and less stable, which favours the initiation of localised corrosion and EAC.

However, in some instances, there can be an inversion of this tendency at high temperature for localised corrosion and EAC that is often due to the fact that increased general corrosion rates make the development of faster localised damaging processes more difficult. Hydrogen embrittlement, which is involved in some EAC processes, also decreases as temperature increases.

Depending on whether corrosion rates are controlled by liquid phase mass transport, by surface reaction rates or by solid phase mass transport rates, the effect of temperature may strongly change from low to high apparent activation energy.

Presence of deleterious solutes

The presence of dissolved species in water may be damaging directly as a result of increased conductivity. This has been clearly demonstrated in the case of intergranular stress corrosion cracking in BWRs with Normal Water Chemistry (NWC) (Figure 4-4). One reason for this effect is that in high purity water, in the absence of ionic species, the dissolution of metallic cations whose positive charge must be balanced by anions becomes more difficult.

In addition among the solutes, several classes are almost universally deleterious, due to their chemical or electrochemical properties:

- Chloride ions are the most widespread harmful solute in aqueous environments and they are dangerous in several aspects: they impair stability and repair of passive films, they can be at the origin of low pH values, and they may enhance active dissolution;
- Reactive sulphur species, like sulphides, sulphites, thiosulphates, thiocyanates, polythionates, readily and strongly adsorb on bare metal surfaces and inhibit formation of passive films;
- Complexants increase the solubility of metallic cations. For example, amines form complexes with copper and increase its corrosion rates, which is a problem in PWR plants with brass condensers. On the other hand, EDTA is used for boiler cleaning by enhancing dissolution of Fe corrosion products.

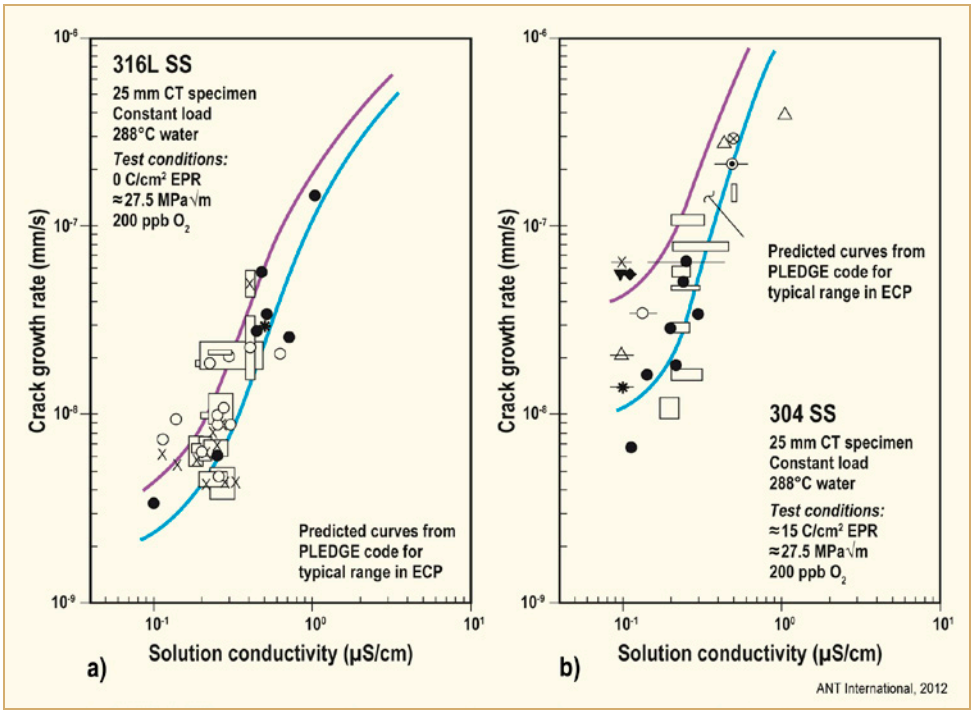

Figure 4-4: Effect of water conductivity on the crack propagation rate in non-sensitised Type 316L stainless steel (left) and sensitised Type 304 stainless steel (right) in 288°C water, after [Ford, 1988] and [Ford, 1996].

4.3.2 Material parameters

Among material parameters of importance for corrosion behaviour, elemental composition and microstructure are very important.

4.3.2.1 Alloy composition

The effect of composition on resistance to corrosion is due to the presence of alloying elements but also to the residual elements that are often deleterious.

In the particular case of stainless alloys, i.e. Fe-Ni-Cr alloys which are the most used materials in LWRs, the effect of alloying elements can be summarized as follows:

- Chromium is the alloying element which is responsible for the formation of very protective oxide films because its solubility is extremely low in deaerated water. However, it can be oxidised into soluble chromates when the environment becomes highly oxidising, as is the case in BWR NWC in the presence of dissolved oxygen and hydrogen peroxide.
- Molybdenum is a very efficient alloying element for improving resistance to localised corrosion at low temperature. However, it has no significant effect in high temperature water.
- Nitrogen added at levels of the order of 0.25 to 0.4% in conjunction with molybdenum dramatically improves resistance to localised corrosion in low temperature chloride environments.
- Nickel has a strong effect on the microstructure of stainless alloys as it stabilises austenite and avoids the presence of ferrite or martensite that may influence corrosion behaviour. Also, nickel increases the stability of passive layers at room temperature and has some positive (but limited) effect on resistance to localised corrosion.

Regarding the effects of residual elements in stainless alloys, the most important are due to:

- Carbon that may be deleterious as it promotes precipitation of chromium carbides on grain boundaries with associated chromium depletion (sensitisation, see Sections 3 and 9);
- Sulphur is very harmful for resistance to localised corrosion and to EAC in chloride environments.

4.3.2.2 Alloy microstructure

Two important factors may influence corrosion behaviour:

- The presence of phases, precipitates and inclusions:
  - in the case of stainless steels, the presence of ferrite or martensite (often formed by deformation) may be beneficial or deleterious depending on specific environmental conditions; in particular, martensite may be susceptible to hydrogen embrittlement;
  - On stainless alloys, the presence of precipitated fine intergranular carbides, apart from any associated chromium depletion, may be beneficial for resistance to intergranular SCC in low oxidising power environments (PWR coolants);
  - On stainless alloys, all non-metallic inclusions are more or less deleterious to resistance to localised corrosion, particularly manganese and calcium sulphides that can be dissolved or oxidized and promote initiation of localised corrosion.

5 Low temperature EAC in LWRs (Pierre Combrade)

In addition to the normally well-controlled aqueous environments used in LWR primary coolant circuits, , austenitic stainless alloys can also be occasionally exposed in dead-legs of those circuits with restricted flow and in many auxiliary circuits to aqueous contaminants and dissolved oxygen that cause SCC.

The most widespread and most dangerous contaminant is obviously chloride ions although other contaminants like sulphur species may also be of concern. This chapter addresses mainly the consequences of contamination by chlorides. Other SCC phenomena that may possibly relevant to LWRs are also briefly described.

5.1 Low temperature SCC of stainless steels in LWRs

5.1.1 Low temperature SCC in primary and auxiliary circuits

A relatively recent EPRI review of SCC in the primary circuits of American PWRs revealed that 85% of SCC events in austenitic stainless steel occurred in "occluded" regions (see the blue bars in Figure 5-1), most cracks being transgranular. Only 15% of events apparently occurred in the nominal flowing environment. The extremely low number of SCC events on stainless steels reported in this review, as well as in a German review summarized in Figure 5-2, emphasizes the excellent field experience of these materials over several decades of exploitation of PWRs for electric power production.

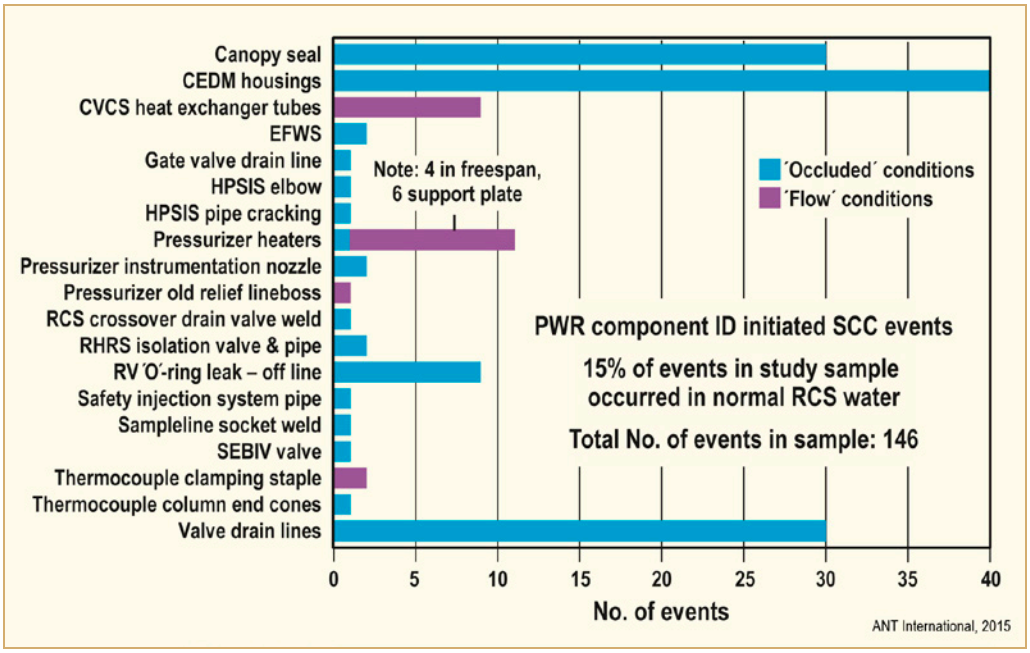

Figure 5-1: Summary of reported events of SCC in austenitic stainless steels in PWR primary circuits, after [Ilevbare et al, 2008].

In addition, the distribution of cases of transgranular cracking (Figure 5-2) shows no increasing frequency with time, which means that these events, albeit recurrent, are not a problem related to plant aging but a problem of transient operating conditions.

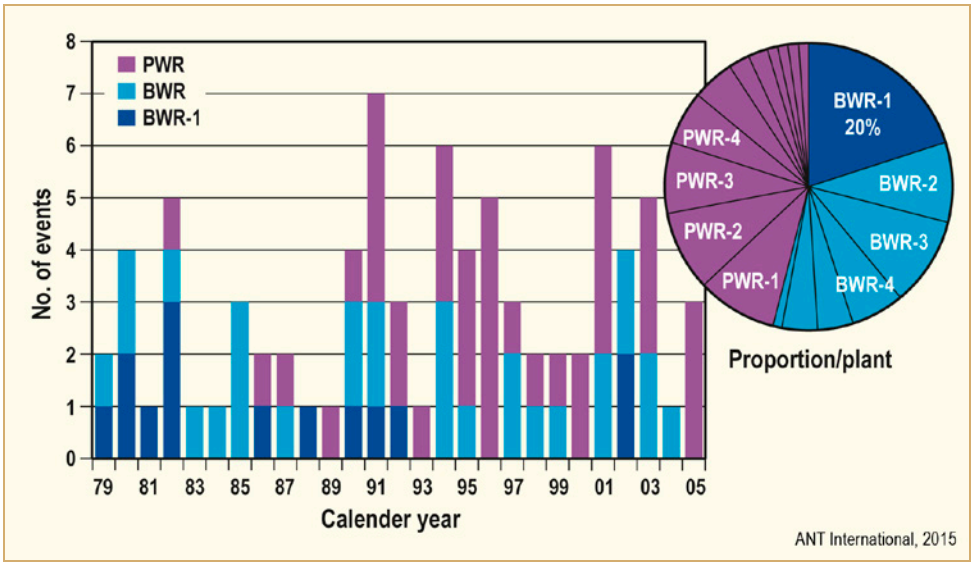

Figure 5-2: Evolution with time of transgranular SCC events in austenitic stainless steels and the proportions per LWR plant type in Germany, after [Jendrich et al, 2006].

When analysis of local environments in contact with cracked stainless steels in "occluded" zones has been possible, they usually reveal the presence of chlorides and/or ionic sulphur species.

According to the EPRI review, the main "occluded" zones in primary circuits affected by SCC are Canopy seals, CRDM housings, and dead legs near valves. The German review mentions that small bore pipes are the main locations for TGSCC, which has also been observed in auxiliary circuits. TGSCC of fasteners used to connect core barrels to baffle formers in reactor vessel internals has been attributed to the use of inappropriate lubricants during installation. In French PWRs, a significant number of TGSCC events have also occurred in dead legs of PWRs (Figure 5-3), notably between isolations valves. These zones are characterised by stagnant water at temperatures that can exceed 250°C with possible thermal stratification as well as the presence of water and steam phases (Figure 5-4) that may lead to concentration of impurities by evaporation near the water line.

Similarly, air bubble trapped in canopy seals (Figure 5-5) when filling primary circuit causes the formation of a temporarily aerated environment, possibly contaminated by impurities coming from thread surfaces. Transgranular cracking may occur during and after plant heat-up transients (Figure 5-6) before trapped oxygen has been consumed or eliminated by diffusion. Note that in an air bubble trapped at the pressure of the primary circuit, the oxygen partial pressure may exceed 20 bars, creating highly oxidising conditions that are very favourable for SCC in presence of chlorides (see below).

Impurity sources are often unknown but those that have been identified include asbestos gaskets, sealing materials and lubricants. Silicate filler materials are also suspected as well as palladium gels dryers and palladium catalysers used to recombine hydrogen. In cases where evaporation plays a part, the very low amount of impurities contained in reactor coolants of nominal purity has been claimed to possibly lead to critical chloride concentrations even if no additional contamination is present.

Contamination of surfaces during fabrication is also a well-known cause of stress corrosion cracking of austenitic stainless steels: e.g. skin moisture due to handling without gloves, adhesive tapes and markers have been identified in a significant number of cases as the sources of chlorides responsible for TGSCC.

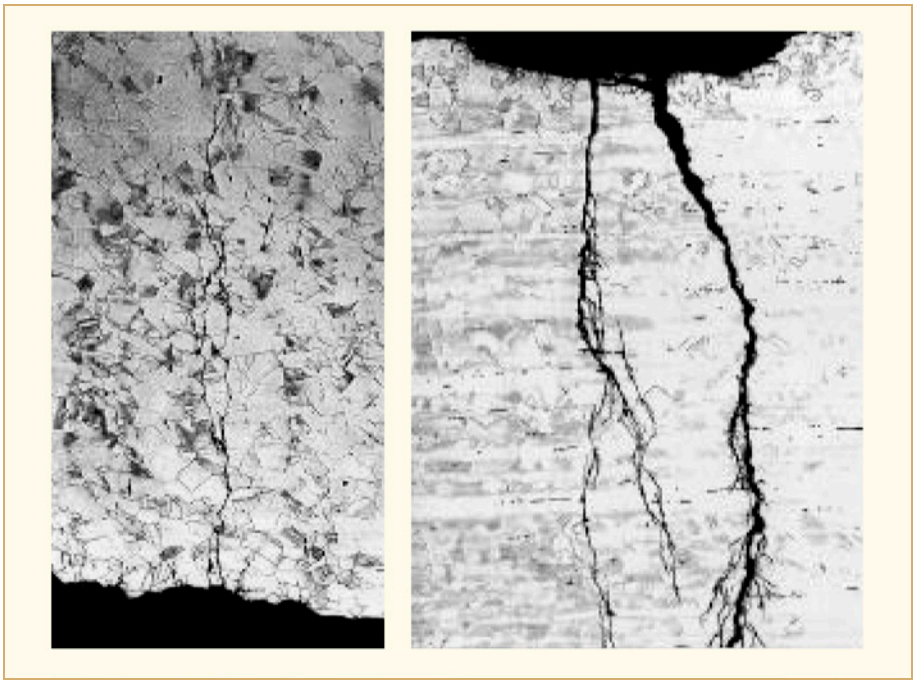

Figure 5-3: Transgranular stress corrosion cracking of Type 316L stainless steels in dead legs between isolation valves of a PWR primary circuit, after [Boursier et al, 2002].

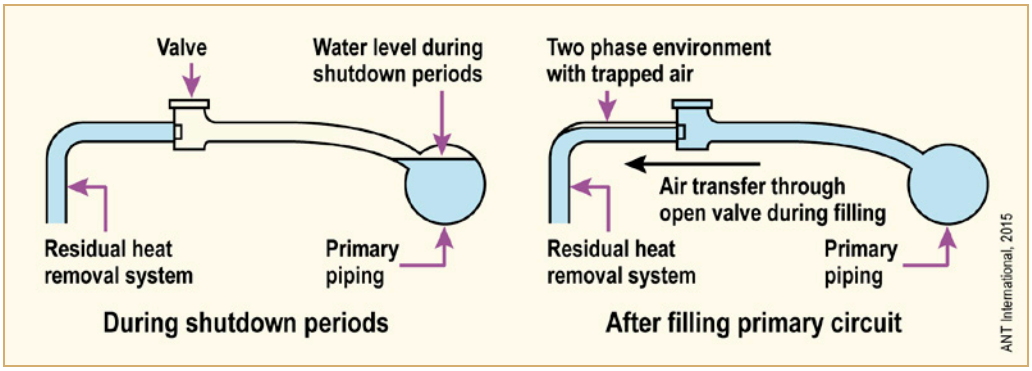

Figure 5-4: Formation of a two-phase, aerated environment when filling the primary circuit after a shutdown period in dead legs between isolation valves, after [Economou et al, 1990].

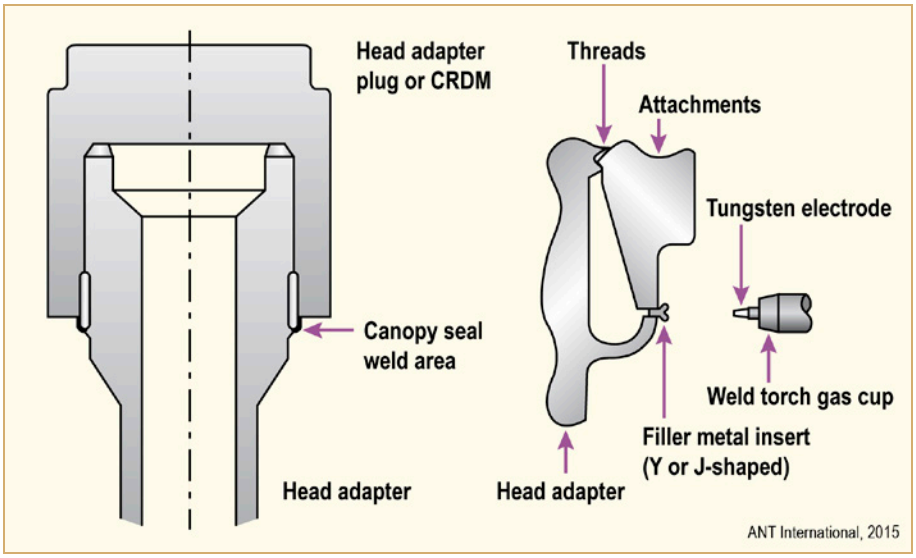

Figure 5-5: Schematic views of canopy seals and welding procedure [Pezze & Wilson, 1990].

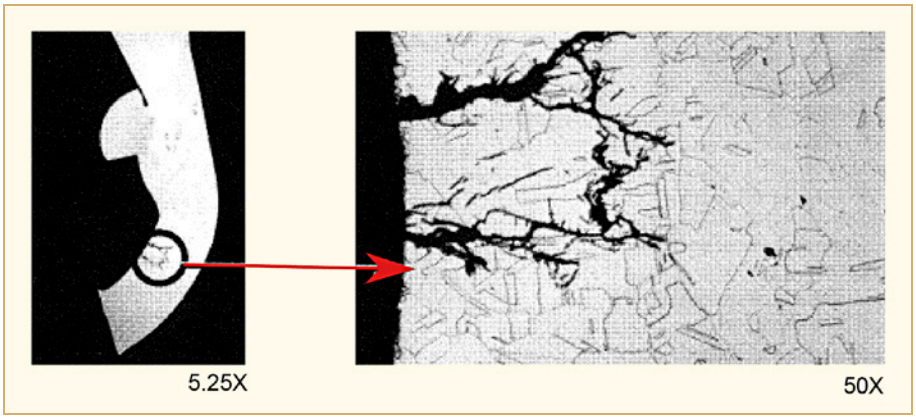

Figure 5-6: Example of TG cracks in the base metal of canopy seals [Pezze & Wilson, 1990].

5.1.2 External SCC

SCC is called "external" when occurring on surfaces not exposed to the process fluid but to the external atmosphere in which the plant operates. External SCC includes corrosion under insulation and corrosion without insulation, i.e. mostly atmospheric corrosion.

Corrosion under insulation (CUI) is a very common phenomenon in the chemical industry due to improper selection of insulating materials and/or to ingress of contaminated water between the insulation and component, very often during washing and during fire exercises. No recent case of CUI has been reported in LWRs.

Atmospheric SCC has occurred, for example in both Koeberg units, on stainless steel components exposed to marine atmosphere. Numerous externally initiated cracks, some through-wall, were observed in both Koeberg units on seam welded piping of safety related water injection systems, the refuelling storage water tanks, and cast valves. The cracking was almost exclusively initiated from surface pits (Figure 5-7). The tanks, piping and valves were manufactured from Type 304L austenitic stainless steel and the systems concerned typically operate at temperatures below 50°C with no thermal insulation.

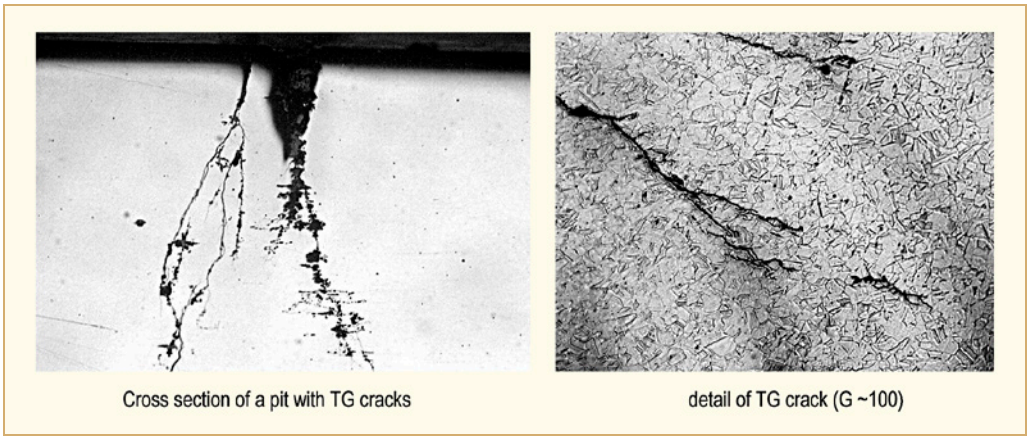

Figure 5-7: Pitting and TG cracks on the outer surfaces of Type 304L stainless steel equipment at Koeberg [Basson & Wicker, 2002].

5.2 SCC of stainless steels in chloride environments

SCC of austenitic stainless steels in chloride environments is usually transgranular (Figure 4-49 in Section 4.8.2.2). The fracture surfaces (Figure 4-50 in Section 4.8.2.2) have a brittle aspect with many crystallographic patterns and often without any visible trace of plasticity, at least at an optical microscopic scale. In some instances, cracks may have propagated intergranularly, but this is mainly due to very high mechanical loads or to sensitisation.

5.2.1 Effect of environment (potential, pH and temperature)

In very acidic environments (H_2SO_4 + NaCl, H_2SO_4 + HCl or HCl), where stainless steels exhibit an activity peak and weak passivity, SCC can occur at room temperature, either above a critical potential or near the active to passive transition (in common with many SCC systems).

In near neutral or moderately acidic environments, SCC of austenitic stainless steels occurs when the corrosion potential exceeds a critical value (Figure 5-8) that is often close to or slightly lower than the pitting potential.

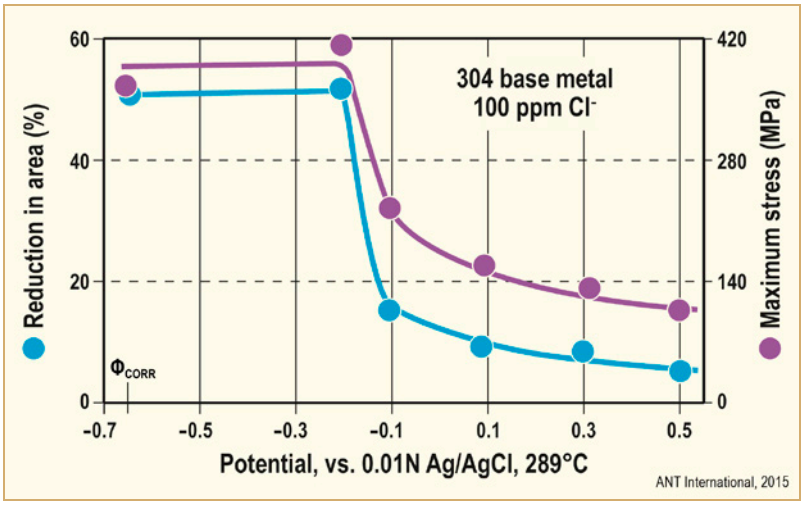

Figure 5-8: Effect of applied potential on tensile specimens continuously strained in 100 mg/L chloride, deaerated solution at 290°C. TGSCC occurs above a critical potential ~-0.15 mV/Ag/AgCl and causes a decrease in reduction in rupture surface area and maximum stress in SSRTs, after [Andresen & Duquette, 1980].

- **In moderately acidic, concentrated environments**, such as the classical boiling $MgCl_2$ test solutions at 154°C, the presence of an oxidising species other than water is not necessary for the corrosion potential to exceed the critical value. Thus, SCC can occur in deaerated environments although dissolved oxygen accelerates cracking.

  In these environments, SCC may occur at a relatively low temperature, or even at room temperature if the concentration of chloride is very high. This could account for SCC in marine atmospheres at low temperatures (see below).

- **In near-neutral dilute environments**, SCC requires the presence of a species more oxidising than water, usually dissolved oxygen, and is often initiated from localised corrosion.

  As shown in Figure 5-9, the higher the chloride content, the lower the dissolved oxygen concentration required for cracking of non-sensitized stainless steel. However, in the range of interest of most contaminated LWR environments, i.e. very low concentrations of chloride, the threshold for cracking is not reliably established and requires more study.

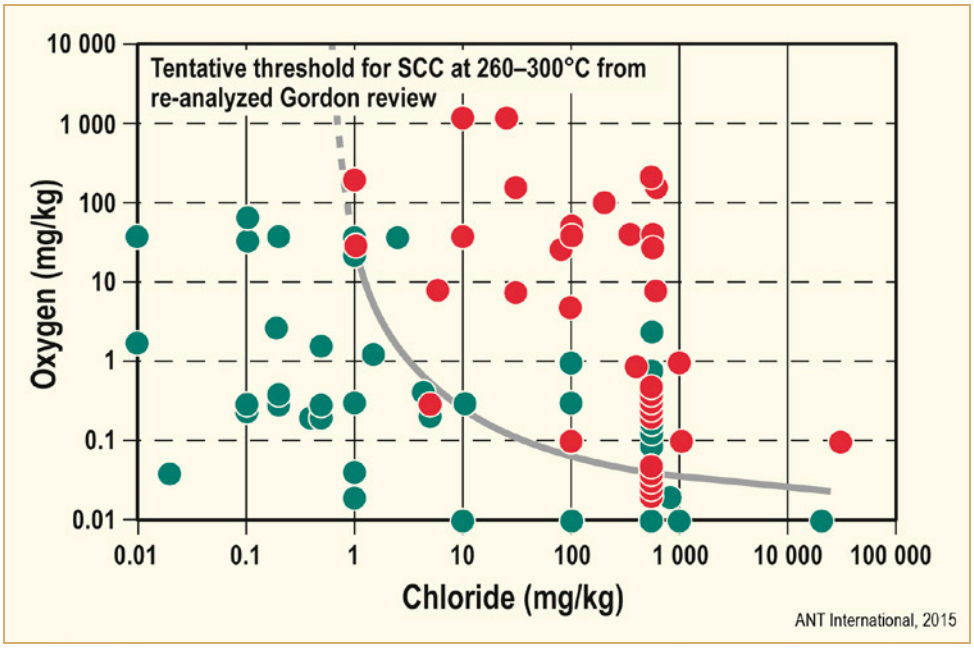

Figure 5-9: Effect of chloride concentration on the critical concentration of dissolved oxygen for SCC in high temperature water: data collected by [Gordon, 1980] and re-analysed.

The presence of sulphates has been found to decrease susceptibility to SCC by increasing the critical potential for cracking at 290°C (Figure 5-10).

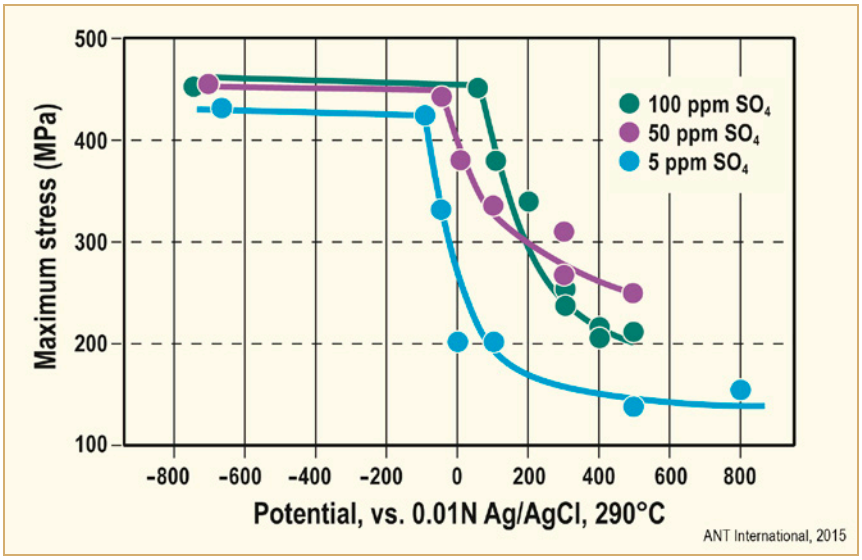

Figure 5-10: Effect of sulphate concentration on SCC on annealed Type 304 stainless steel in 100 ppm Cl^- solution at 290°C, after [Poznanski & Duquette, 1983].

Laboratory results and field experience surveys show (Figure 5-11) that, in near-neutral environments, SCC occurs only above ambient temperature, typically above 50 to 60°C. However, propagation of existing cracks cannot be excluded at lower temperatures.

In all cases, increasing temperature increases susceptibility to cracking since it lowers the critical potential for cracking and increases crack propagation rates.

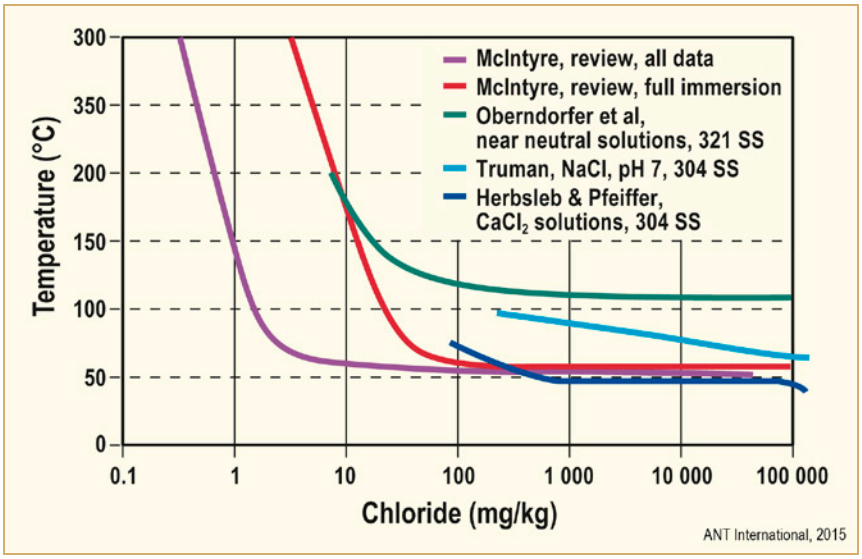

Figure 5-11: Threshold temperature for SCC of Type 304 SS as a function of chloride content, after [McIntyre, 1987], [Oberndorfer et al, 2004], [Truman, 1977] and [Herbsleb & Pfeiffer, 1984].

6 Water chemistry in light water reactors (Pierre Combrade)

Water chemistry in light water reactors is a critical issue regarding the degradation of materials by corrosion. Except for the role of primary water chemistry in participating in the control of nuclear reactions in PWRs, all the main goals of water chemistry in LWRs are aimed at minimising problems related to different aspects of aqueous corrosion, i.e. degradation of metals and the deleterious effects of corrosion products (leading to activity transport and fouling of the coolant circuits):

- The degradation of LWR structural materials includes:
  - Oxidation of Zr-alloy cladding on fuel rods, which controls the lifetime of the fuel;
  - Stress corrosion cracking including:
    - SCC of sensitised and/or cold worked stainless steels in BWRs (see Section 9);
    - SCC of Ni-based alloys and cold worked stainless steels in the primary circuits of PWRs (see Section 10);
    - IASCC of irradiated stainless steels both in PWRs and BWRs (see Section 9 and 10);
    - Secondary side corrosion of steam generators tubes in PWRs (see Section 10.8),
    - Stress corrosion cracking of stainless steels in auxiliary circuits (see Section 5);
  - General corrosion:
    - General corrosion of stainless alloys in primary coolant circuits (see Section 7)
    - Flow assisted corrosion of carbon steels LWRs (see Section 8);
  - Localised corrosion, mainly in auxiliary circuits;
    - Pitting and crevice corrosion (see Section 4.6.2);
    - Microbially Induced Corrosion (see Section 4.7);
- Corrosion products are responsible for:
  - Deposition on fuel rods;
  - Activity of primary circuits due to cation release of stainless steels and Ni-base Alloys (see Section 7);
  - PWR steam generator fouling in the secondary side;
  - Water purification and treatment of radioactive effluents.

6.1 Water radiolysis

An issue specific to LWRs is the radiolysis of water under the influence of the core radiation field. Neutrons, β and γ radiations cause the decomposition of water molecules into radical species and aqueous electrons with subsequent reactions leading to the formation of molecular species, mainly hydrogen peroxide, oxygen (a decay product of hydrogen peroxide), and hydrogen.

$$H_2O \rightarrow e^-_{aq}, H^\bullet, OH^\bullet, H^+, HO_2^\bullet, H_2, H_2O_2 (\rightarrow O_2)$$

The concentrations of the primary products of radiolysis are controlled by the linear energy transfer rate (LET) for each radiation type and energy. The reaction yields are given by the so-called G-values, i.e. the number of molecules, ions or radicals formed for each 100 eV of energy absorbed. G-values can vary sharply with the LET so that radiation quality (neutron/γ ratio, energy) and intensity have a significant impact on the primary reaction product concentrations. Table 6-1 gives typical values of LET and G-values for neutron and γ-radiations.

Table 6-1: LET and yields for reactor irradiations [Cohen, 1980] and [Burns & Moore, 1976].

Radiation type	Mean LET	G-values: yield/100eV absorbed						
	eV/nm	e^-_{aq}	H^+	H_2O_2	$OH\cdot$	$HO_2\cdot$	$H\cdot$	H_2
β, γ	0.1	2.70	2.70	0.61	2.86	0.03	0.61	0.43
Fast neutrons	40	0.93	0.93	0.99	1.09	0.04	0.50	0.88
ANT International, 2015								

Radical species do not survive for long periods and their presence via subsequent radical-molecule reactions may be effective only in the core. The $HO_2\cdot$ radical is believed to be the most concentrated of all the short lived products of radiolysis. Molecular species, including hydrogen peroxide that now appears to be much more stable than expected in high temperature water, can be present in all LWR core coolants if no countermeasure is taken. Oxidising species (oxygen and hydrogen peroxide) have, in most cases, a deleterious effect on materials as they cause a dramatic increase in corrosion potential, which results in the occurrence of IGSCC of sensitised and/or cold worked materials in BWRs.

The countermeasure used both in PWRs and now in BWRs with HWC is to eliminate most of the oxidising species by adding dissolved hydrogen to the core coolant, which then scavenges the oxidising products of radiolysis, as shown in Figure 6-1.

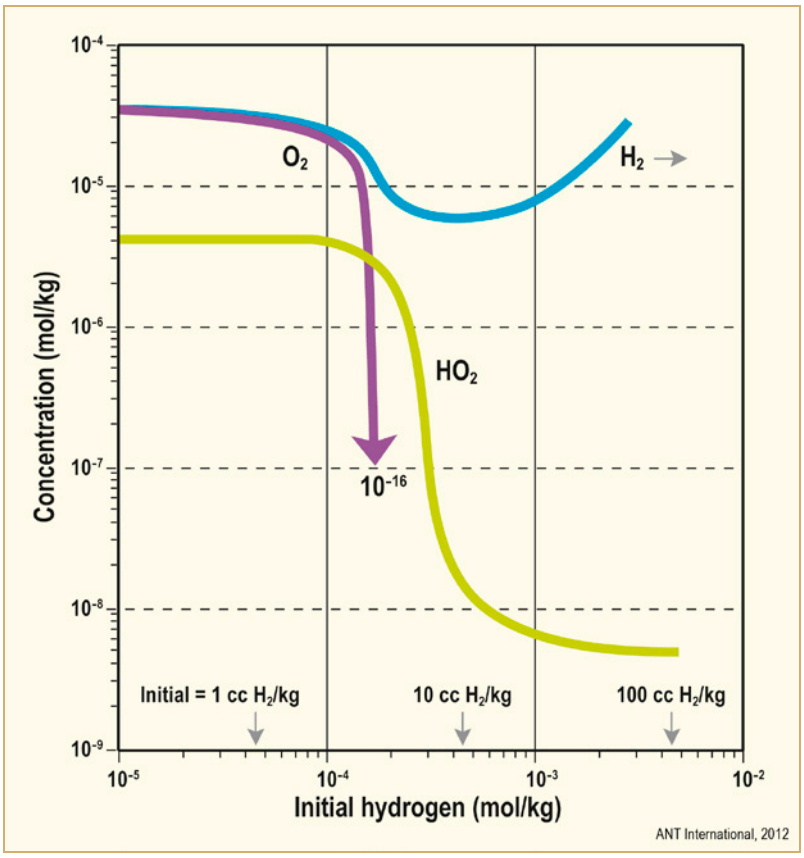

Figure 6-1: Steady state concentration of O_2 and HO_2 under irradiation conditions as a function of initial dissolved hydrogen concentration, after [Solomon, 1978].

More details on radiolysis and its consequences can be found in ANT International LCC4 STR [Riess et al, 2010] and Introduction to Boiling Water Reactor Chemistry – Volume I [Cowan et al, 2011].

6.2 PWR primary water chemistry

The water chemistry of PWR primary circuit is mainly aimed at:

- participating in the control of the nuclear reaction by the addition of a neutron absorber (boric acid);
- maintaining "low" corrosion potentials of metallic materials to minimise corrosion problems;
- minimising the activity of the primary coolant circuit and deposition of crud on the fuel rods.

Details on the water chemistry of primary PWR and VVER plants can be found in two ANT International reports on "PWR/VVER Primary Side Coolant Chemistry": "Volume I - Technical Basis and Recent Discussions" [Riess et al, 2011] and Volume II - Water Chemistry Tool to Mitigate the Concerns" [Riess & Odar, 2012].

Table 6-2 shows a typical water chemistry of PWR primary circuit:

Table 6-2: Typical water chemistry conditions in PWR primary system, after [Scott & Combrade, 2006].

	Typical
Pressure (MPa)	14.2
Temperature (°C)	286-323
Oxygen (ppm)	<0.1
Conductivity ($\mu S.cm^{-1}$)	1-40
Hydrogen (ml/kg) at STP	20-50
Lithium (ppm) as LiOH	0.1-3.5
Boron (ppm) as H_3BO_3	0-2300
Chloride (ppm)	<0.15
Fluoride (ppm)	<0.15
SiO_2 (ppm)	<0.20
pH_T	6.8-7.4
	ANT International, 2015

Pressure is maintained high enough by the higher temperature of the pressurizer to avoid boiling in the primary circuit. However, in some plants with high duty cores, nucleate boiling may occur on the upper part of the fuel rods; this favours the formation of crud deposits and may lead to the so-called Axial Offset Anomaly (AOA) due to unbalanced core burn-up.

Oxygen is kept very low, usually of the order of a few µg/kg, i.e. much lower than the specified value.

Boric acid contributes to controlling the nuclear reaction (together with the water coolant and the control rods) due to the neutron absorbing properties of the ^{10}B isotope. The concentration of boron at the beginning of a fuel cycle is 1000 to 1800 mg/kg and continuously decreases to about zero as the excess reactivity of the nuclear fuel decreases. The use of boric acid with enriched ^{10}B enables the concentration of boric acid to be decreased and thereby facilitates the control of pH.

Lithium hydroxide is added to control the pH. It was selected because it is a weak base and lithium is also a fission product of boron. The lithium concentration is maximum at the beginning of a fuel cycle because of the elevated concentration of boric acid. Due to its possible deleterious effect by boiling concentration on Zr alloys of the fuel cladding, the initial lithium concentration was limited to 2.2 mg/kg for many decades. Presently, the trend is to increase this limit to 3.5 mg/kg or even higher. As the concentration of boron decreases, the concentration of lithium is also decreased to values as low as 0.1 mg/kg.

pH at temperature (pH_T)[28] is maintained slightly alkaline to minimise the solubility of oxides formed on primary circuit structural alloys and particularly their transport from steam generator tube bundles to the core and vice versa. In the past, the optimum $pH_{300°C}$ was estimated to be ~6.9 based on magnetite solubility. Today, the solubility of nickel oxide and nickel ferrite are taken into account and the optimum $pH_{300°C}$ is estimated in the range 7.2 to 7.4. To maintain optimum pH during the fuel cycle the so-called "coordinated Li/B chemistries" have been defined. Figure 6-2 shows different Li/B coordinated chemistries that have been used or foreseen for use in French PWRs. Note that due to the maximum limit applied to the Li concentration of the primary coolant, the pH is more acidic than optimum at the beginning of a fuel cycle. The use of high initial Li chemistries allows the optimum pH_T to be reached sooner in the fuel cycle.

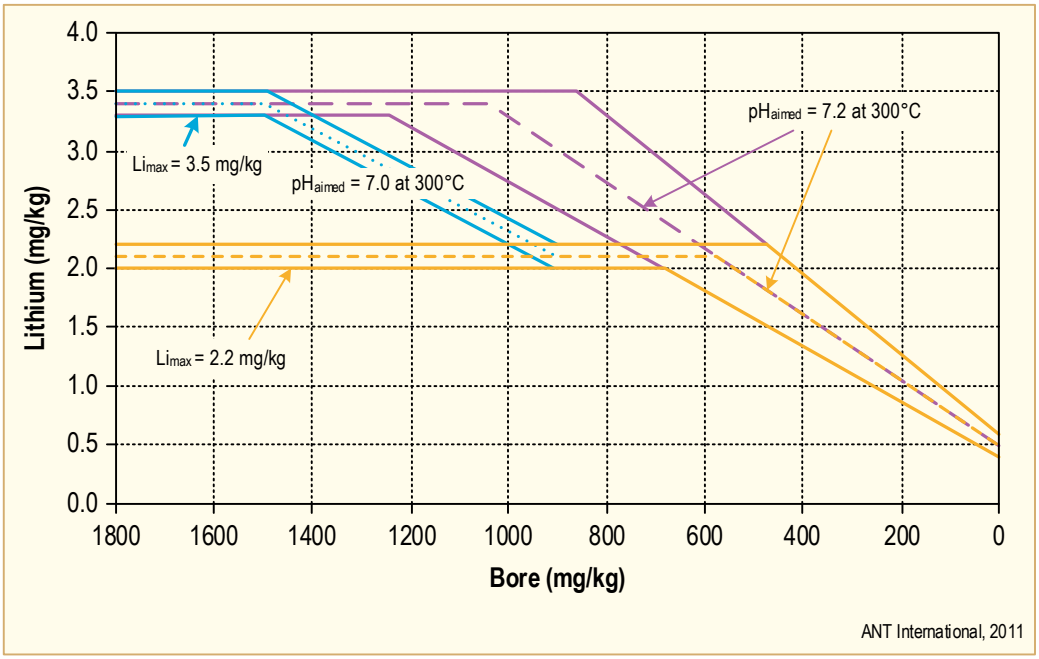

Figure 6-2: Diagram of the three B/Li coordinated chemistries used or considered for use in EdF PWRs: Classic coordination (orange), modified coordination (blue) and elevated lithium coordination (purple), after [Taunier et al, 2010].

Dissolved hydrogen is added to scavenge the radiolytic decomposition products of water and to maintain low corrosion potentials of all materials in the primary circuit. A few cm^3/kg are sufficient to reach this goal in theory (Figure 6-1), but in practice higher concentrations are usually specified. As a consequence of the high exchange current density of the H^+/H_2 redox reaction on all the common structural alloys in PWR primary circuits that is more than one order of magnitude higher than any oxidation currents of the same materials exposed to the primary coolant, the corrosion potentials of all steels and Ni-base alloys are within few millivolts of the redox potential of the Reversible Hydrogen Electrode (Figure 6-3), at least for temperatures higher than ~150°C (Figure 6-4).

[28] Note that at 300°C, neutrality of water where $[H^+] = [OH^-]$ occurs at pH ~5.7.

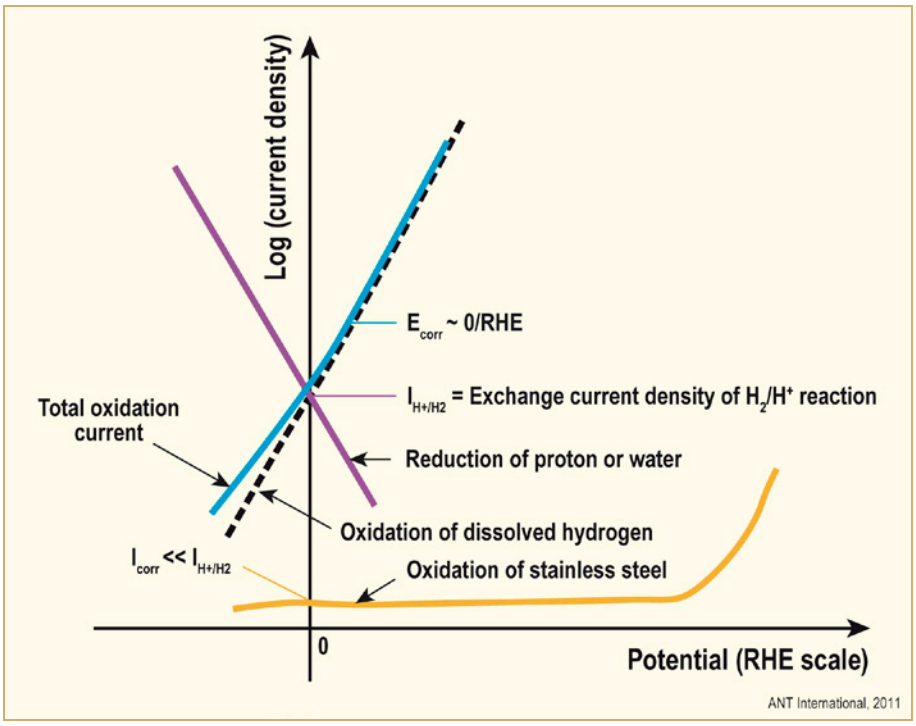

Figure 6-3: Evans diagram showing how the corrosion potential of stainless steel in PWR primary water is almost equal to the RHE potential because the exchange current density of the H^+/H_2 reaction is much higher than the oxidation current density of stainless steel.

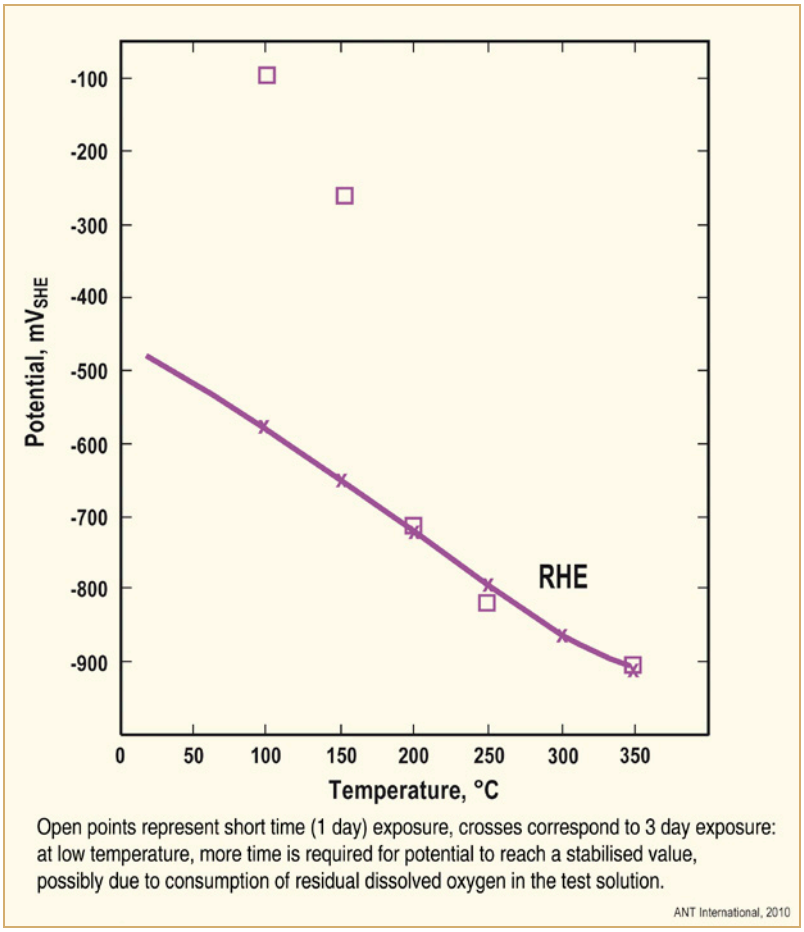

Figure 6-4: Corrosion potential of Type 304 stainless steel in lithiated, hydrogenated water compared to the Reversible Hydrogen Electrode (RHE) potential as a function of temperature, after [Szklarska-Smialowska et al, 1991].

For most PWRs, the dissolved hydrogen was specified to be in the range 25 to 50 cm^3/kg. However, there has been a recent debate to optimise this concentration with two purposes:

- To minimise the activity of the primary circuits. The effect of dissolved hydrogen on activity transport in PWR primary circuits is not completely clear but recent results tend to show that low dissolved hydrogen minimise deposition of crud on fuel rods. This seems to be the main reason why Japanese and Swedish operators favour a low hydrogen chemistry. A low concentration of dissolved hydrogen is preferred in Japan and is currently specified for French EPR [Ryckelynk et al, 2012];

- To delay stress corrosion cracking (PWSCC) of Alloy 600 and the related weld metals Alloys 182 and 82. This second goal is only relevant to old plants with Alloy 600 and its related weld metals that are susceptible to PWSCC. Lowering the dissolved hydrogen can delay crack initiation but the hydrogen concentrations necessary to obtain significant benefit are deemed too low to guarantee full suppression of water radiolysis. The present trend in US and, more recently, in France is therefore to increase dissolved hydrogen towards the top end of the present specification, which definitely slows down crack propagation rates with no significant deleterious effect on crack initiation at the highest temperatures.

More details on this debate can be found in ANT International report "PWR/VVER Primary side coolant chemistry – Volume II" [Riess & Odar, 2012].

7 Oxidation and cation release of stainless alloys in light water reactors (Pierre Combrade)

All materials of PWR primary circuits exposed to the primary coolant and all materials in the high temperature part of BWR circuit are stainless alloys (except the fuel cladding), i.e. stainless steels and nickel-base alloys. General corrosion of these materials has no impact on the integrity of these components. However, release of Ni and Co cations and oxide particles into the primary water leads to the formation in the core of ^{58}Co and ^{60}Co isotopes, which are the main sources of radioactive contamination of the primary coolant circuits. In PWRs, steam generator tubes are the major contributor to the cation release and to primary circuit activity due to their high surface area and their higher nickel content.

7.1 Oxidation in high temperature water

In high temperature water, stainless alloys are protected by thin oxide films that are significantly different from passive films formed near room temperature but have similarities with oxide films formed in hot oxidising gases. The transition between low and high temperature oxide layers occurs between 150 and 200°C. Compared to low temperature passive films, oxides grown in high temperature water are much thicker. They also have a duplex inner and outer structure but both layers are well crystallised and their composition and semiconducting properties are significantly different.

In addition, by contrast with oxidation in low temperature environments, oxidation processes in high temperature water can involve mass transport in the base metal other than diffusion of hydrogen (which also occurs in low temperature aqueous environments). This aspect of high temperature aqueous oxidation will be examined in more detail in Section 10.6.

7.2 Surface oxide films

7.2.1 Nature of oxides formed in high temperature water

In high temperature water, oxide films are generally fully dehydrated with no significant formation of hydroxides. The following oxides are usually identified on stainless alloy surfaces:

- Iron-rich spinel oxides $(Ni_xFe_{1-x})(Fe_{1-z}Cr_z)_2O_4$ with an "inverse" spinel structure: nickel ferrite $NiFe_2O_4$ and magnetite Fe_3O_4 are the limiting forms of these spinels corresponding to z= 0 and respectively x = 1 and x = 0. Depending on x, these oxides can contain up to 5 to 25% chromium.
- Chromium-rich spinel oxides (chromite type) $(Ni_xFe_{1-x})(Cr_{1-y}Fe_y)_2O_4$ with a "normal" spinel structure, which can contain up to ~30% iron.
- Chromium oxide containing some iron $(Cr_xFe_{1-x})_2O_3$ with a corundum structure.
- Nickel oxide NiO, with a rock salt crystal structure,
- Iron oxides, magnetite (see above) in low potential environments and, in high potential conditions, haematite (α-Fe_2O_3) with a corundum structure and maghemite (γ-Fe_2O_3) with an inverse spinel structure that is similar to magnetite but saturated in cation vacancies.

7.2.2 Oxide layers formed in "low potential" conditions

"Low" potential signifies potentials lower than the equilibrium potential between magnetite and haematite and are typical of PWR coolants and of BWR-HWC with NobleChem™.

Oxide films formed on stainless materials at "low" potentials exhibit a duplex structure that is summarised by Figure 7-1. Examples of oxide layers formed on Alloy 600 are shown in Figure 7-2 and Figure 7-3. Figure 7-4 summarises the main processes involved in oxide growth.

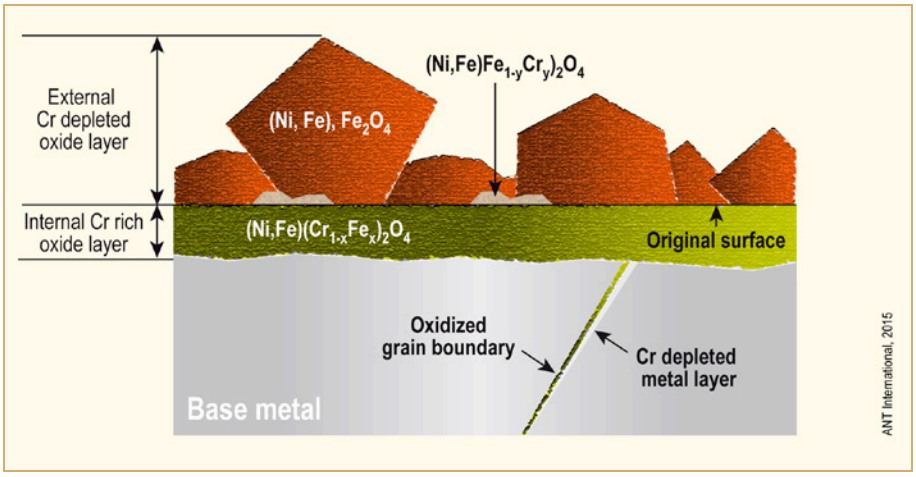

Figure 7-1: Structure of oxides formed on stainless alloys in high temperature water, at low potential.

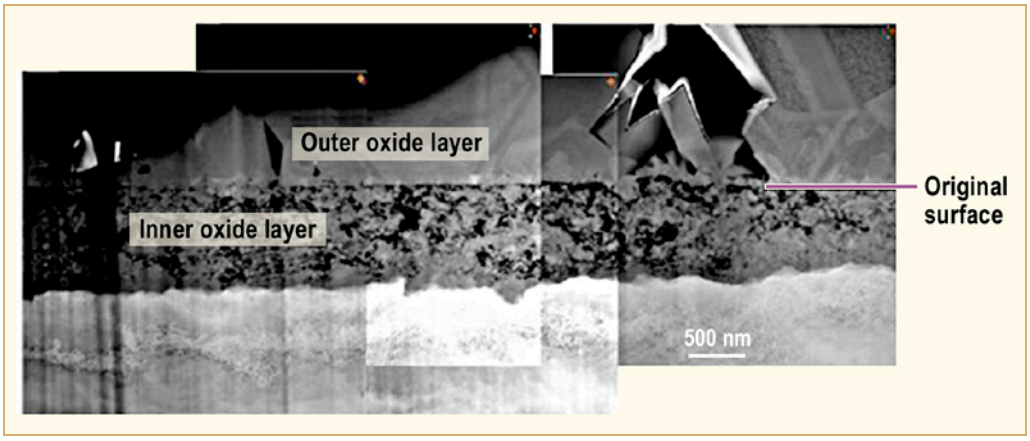

Figure 7-2: Duplex structure of the oxide layer observed by TEM on a cross-section machined by FIB of an Alloy 600 surface oxidized for 12500 h in PWR primary water at 330°C [Scott et al, 2007a] see also [Combrade et al, 2005].

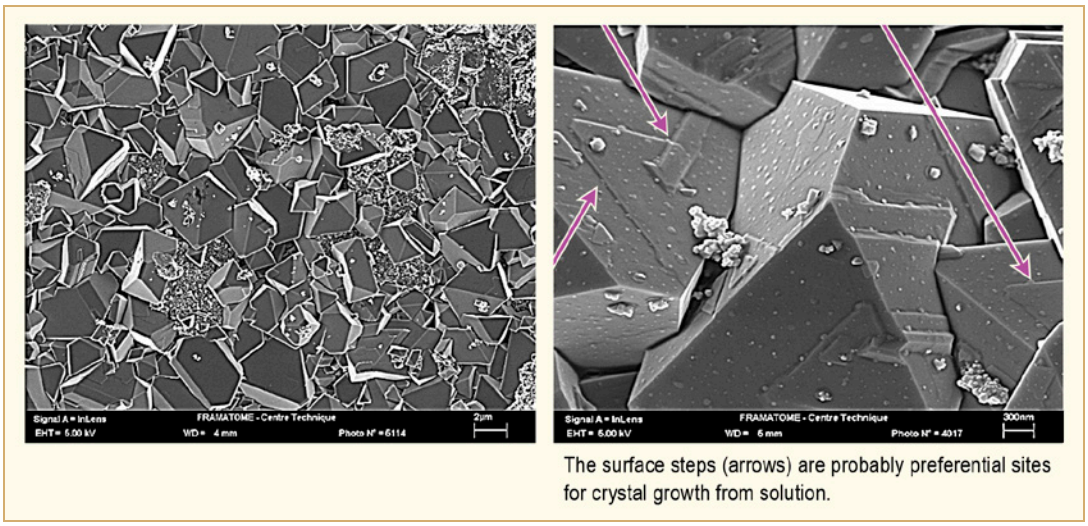

Figure 7-3: SEM observations of the outer oxide layer on an Alloy 600 surface oxidized for 34750 h (left) and 20500 h (right) in PWR primary water at 330°C [Scott et al, 2007a].

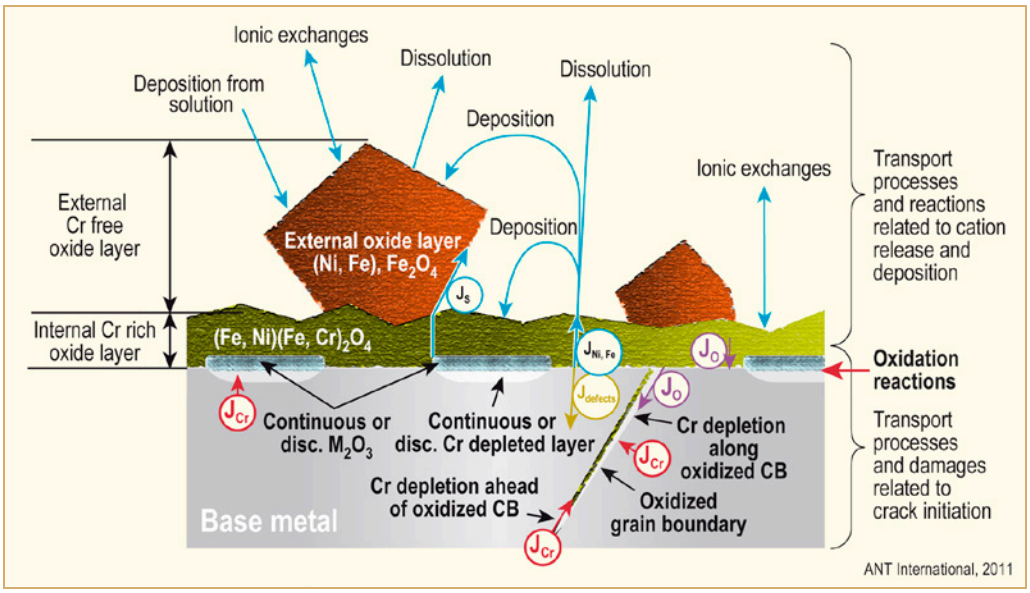

Figure 7-4: Mass transport processes involved in the oxidation of Ni-Base Alloys in de-aerated high temperature water.

- The inner oxide layer is Cr-rich and constitutes the main protective layer. It grows primarily by an anionic process, i.e. at the metal/oxide interface. It is very generally composed of spinel oxides but the presence of Cr_2O_3 (not shown in Figure 7-1) is also possible, particularly on high chromium nickel base alloys like Alloy 690. Some nickel and iron cations diffuse through this layer and are dissolved (released) into the aqueous environment at the interface between the inner oxide layer and solution. These dissolved cations that can then be precipitated on the surface (see below) or flushed away in the bulk coolant are the source term for radioactive contamination of primary coolant circuits. The thicknesses of inner oxide layers range from a few tens of nm to a few µm depending on exposure time. Increasing chromium concentration of the alloy decreases oxide layer thicknesses.

- The outer oxide layer is usually an iron rich spinel and does not contribute significantly to corrosion protection. It is composed of facetted crystallites (Figure 7-3) spread over the surface. It grows mainly by precipitation of cations either dissolved from the inner oxide layer or present in the bulk solution. On nickel base alloys, the outer oxide layer may include nickel oxide if the potential is high enough. On stainless steels, this layer is usually thicker than on nickel alloys and its composition is generally close to that of magnetite. This layer may be dissolved if the aqueous environment becomes unsaturated in Ni and Fe cations. Indeed, Hot Functional Tests (see below) during plant commissioning and plant shut down procedures include final steps aimed at dissolving this outer layer to minimise subsequent surface activity of PWR primary circuits.

- Underneath the inner oxide layer, some intergranular penetration of oxide and, in some cases, a thin Ni-rich metal layer may be formed. These points will be discussed in Section 10.6.

7.2.3 Oxide layers formed in "high potential" conditions

"High" potential signifies potentials in the range of stability of haematite (or maghemite) instead of magnetite that is characteristic of "low" potentials. "High" potentials are typical of stainless steels in BWR-NWC and, at least in some parts of the coolant circuits where hydrogen is not fully effective for removing dissolved oxygen and hydrogen peroxide in BWR-HWC conditions. Stainless steels are the main alloys exposed to these conditions in BWRs.

Two cases must be separated depending on whether or not chromium oxide can be oxidised into soluble chromate, which occurs at potentials > ~0 mV/SHE in neutral environments:

- If chromium oxides are stable, the oxide layer formed on stainless steels are quite similar to those obtained in "low" potential conditions, with the exception of the presence of haematite and/or maghemite in the outer oxide layer, which often contains two families of iron oxide crystals (Figure 7-5). On nickel-base alloys or in environments containing large concentrations of dissolved nickel, spinel oxides containing nickel may also be formed in the outer oxide layer.

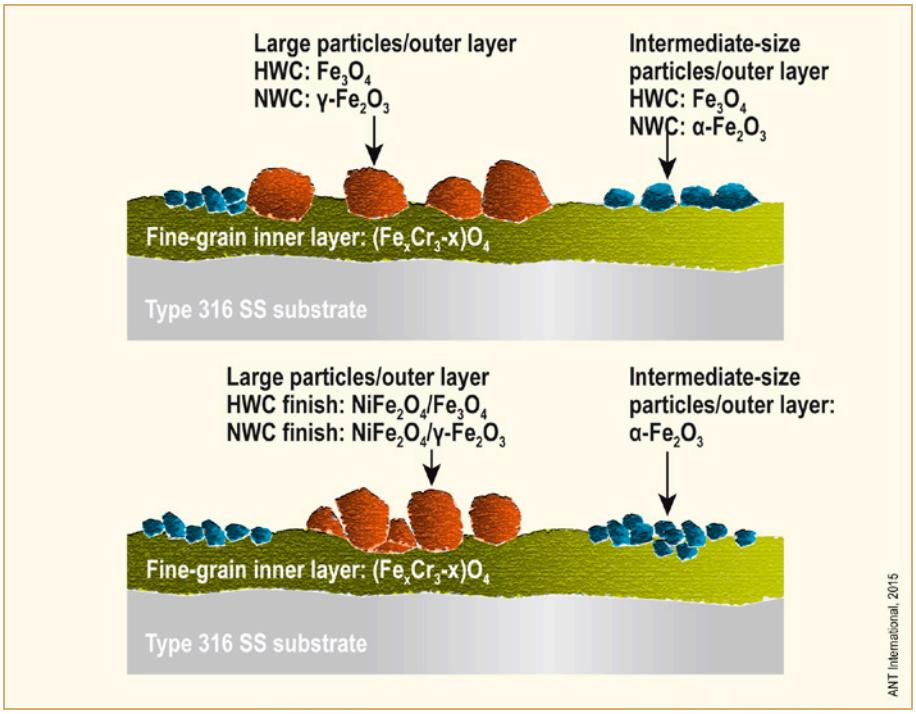

Figure 7-5: Structure of oxide films formed on Type 304 stainless steel in BWR-NWC and BWR-HWC water (top) and on alternating NWC and HWC environments (bottom), after [Kim, 1995].

- If potential is high enough for chromium to be oxidised into soluble chromate, which may occur at high flow rates in BWR-NWC water, particularly if hydrogen peroxide is present, the inner oxide layer dissolves (Figure 7-6) and its chromium content decreases as the corrosion potential increases. This situation may be considered as analogous to the transpassive condition in low temperature water (see section 4.5.2).

  On stainless steels, the outer oxide layer of haematite becomes more developed and compact and may play some protective role that becomes more and more important as the potential increases.

  On nickel alloys, the outer oxide layer is mainly composed of nickel oxide, which may not be as protective as haematite and this can lead to high corrosion rates, particularly on Alloy 690 due to its high chromium concentration.

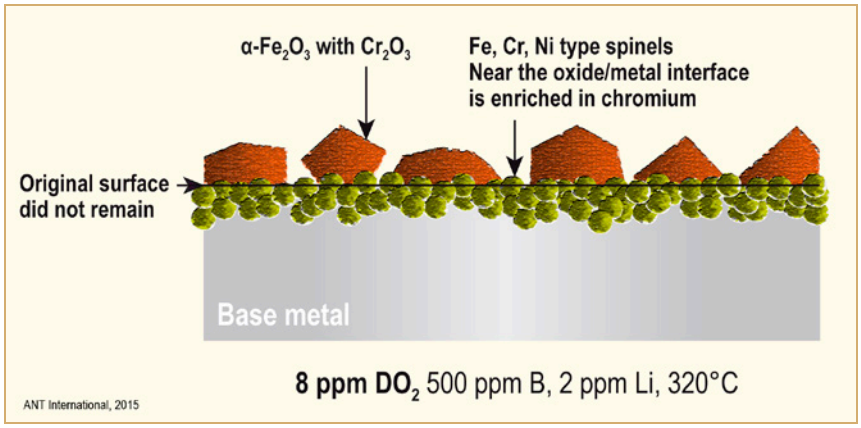

Figure 7-6: Structure of oxide films on stainless steels in "high "potential conditions leading to dissolution of chromium into chromates, after [Terachi & Arioka, 2006]. The trace of the original metal surface, which is visible on cross section of oxides grown in "low" potentials conditions (Figure 7-2), does not remain because of dissolution of the Cr-rich inner oxide layer.

7.3 Oxidation and cation release rates in PWR primary water

7.3.1 Oxidation rates

The rate laws for oxidation of stainless alloys in high temperature water are not well established and several functional forms have been proposed to describe the oxidation rates as a function of time:

- A parabolic law $e = a.t^{1/2}$ has been proposed by several authors;
- A power law $e = a.t^{b}$ where values of b range from ~0.15 to ~0.5 depending on Alloy type (600 or 690) and surface conditions;
- A combination of a parabolic law for short durations followed by an asymptotic function $e = k.(1-e^{-t/\tau})$ has been proposed for Alloy 600;
- A logarithmic function $e = e_0 + a.\ln(t+t_0)$ is strongly suggested for Alloys 600 and 690 by a recent review and re-analysis of past results [Marcus et al, 2009] and [Marcus et al, 2010] as well as recent results. A similar law has also been proposed for stainless steels.

After an initial transient due to the build-up of the inner protective oxide layer, the general corrosion rate of Ni-base alloys in PWR primary water is very low.

According to [Lister et al, 1986], corrosion rates of Alloy 600 are significantly lower than those of stainless steels. The results of short-term laboratory experiments show rates that are usually of the order of few mg/dm^2/month. Early measurements produced values of the order of ~1 to 10 mg/dm^2/month in flowing and static lithiated, hydrogenated water. [Lundgren et al, 2005] mention values of the order of 1 to 2 mg/dm^2/month for austenitic stainless steels and Ni-base alloys.

Based on this type of rate data, [Bosma et al, 2004] have fitted the curves shown in Figure 7-7 for Alloy 600 and 690 SG tubes. According to these curves, the oxidation rate of Alloy 690 is lower than that of Alloy 600 and rates of loss of thickness for both alloys should not exceed ~50 nm/year after the first few fuel cycles.

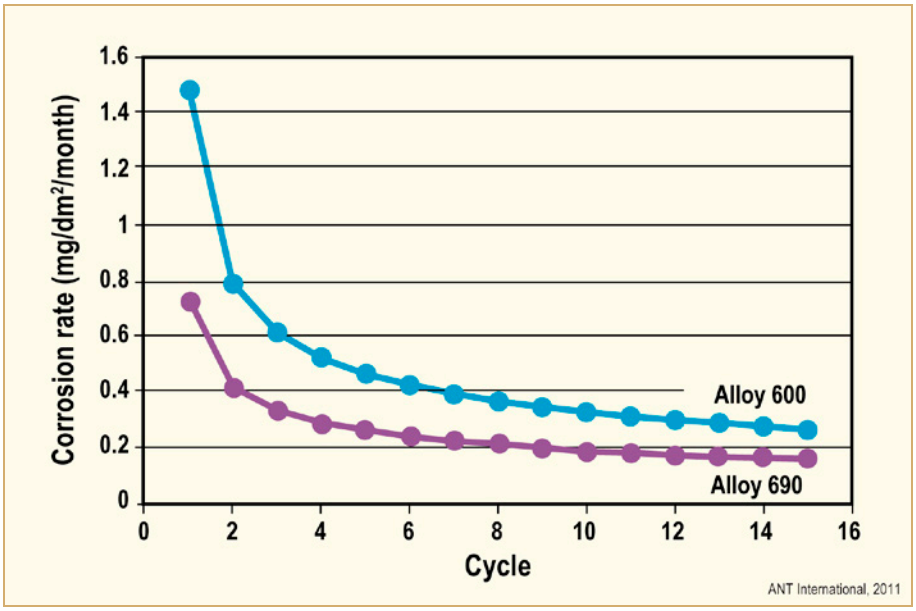

Figure 7-7: Long-term SG tubing alloy corrosion rates predicted from short term laboratory experiments, after [Bosma et al, 2004].

7.3.2 Cation release of nickel base alloys in PWR primary water

The source of cation release into the primary water environment is the flux of Ni and Fe (and Co) through the inner oxide layer (Figure 7-4). However, the actual cation release into the bulk environment also depends on the formation or dissolution of the outer oxide layer, i.e. on the hydrodynamic conditions and on the concentration of cations dissolved in the bulk environment, which may change according to the plant operating conditions. In PWRs, a key point is the relative solubility of oxides in the core and in the steam generators, which dictates the direction of cation exchanges towards the region where solubility is a minimum. Accordingly:

- very high release rates may occur under transient conditions, particularly when the temperature decreases, which may then increase oxide solubility;
- overall release may be negative (i.e. cation pick-up) when the solution is super-saturated.

Laboratory results [Lister et al, 1986] suggest that the oxidation rate is not significantly dependent on the formation of an outer oxide layer and, thus, the flux of Ni and Fe through the inner oxide layer represents the maximum possible cation release rate in steady state conditions. However, measuring cation release in laboratory tests is difficult due to the presence of the outer oxide layer. Indeed, the available laboratory results are somewhat inconsistent, even when generated in experiments with unsaturated bulk environments:

- Power laws $R = At^b$ have been proposed both for stainless steels (b ~0.44) and nickel-base alloys (b ~0.6 to 0.7 according to [Lister, 1987] but b ~0.15 to 0.4 according to [Carrette, 2002]);
- More recently, [Carrette et al, 2008] proposed a cation release law including an initial exponential decay and then a steady state constant release rate (Figure 7-8):

$$R = At + C(1- \exp(-Bt^{1/2})),$$

Figure 7-9 shows an example of the excellent fit of the experimental data to this rate law. The long term cation release rate (parameter A) increases with temperature.

The order of magnitude of the total cation release rate, expressed as an equivalent loss of thickness for Alloys 600 and 690, seems to be of the order of few tens of nm/year after long exposure times.

The following points should also be noted:

- Oxygen ingress into PWR primary water causes Cr release (if the potential allows the formation of soluble chromates and also increases the release of the other elements;
- When normalised to their concentration in the alloy, the release of Co cations is significantly higher than that of other elements, while that of Ni is much lower than that of Fe.

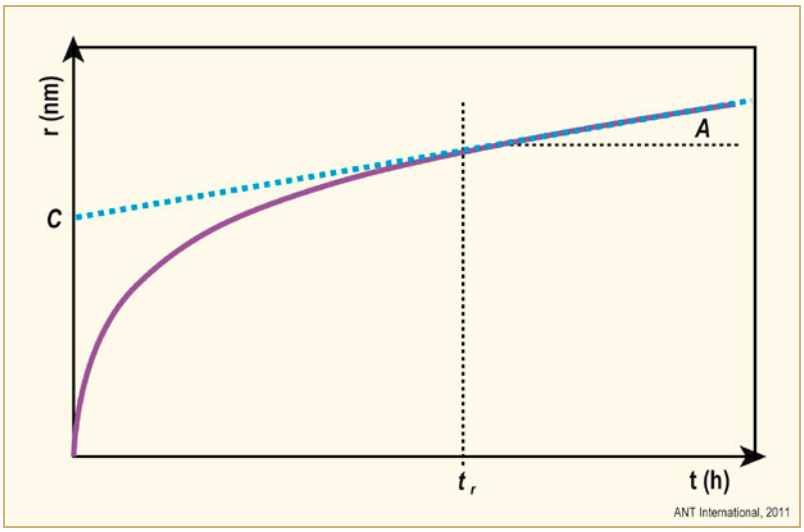

Figure 7-8: Rate law for total cation release of Alloy 690, after [Carrette et al, 2008].

8 Flow accelerated corrosion & boric acid corrosion (Peter Scott)

In contrast to the very low passive corrosion rates of structural iron and nickel base alloys used in BWRs and PWRs discussed in the preceding chapter, two mechanisms of very rapid corrosion are described here that only affect Carbon & Low Alloy Steels (C&LAS). These are Flow Accelerated Corrosion (FAC) and Boric Acid Corrosion (BAC), the latter being directly linked to leaks of PWR primary coolant onto C&LAS components. These two mechanisms of rapid corrosion of C&LAS, their consequences and mitigation actions applied in LWRs were described in a previous ANT International report [Ford & Scott, 2008] and updated in [Combrade et al, 2012] where full lists of original references may be found. A summary is presented here together with some additional key publications that have appeared more recently.

8.1 Flow accelerated corrosion (FAC)

According to the ISO standard 8044, FAC is a form of "erosion-corrosion" involving conjoint corrosion and erosion and can occur in pipes with high fluid flow velocity as well as in pumps and pipe lines carrying fluids containing abrasive particles in suspension. This is not, however, the convention usually adopted in the nuclear industry where the terminology FAC is normally used to describe enhanced dissolution of passive oxide films on C&LAS (and copper base alloys) that can occur in flowing water or wet steam under single- or two-phase flow conditions. The terminology "erosion-corrosion" is usually reserved for those circumstances where some mechanical abrasive effect contributes to the loss of surface oxide and metal and is not confined to C&LAS. Cavitation is a another category of mechanical damage to otherwise protective oxide films encountered occasionally in the nuclear industry but not necessarily confined to C&LAS, in which vapour bubbles implode on the surfaces of components such as pump impellors and can also lead to severe and rapid metal loss. Metal loss by abrasion and cavitation exhibit no particular sensitivity to the water chemistry, they obey different kinetic laws to FAC, and they exhibit a different ragged morphology of the damaged surfaces with evidence of surface cold work.

FAC is generally associated with changes in the mass-transport controlled oxidation and reduction electrochemical reaction rates occurring on an oxidized surface next to flowing water or wet steam. It is most commonly observed on carbon steel used in feedwater, extraction steam and drain lines, and on copper-based alloys used in condensers and heat exchangers. FAC is often associated with geometrical discontinuities or abrupt changes in flow direction where high turbulence is encountered. As an example, typical metal losses from carbon steels can easily be >1 mm/year for single phase flow velocities of >6 to 10 m/s at 200°C. It is possible to accelerate the corrosion rate even further due to the removal of oxide by impact of water droplets on the surface in wet steam systems or by abrasive particles such as sand in tertiary cooling water systems using river, lake or seawater.

Carbon steels in direct contact with water/steam are commonly used in the secondary and tertiary circuits of PWRs and in the feedwater systems and steam lines of BWRs. The impact of water droplets on the surface of main steam lines, upper support plates in PWR steam generators, or cross-around piping in turbines can enhance metal removal by erosion. For reasons that will become apparent, carbon steels have often been replaced by low alloy steels or even stainless steels where severe cases of FAC have occurred. Copper-base alloys have been used predominantly in condensers and for some tertiary cooling water system components such as pumps. However, the use of copper-base alloys has been widely phased out in favour of titanium alloys where seawater is used for cooling or stainless steels where river or lake water cooling is used.

The consequences of FAC (and/or erosion-corrosion) include: (a) outright failure of the component due to thinning until the system pressure or stress can no longer be supported, (b) significant contribution to the feed water iron content, (c) an increase in radiation levels in the balance-of-plant of BWRs and, (d) the fouling of flow measurement devices and ion exchange resins by released iron oxides and of PWR steam generators. Extreme examples of the consequences of FAC are the ruptures of an 18 inch diameter carbon steel condensate line on the secondary side of the Surry-2 PWR in 1986, and a 24 inch diameter carbon steel steam line between the low pressure heater and deaerator at the Mihama-3 PWR in 2004 (Figure 8-1). In both cases, FAC occurred near geometrical discontinuities such as elbows and/or orifices, which disturbed the fluid flow. Both these accidents caused fatalities.

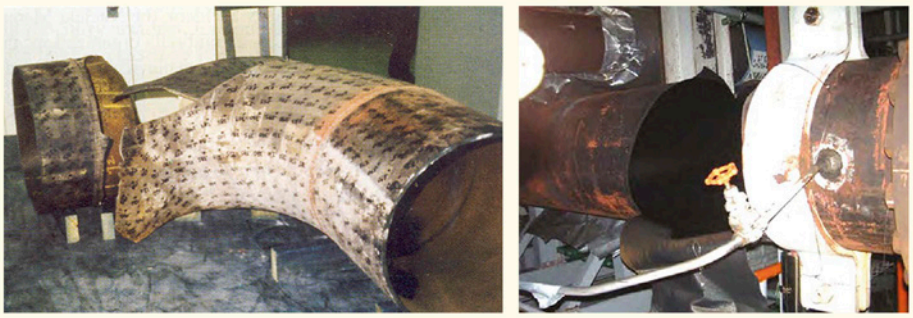

Figure 8-1: FAC related failure of the condensate line at Surry-2 in 1986 (left) [Czajkowski, 1987] and of a steam line between the low pressure heater and deaerator at Mihama-3 in 2004 (right) [NISA, 2005].

8.1.1 Phenomenology and mechanism of FAC

In LWRs, FAC of carbon steel when well-developed has two distinctly different appearances; an orange peel-like, shiny surface with shallow pits or scallops in the metal in the direction of single phase flow, and tiger striping perpendicular to the direction of two-phase flow in wet steam.

The basic mechanism by which flow increases corrosion rates of carbon steel in high temperature water is well known. In the absence of oxygen, the magnetite film on carbon steel undergoes reductive dissolution, i.e. depends on the dissolved hydrogen concentration, as follows:

Eq. 8-1: $$1/3Fe_3O_4 + (2-b)H^+ + 1/3H_2 \rightarrow Fe(OH)_b^{(2-b)+} + (4/3-b)H_2O$$

where 'b' is the number of OH^- ligands, which varies from 0 to 3 for soluble ferrous species. Increasing flow rate increases the dissolution rate of magnetite and causes thinning of the protective magnetite film and a higher corrosion rate. How flow and turbulence affects the rate of this reaction can be understood in terms of their influence on the diffusion of soluble species to and from the dissolving oxide surface. Other important variables are the solubility of magnetite as a function of temperature, corrosion potential and pH, and the quality, composition and adherence of the oxide at the metal surface. Most of the ensuing discussion on the influence of these variables concerns carbon steels unless otherwise noted.

It is generally accepted that the parameter characterising the water flow that best describes the loss of metal due to FAC is the mass transfer coefficient, on which depends the diffusion rate of soluble species across the laminar flow boundary layer between the oxidizing metal surface and the fluid. In practice, FAC in single phase flow is observed mainly where there are changes of section or flow direction provoking turbulence in the fluid, e.g. at elbows, T and Y-junctions, valves, diaphragms, orifices, and even welds. It is usual to consider the mass transfer coefficient for a straight tube and then apply a coefficient for each specific geometry. The kinetics of FAC in smooth straight tubes carrying fluids in which magnetite has a comparatively high solubility increase generally as a function of the mass transfer coefficient raised to the power 0.8. If a straight tube has a rough surface then the FAC rate is directly proportional to the mass transfer coefficient (and to the fluid velocity). Significantly higher dependencies on the mass transfer rate are possible up to the third power, for example when magnetite solubility is minimized (due to the presence of ~0.2%Cr in the substrate) and particle erosion becomes more important. These dependencies have been verified in the laboratory for single phase flow mainly in the temperature range from 150 to 250°C.

The above mass flow dependencies for single phase flow are consistent with observations for two phase flow. Empirically, it is observed that the kinetics of FAC increase very quickly when the steam quality attains 20 to 40% and is maximum between 40 and 80%.

FAC of carbon steel depends strongly on the temperature and tends to be a maximum at around 130 to 150°C, as shown in Figure 8-2. In two phase flow conditions, the maximum is typically at 180°C. The effect of temperature parallels its effect on the Schikorr reaction:

Eq. 8-2: $$3Fe(OH)_2 \rightarrow Fe_3O_4 + 2H_2O + H_2$$

which becomes progressively more efficient as the temperature increases above ~150°C and effectively counterbalances the thermal activation of the oxidation rate of iron by forming a more protective layer of magnetite at higher temperatures.

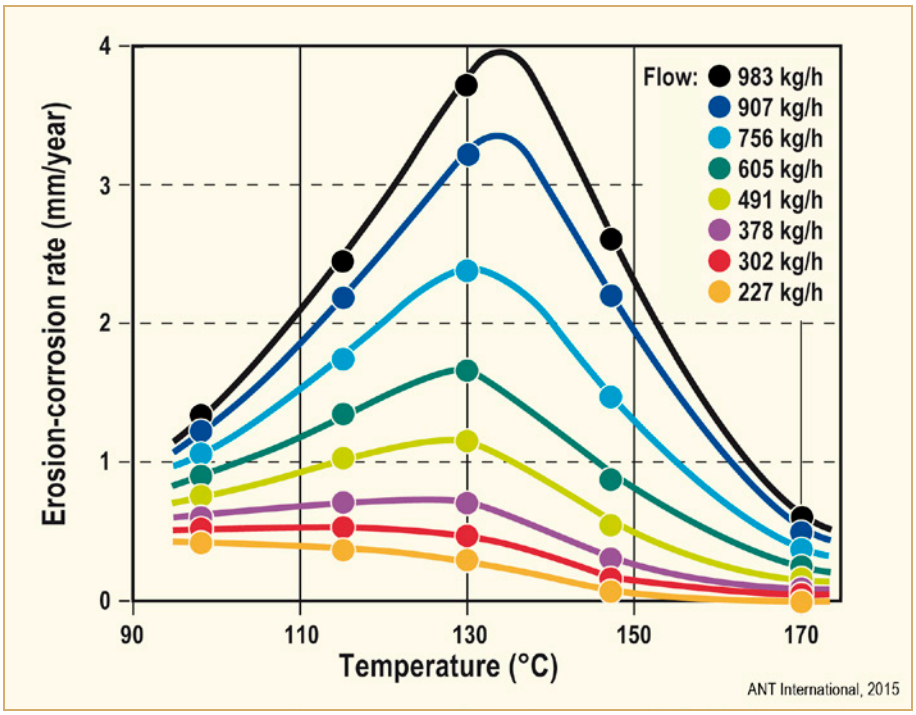

Figure 8-2: Effect of temperature on the flow accelerated corrosion rate of carbon steel in deoxygenated ammonia *AVT* water at pH 9.04, after [Bignold et al, 1981].

The influence of temperature can be more or less marked according to the pH, single or two phase flow, and fluid velocity. Although FAC rates decrease at temperatures on either side of the peak temperature, FAC is often localized because of mass transfer effects and the rates of metal loss at higher or lower temperatures may still be sufficient to result in wall thinning and piping failure in thin-walled pipes. Operating experience with PWR steam generators shows, for example, that feedwater distribution J-tubes fabricated from carbon steel can lose metal at up to 1 mm/year in single phase water at 220°C flowing at 8 to 9 m/s. Significantly more highly alloyed materials are used today to fabricate the J-tubes in replacement steam generators.

Carbon steel feedwater systems for both BWRs and PWRs are particularly at risk from FAC, and are typically inspected on a routine basis to ensure that wall thinning is monitored in vulnerable locations. In unfavourable conditions, metal loss rates up to 10 mm/year have been observed. This is of particular significance for LWR operators applying for power uprates since the extra power can be achieved by, among other things, increasing the coolant and feedwater flow rates.

Corrosion potential can have a strong effect on FAC rates since haematite (Fe_2O_3), the oxide of iron that forms at high corrosion potential, is several orders of magnitude less soluble in water than magnetite that forms at low corrosion potential. Thus, dissolved oxygen at concentrations ranging from a few ppb to a few tens of ppb, depending on the flow rate (which affects the efficiency of mass transport to and from the corroding surface), can have a dramatic effect by increasing the corrosion potential by 400 to 600mV. This has led to the practice of adding oxygen to reduce FAC rates in the feedwater systems of conventional boilers, BWRs (Figure 8-3), and more recently on an experimental basis, of a few PWR steam generators. In the latter case, all the added oxygen is consumed by hydrazine before the feedwater reaches the steam generator.

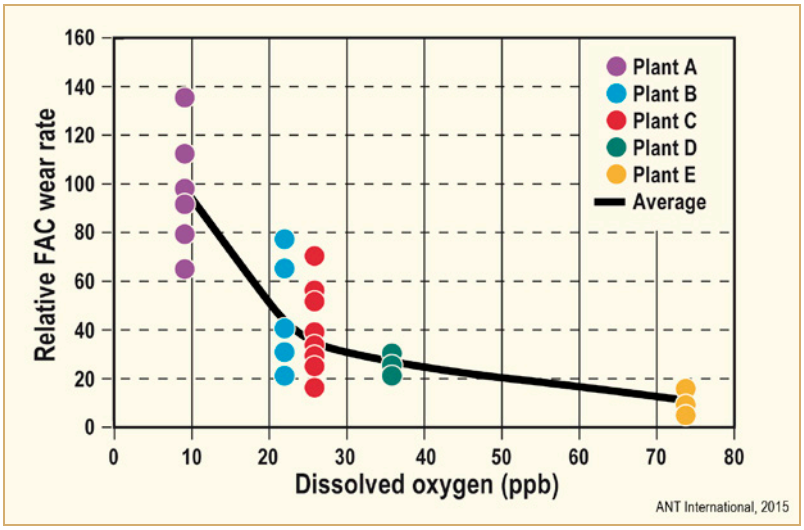

Figure 8-3: Flow-accelerated corrosion data for condensate and moisturizer separator re-heater drain systems in four *BWR* plants as a function of the local dissolved oxygen concentrations, after [Wood, 2004].

The pH of PWR secondary circuit water has a strong influence on the FAC rate in feedwater systems of PWR steam generators. For carbon steels in secondary water circuits, the pH (as measured at 25°C, the conventional temperature at which PWR secondary water pH is specified) should be between 9 and 10 to minimize general corrosion. This is usually achieved using an AVT secondary water chemistry with ammonia/hydrazine and/or organic amines such as morpholine or ethanolamine. The organic amines are stronger bases at the higher temperatures than ammonia for the same pH at 25°C and their partition coefficients between steam and water are lower than that of ammonia, which also favours a higher pH in the liquid phase of two phase mixtures of water and steam. Maintaining a $pH_{25°C} > 9.5$ at the intermediate temperatures of feedwater heaters and moisture separators has a significant beneficial effect on reducing FAC of carbon steels.

The protective quality of passive films against FAC on carbon steels can be markedly improved by certain minor alloying elements, notably chromium, but also copper and molybdenum, that would not normally be specified in a plain carbon steel. Chromium levels as low as 0.05wt% have been shown to be beneficial and levels 0.1 to 0.2wt% appear largely sufficient for avoiding the problem of FAC in single phase conditions in PWR steam generator J-tubes (Figure 8-4). Current practice is to specify chromium levels of >0.15 or 0.2wt% for the construction of PWR secondary side feedwater piping. Recognized low alloy steels such as 1¼Cr Mo or 2¼Cr Mo might, on the face of it, seem a better choice that has been widely adopted, particularly for two-phase fluids that are typically at very much higher velocity than single phase flows. However, these low alloy steels necessitate stress relief heat treatment after welding and some operators baulk at the extra cost involved. Stainless steel has also been used in secondary side feedwater piping in newer plants where susceptibility to FAC is anticipated to be most pronounced in two-phase flows.

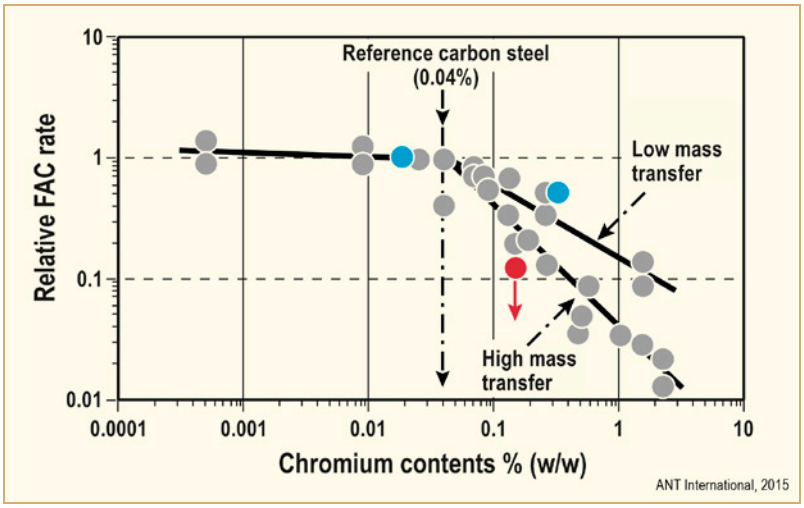

Figure 8-4: Flow-accelerated corrosion rates on carbon steel as a function of Cr-impurity content, after [Trévin et al, 2010].

FAC of copper–based alloys, and especially Cu-Zn Admiralty brass, has been a significant problem in both nuclear and fossil-powered plant. In seawater systems fabricated from Admiralty brass, fluid velocities >1 m/s can cause FAC or impingement attack problems while the cupro-nickels can be used up to about 3 m/s. In nuclear plant, the release of copper cations from the process water side of heat exchangers have been instrumental in exacerbating various corrosion modes, for example on fuel cladding in direct cycle BWRs or on the secondary side of Alloy 600 steam generators tubes in PWRs where copper deposits have been implicated in aggravating IGA/IGSCC. Consequently, this has led to the replacement of Cu-Zn, Cu-Ni or Cu-Al condenser and heat exchanger tubing with stainless steels for fresh water cooled plants or titanium tubing for seawater cooled stations.

Steam droplet impingement erosion has also occurred on the outer tube bundles of condensers where the steam inlets are located. This phenomenon has even occurred in condensers with titanium alloy tubes but can be resolved by design changes to the flow inlets and/or by using stainless steels in this area.

8.1.2 Managing FAC

Although there is extensive knowledge of the underlying principles affecting the kinetics of FAC of carbon steels, approaches have varied between different teams in attempts to formulate predictive algorithms from the purely empirical through to a detailed understanding of the effect of flow on the oxidation and reduction kinetics as a function of various thermal-hydraulic parameters.

The completely empirical approach to FAC analysis and management of inspection priorities is based on empirical relationships encapsulated in the CHECWORKS™ prediction code [EPRI, 2010]. For each of the parameters affecting the phenomenology of FAC described earlier, empirical predictive algorithms were developed. The code is widely used by LWR operators to predict the most likely areas that may experience FAC as well as the rate of metal loss in order to fix inspection priorities. CHECWORKS™ is claimed to be accurate to within a factor of 2 when compared with plant measurements, with a confidence level of 98%.

A similar empirical approach is taken in the COMSY™ code that includes flow-induced degradation mechanisms such as FAC, liquid droplet impingement corrosion and cavitation [Zander & Nopper, 2008], [Zander & Nopper, 2014]. The FAC module is based on all the known experimental and plant data on FAC. It incorporates detailed modelling of the plant geometry and thermal hydraulic characteristics and then, based on the water chemistry and material compositions, evaluates the zones at risk from FAC. For sub-systems identified as vulnerable to FAC, a detailed analysis is performed to provide life predictions for individual components. An integrated inspection management module enables inspection data to be incorporated as they become available and to optimize the inspection scope, locations and intervals.

The BRT-CICERO™ software developed by Electricite de France (EDF) is based on a physical model of ferrous ion transfer between the boundary layer in equilibrium with magnetite reduction and the ferrous ion concentration in the bulk water [Trévin et al, 2010], [Trévin et al, 2014]. The water chemistry and temperature are taken into account through the equilibrium ferrous ion concentrations in the boundary layer and in the bulk water as well as thermal hydraulic parameters. Material composition parameters affect primarily the oxide thickness and porosity in the model. Version 3 of the BRT-CICERO™ model has been extensively tested against pipe thickness measurements taken over the last 24 years on the 58 plants of the French PWR fleet. The results of a statistical analysis have shown that conservative predictions were made in 99.83% of cases leaving only 94 non-conservative predictions (in over 14000 measurements) (Figure 8-5). In some cases the predictions have a high degree of conservatism that is thought to be generally due to lack of information on the chromium content, or to significantly thicker initial pipe thicknesses than specified, or to geometry factors that were too conservative. The average deviation between the measured and calculated thickness was -1.07 mm.

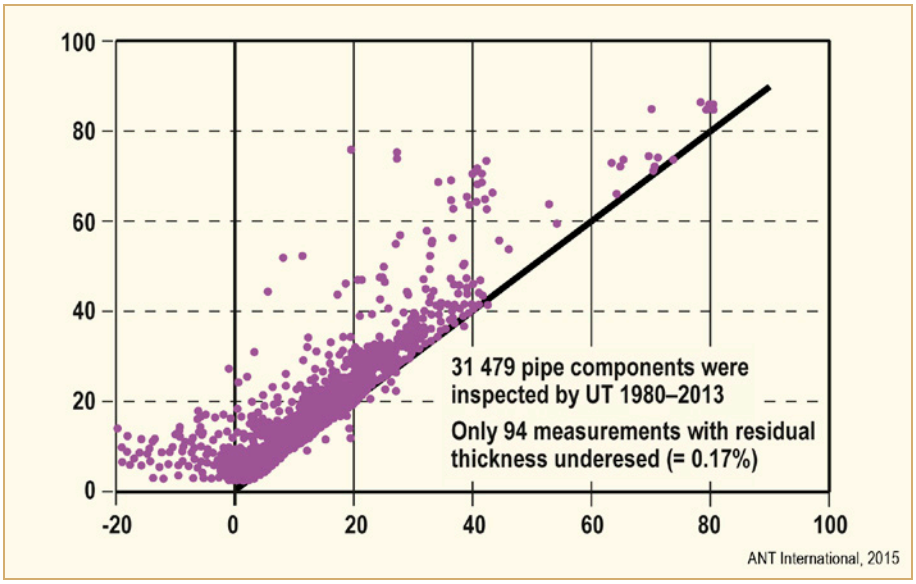

Figure 8-5: Comparison of measured and predicted FAC with BRT-CICERO™ version 3 in French PWR secondary circuits, after [Trévin et al, 2014].

Another calculation code for plant evaluations has been publicised in recent years by joint Japanese and Canadian authors developed in response to the Mihama-3 secondary circuit pipe failure in 2004 (see Figure 8-1) [Uchida et al, 2012] and to FAC encountered in Canadian PHWR carbon steel (primary side) feeder pipes [Phromwong et al, 2011], [Lister et al, 2010]. The main parametric trends in FAC of carbon steels in these two cases are seemingly correctly predicted. The code like the French BRT-CICERO™ treats diffusion of Fe^{2+} cations from the surface towards the bulk environment through a boundary layer and takes the local dissolved hydrogen concentration into account to define iron solubility. It also includes the effects of droplet impingement on particle erosion in two-phase flow as well as the beneficial effects of chromium in the metal substrate and of dissolved oxygen in the liquid phase. The code correctly predicts the non-linear dependence of FAC on mass transfer rate when erosion of oxide particles by the shear forces induced by flow dominates over iron dissolution on chromium containing carbon steels. Chromium is assumed to promote the formation of a mixed Cr-Fe protective oxide layer at the metal/oxide interface via the introduction of a "Passivation Parameter" proportional to the Cr content of the steel.

8.2 Boric acid corrosion

Operating experience of *PWR*s has shown that primary water leaks can cause serious wastage corrosion of the external surfaces of *C&LAS* components where boric acid is able to concentrate or if exposed directly to escaping steam jets. Serious metal loss has occurred where leaks were either not detected sufficiently early or were detected and unwisely left uncorrected, usually until the next planned refueling outage. Rates of corrosion up to several tens of millimeters per year over significant areas have been observed that have in some cases presented potentially serious threats to structural integrity. Major pressure vessels, particularly reactor vessel upper heads and pressurizers, some types of (non-stainless steel) primary piping, and bolted connections with leaking gaskets have all been affected.

Large pressure retaining components of the primary coolant circuits of *PWR*s, pressure vessels, steam generator shells, pressurizers, and primary piping of some *PWR* designs, are fabricated from ferritic *C&LAS* such as A533B, A508 class III and A106B. The internal surfaces of these components exposed to *PWR* primary water are clad with stainless steel in order to reduce general corrosion to a minimum. However, even where the stainless steel cladding has occasionally been damaged or deliberately removed locally to expose the underlying ferritic steel, the corrosion rate at 300°C is very low (~0.003 mm per year) in *PWR* primary water. This is because even in the presence of up to ~1% boric acid (at the beginning of a fuel cycle) the pH is adjusted by lithium hydroxide additions so that the solubility of protective oxides such as magnetite and other spinels is at a minimum and a protective oxide layer is formed. By contrast, the external surfaces of these *C&LAS* components, which are not clad because the oxidation rate in the containment atmosphere is negligible, can experience severe corrosion when exposed to leaks of primary water. The observed corrosion is usually caused by boric acid as its concentration rises due to steam flashing or evaporation at near atmospheric pressure in the containment building. Under such conditions the corrosion rate increases due to the high solubility of magnetite in acidic environments and corrosion rates up to 250 mm/year are possible.

8.2.1 Operating experience

Many cases of significant corrosion damage of the external surfaces of ferritic primary circuit components have occurred by this mechanism in *PWR*s. The most infamous case of boric acid wastage of *C&LAS* was that which was discovered at the Davis-Besse plant in early 2002. This incident gave rise to major new research initiatives designed to better understand the mechanism of attack and avoid such events in future [White et al, 2013]. The Davis-Besse plant had started power operation in 1977 and had been operating for nearly 16 Effective Full Power Years (*EFPY*) when a large rugby football (or pineapple) size cavity in the ferritic steel of the upper head was discovered between *CRDM* nozzles #3 and #11 in early 2002 (Figure 8-6). In this case, primary water had escaped through cracks caused by PWSCC in one or more of the Alloy 600 *CRDM* penetrations in the upper head, evidently over a period of several years.

9 Environmentally assisted cracking in boiling water reactors (Peter Ford)

9.1 Introduction

Environmentally Assisted Cracking (EAC) is, as discussed in Section 4.6, a materials degradation mode that encompasses a number of cracking sub-modes, namely:

- *Stress Corrosion Cracking*, (SCC). This sub-mode of cracking is associated with crack initiation and propagation in components primarily under *constant displacement or constant load* conditions.
- *Strain Induced Corrosion Cracking* (SICC) is an extension of SCC that is accelerated by the application of a rising tensile load. Such a nomenclature was initially applied to the cracking observed in carbon steel feedwater piping in BWRs in Germany, but it is now recognized as a potential phenomenon for all structures exposed to dynamic loading during, for example, reactor start up and turbine roll.
- *Corrosion Fatigue* (CF) is relevant to the effect of the environment decreasing fatigue resistance.

As will be discussed later, there is a spectrum of cracking susceptibility between the SCC, SICC and CF sub-modes of EAC in Light Water Reactor (LWR) systems in general and, as discussed in this Section, in BWRs in particular.

The degree of cracking susceptibility and morphology may change in any given alloy/environment system with, sometimes, relatively subtle changes in the combinations of material, stress and environment conditions. The interactions between these conditions are "conjoint", as was indicated in Figure 1-1 for design and operating conditions and, more specifically in Figure 9-1, for system conditions such as stress, material, water chemistry, etc.

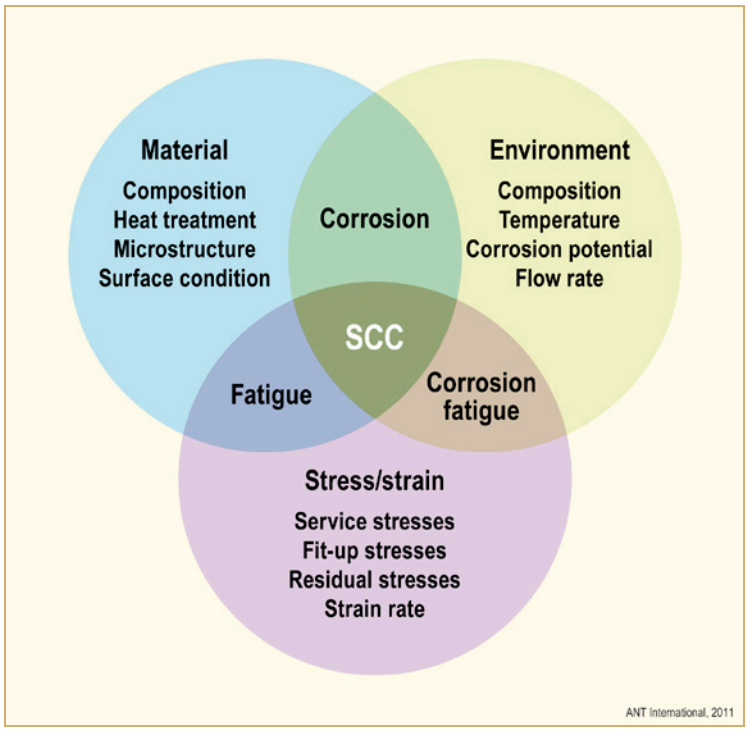

Figure 9-1: Conjoint material, stress and environment requirements for stress corrosion cracking in BWRs, after [Speidel, 1984].

Such Venn diagrams were widely used in the 1970s and early 1980s to give a *qualitative* indication of the effect of the various system parameters on EAC of structural alloys in BWRs. For instance, the influence of each of the major material, environmental and stress factors may be represented by the diameter of each circle in Figure 9-1, and the resultant area of overlap of these three circles would give some indication of their effect on the cracking susceptibility (i.e. the shaded region in Figure 9-1). The limitation of this representation became apparent with the need for a more quantitative prediction of the benefits of various mitigation actions, and the realization that the actual cracking process was a good deal more complex than depicted in Figure 9-1. For instance, system parameters such as cold work could affect two of the circles of influence (material and stress), and irradiation could affect all three circles of influence.

Consequently the qualitative understanding of cracking represented by Figure 9-1 was replaced by *quantitative* analyses of the effects of, and interactions between, all the relevant system parameters on cracking susceptibility.

9.2 Chronology of environmentally-assisted crack growth events

It is recognized that the development of EAC in ductile alloys in LWR systems can follow a sequence of four distinct periods (Figure 9-2), namely:

a) ***A precursor period*** during which specific metallurgical or environmental conditions may develop at the metal/solution interface that are conducive to subsequent crack initiation. For example, the relevant phenomenon during the precursor period may be pitting corrosion associated with breakdown of the normally protective surface oxide film, and this pitting may lead to subsequent crack initiation. Other precursor phenomena might be associated with the creation of localized environments within crevices or on heat transfer surfaces. These "precursor" periods may be very short if stresses are high or if severe water impurity transients occur during initial reactor operations. An example of such short-lived precursor periods would be the cracking of weld-sensitized Type 304 stainless steel BWR piping whose surface had been ground following welding in order to facilitate ultrasonic inspection. On the other hand, the precursor events may take years if they are associated with a change in metallurgical microstructure involving thermal aging, irradiation embrittlement, grain boundary diffusion or oxidation, or the creation of the necessary stress due to corrosion product formation and expansion.

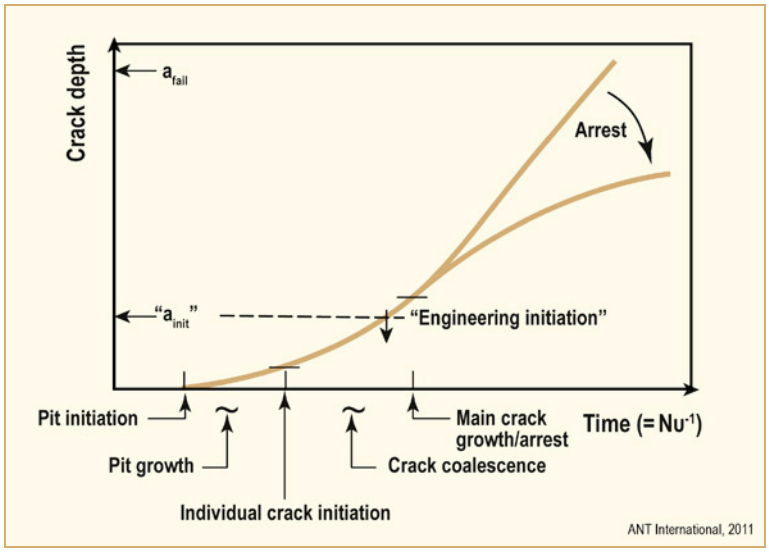

Figure 9-2: Sequence of crack initiation, coalescence and growth during sub-critical cracking in aqueous environments. Note the arbitrary definition of "Engineering Initiation", which generally coincides with the NDE resolution limit, after [Ford, 2006].

b) ***The initiation of individual cracks*** when the local environment, microstructure, stress and crack geometry conditions have reached a critical state.

   The criteria for crack initiation (and the subsequent short crack growth) have been extensively reviewed elsewhere [Hickling et al, 2005].

c) ***Growth of shallow individual cracks*** followed by their ***coalescence*** to form a "major" crack. The crack depths during this phase may be <100 μm, but ultimately will reach, during a "short crack" phase, dimensions that are detectable by either non-destructive examination techniques, or by an observable drop in stress in a strain-controlled test or component (such as a bolt), which corresponds to approximately 1-5 mm crack depth. It is at this point that, *in engineering terms*, the crack is deemed to have "initiated" (Figure 9-2).

d) ***Propagation of a single dominant crack*** at a rate that is dependent on the material, stress and environmental conditions. The growth rate is rarely constant, as is too often assumed, but may accelerate or decelerate over time depending on the stress and strain profiles, and the material and irradiation conditions.

It is apparent from this discussion that the development of a life prediction algorithm of the general form given by Eq. 1-1 must take into account all of these phenomenological factors. Such a development poses considerable challenges. For instance, there may be interactions between the various system parameters that control the various sub-modes (e.g., pitting, intergranular attack, short crack coalescence and crack propagation). Moreover, as will become apparent in the following sections, small changes in these interacting factors can significantly affect the final EAC susceptibility.

This immediately leads to the conclusion that there will be a measure of uncertainty in the life prediction capabilities, and these uncertainties can be attributed to two general sources. The first are *aleatory* uncertainties that arise out of random, stochastic events (such as pitting, intergranular attack, crack coalescence) which can occur on a smooth surface. These may dominate the onset of "engineering initiation" and the failure time of relatively thin specimens or components such as springs or thin wall tubing.

The second class of uncertainties are *epistemic* and arise out of incompleteness of the life prediction model that is adopted, the dispersion in the model inputs, and the inadequacy of the system definition or control. These epistemic uncertainties, unlike aleatory uncertainties, may be reduced by improvements in the degradation model and the control/definition of the model inputs.

With this discussion of the chronology of specific EAC phenomena as background, attention is now focused on the state of life prediction of EAC of structural alloys in BWRs, where crack depth as a function of operational time may be controlled by the system parameters schematically depicted in Figure 9-3. The discussion for a particular alloy centres on; (a) operational experience; (b) a quantitative understanding of the mechanism of EAC propagation that is sufficient to provide a *skeleton* around which a life prediction algorithm can be defined, and; (c) a qualification of the life prediction algorithm via comparison between observation and theory.

The discussion starts with stainless steels, followed by ductile and high strength nickel-base alloys and concludes with carbon and low-alloy steels.

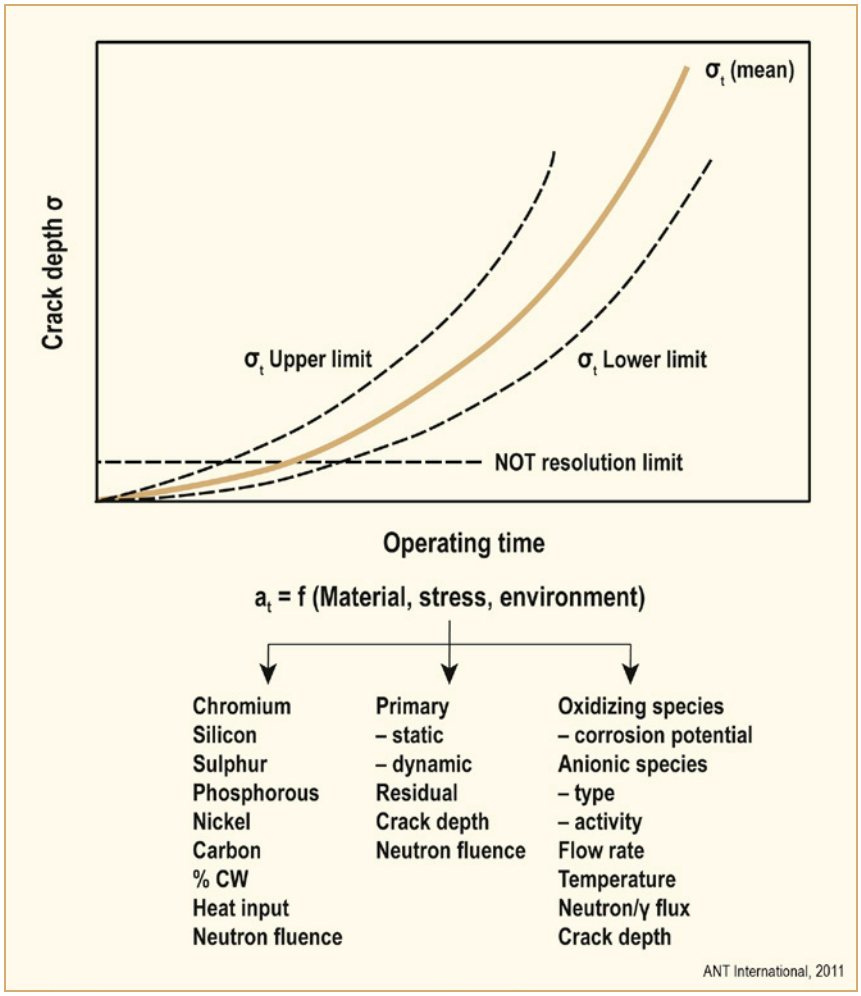

Figure 9-3: Examples of materials, stress and environmental parameters relevant to EAC of structural alloys in BWRs, after [Ford et al, 1988].

9.3 Stainless steels

A more detailed treatment of this section and a more extensive listing of references for EAC of stainless steels in BWRs is given in [Ford et al, 2010].

9.3.1 Operating experience

The earliest incidents of EAC in austenitic alloys in BWRs occurred during the late 1950's and early 1960's and were associated with cracking of Type 304 stainless steel fuel cladding where the driving forces for the cracking were: (a) the increasing tensile hoop stress in the cladding due to fuel swelling; (b) the high degree of irradiation damage to the steel, and; (c) the radiolytically-induced, highly oxidizing conditions in the water. This problem was effectively mitigated when zirconium alloys were substituted for fuel cladding.

The earliest indications of cracking in *unirradiated* austenitic stainless steels occurred in the late 1960's in components where the temperature was <100°C; this was observed primarily during storage Crack initiation was observed on the outside surfaces of the pipes and was exacerbated by: (a) chloride contamination from humid marine environments or from insulation, and; (b) dissolved oxygen (from air) in the water or condensate. These cracking incidents were effectively managed by appropriate control of the chloride contamination and by taking into account the beneficial effect of soluble silicate originating from the glass fibre insulation[29].

These early experiences with cracking of stainless steel fuel cladding and of structures exposed to chloride contamination at low temperatures were followed by cracking (Figure 9-4) in the primary coolant of: (a) sensitized stainless steels; (b) stabilized stainless steels, and; (c) irradiated stainless steels.

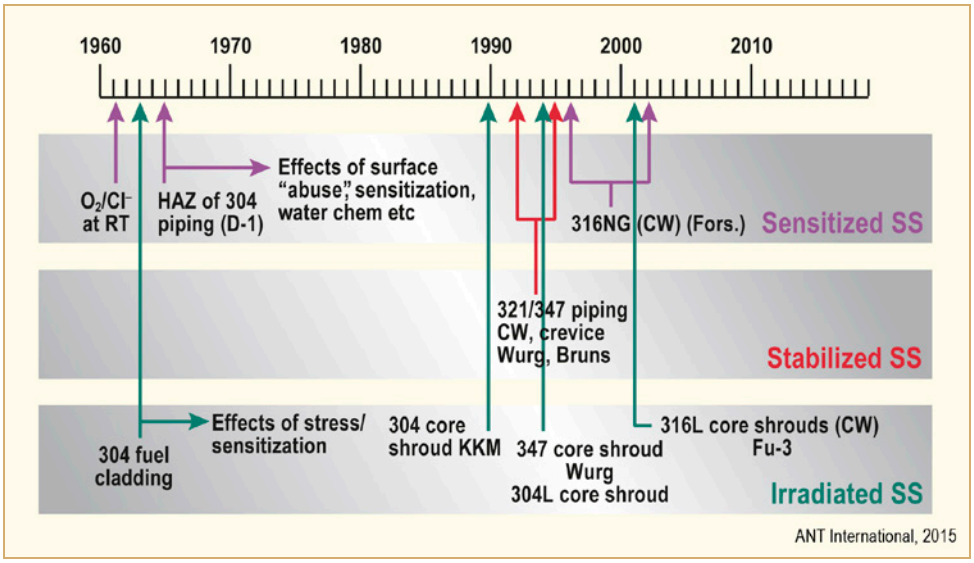

Figure 9-4: Schematic time-line indicating the periods when SCC manifested itself for sensitized stainless steels, unsensitized stainless steels, and stainless steels in irradiated core positions.

The initial EAC incidents in BWR piping (Figure 9-5) were dominated by SCC initiating on the inside surface of the pipe at a position in the heat affected zone (HAZ) relative to the weld fusion line where the steel had become sensitized (i.e. chromium depleted in the grain boundary associated with $Cr_{23}C_6$ precipitation) due to the heat/time cycles associated with welding. In addition, these zones in the HAZs were subject to high tensile residual stress due to weld pool solidification. In some cases, cracks in small diameter pipes were detected after relatively short operating times. Indeed both transgranular (TGSCC) and intergranular (IGSCC) stress corrosion cracking were detected in some cases within the first year of operation, especially in plants where there was inadequate water purity control.

[29] Note that the potential substitution of fibrous silicate insulation with mineral wool insulation (an action that would minimize the clogging of sump pump filters during a severe accident) would reintroduce the danger of chloride-induced TGSCC of stainless steel piping since the beneficial effect of silicates would be lost with the new mineral wool insulation.

Major concern arose when IGSCC was observed in late 1965 at Dresden-1 due to IGSCC in the HAZ of a 150 mm (6 in.) diameter Type 304 stainless steel recirculation bypass pipe after 68 months of plant operation.

Initially the Dresden-1 incident was regarded as an "unusual" event but its generic nature was revealed when numerous indications of IGSCC in welded Type 304 stainless steel piping were noted in late 1974 and early 1975; 64 incidents of cracking were identified during this short period. There were also numerous examples of SCC in sensitized Type 304 stainless steel components in the oxidizing BWR "normal water chemistry" (NWC) environment being accelerated by the presence of surface cold work. In these cases the cracking morphology started off as transgranular, but transitioned to the intergranular mode at greater crack depths. Such effects of cold work on SCC of sensitized Type 304 stainless steel piping was observed worldwide in the USA, Germany, Japan and Sweden.

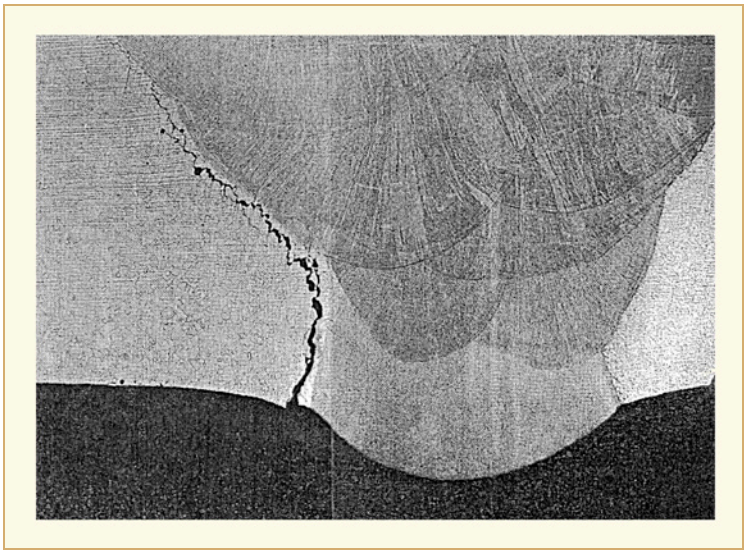

Figure 9-5: Pipe test results showing IGSCC in a 400 mm. (16 ins.) Type 304 pipe HAZ [Gordon & Gordon, 1987].

Most of these early observations were made on smaller diameter (i.e. <250 mm (10 in.)) piping. However during 1978, IGSCC was observed in a large-diameter (610 mm (24 in).) recirculating system pipe and in 1982, extensive IGSCC of 710 mm (28 in.) recirculation piping was found at Nine Mile Point-1 adjacent to the furnace-sensitized safe-end to pipe weld. Additional inspections prompted by USNRC bulletins in 1982 and 1983 for Monticello, Browns Ferry-2,Quad Cities-1, Millstone-1, Hatch-1, Brunswick-1, Oyster Creek and Duane Arnold revealed similar cracking in large-diameter piping [Hazelton & Woo, 1988]. These incidents posed considerable concern since replacement of such large diameter lines would be difficult and costly, and would require additional leak-before-break and degraded pipe behaviour analyses.

The response of the USNRC to these safety-related issues was to issue two Guidance Letters (GL) regarding pipe replacement and weld inspections in 1984. The first, GL 84-07 addressed the overall procedure for pipe replacements, and the second, GL 84-11 addressed the inspection procedures. At the same time a long- term strategy for regulating these issues was defined in the USNRC SECY 84-301 document.

The US utilities formed the BWR Owners Group (BWROG) in 1979 to focus research into repair and mitigation techniques and, following the developments in these areas, the USNRC issued further guidance in GL88-01 [USNRC, 1988] together with a detailed technical argument [Hazelton & Woo, 1988] outlining the regulatory staff position on materials, inspections, repairs and mitigation actions for austenitic stainless steel piping with diameters 100 mm (4 in.) or greater. Subsequently, in 1999, the industry, via the BWR Vessel and Internals Project (BWRVIP), submitted revisions to GL 88-01 [EPRI, 1999a], which were accepted by the NRC in 2000.

Since the late 1970s's the importance of water purity control has become increasingly apparent, especially with regard to creviced components (where the geometry and oxidizing conditions in the bulk environment could give rise to increased anionic activity in the creviced region, even though the bulk water purity was acceptable at that time). This water purity aspect was of importance not only for EAC of stainless steels but also low alloy pressure vessel steels and nickel-base alloys, and is discussed in some detail later in this Section.

These observations led to the EPRI Water Chemistry Guidelines [EPRI, 2000], [Wood, 2004] and [EPRI, 2004] in the US, and similar documents in other countries, that defined the specifications for water purity and corrosion potential.

Since the late 1970's, there have been numerous observations of intergranular cracking in Type 304 stainless steel *core components* that were highly stressed and also exposed to neutron irradiation (>1 MeV) beyond a critical fluence level ($>5 \times 10^{20}$ n/cm^2, E >1 MeV). Initially these incidents were confined to relatively easily replaced components (e.g. absorber tubes) but, more recently, Irradiation-Assisted Stress Corrosion Cracking (IASCC) has been observed in lower stressed components such as instrumentation tubes and in larger welded core structures (beginning with the core shroud in 1990 at KKM). The extent of cracking in these cases depended on the specific combinations of prior thermal-sensitization due to the initial fabrication procedure, fast neutron flux and fluence, coolant purity, weld residual stress and strain localization [Andresen & Ford, 1995], [Bruemmer, 1996], [Scott, 2003].

It became increasingly apparent that the initial hypothesis that there was a critical "threshold fluence" required for IASCC in BWRs depending on whether the component was at "high" or "low" stress was probably in error or, at least, too simplistic.

Various mitigation actions were developed as a result of these evolving problems, and these are discussed in Section 12.2.

However, there are still situations where mitigation effectiveness may be challenged, especially when there is surface cold work. For instance, although the substitution of Type 304 stainless steels with non-sensitized Type 316 L-grade and NG-grade alloys in both unirradiated and irradiated components has increased the operating time before cracking is observed, EAC incidents can still occur [Ehrnsten, 2001], These have been observed in, for example, the Type 316NG piping at Forsmark and the Type 316L core shroud at Fukashima-3, especially if (a) the component has been severely surface cold worked by grinding, straightening, etc. during manufacture, (b) there is evidence of high weld shrinkage strains, and (c) the heat treatment and/or compositional control to avoid sensitization has been inadequate. This observation has also been made for the stabilized stainless steels following the observation in 1992 of stress corrosion cracking of Type 321 piping at Wurgassen and Brunsbuttel. Since the mid-1980s an increasing number of L-grade and NG-grade stainless steel components, such as core internals, control blade sheathing and safe ends have experienced cracking [Horn et al, 1997], [Sandusky, 2007] even though high levels of water purity have been maintained.

In summary, it has become apparent that the original overview of the conjoint rings in Figure 9-1 was, perhaps, simplistic. Although the concept was correct in principle, it was incorrect to assume that cracking resistance would *always* be achieved if one of the conjoint requirements was reduced. For instance, reducing the "material susceptibility", or the "oxidizing environment conditions" are correct mitigation approaches, but they are not necessarily sufficient, since the beneficial effects of using a stabilized stainless steel and/or the adoption of water chemistry purity controls, could be counterbalanced by an increase in the detrimental conditions associated with cold work or neutron irradiation. Furthermore, it also became apparent that the adoption of "threshold" values of stress, corrosion potential, water impurity level, etc. below which "cracking would not occur" should be approached very cautiously, since these "threshold" values depend critically on the other material, stress and environment parameters.

There is no question that such past plant experience is important in developing a quantitative life prediction capability, since this data base provides "calibration points" that must be explained. For example, the methodology must be able to explain quantitatively the relative contributions of the system parameters (such as cold work, sensitization, weld repairs, etc.) to the incidents of SCC that have been observed in a given operating period. In order to accomplish such a prediction capability, it is necessary to have an event data base as exists, for instance, in the STRYK system in Sweden [Gott, 1999] and the "Generic Aging Lessons Learned" (GALL) report by the US [USNRC, 2006]. Although such data bases provide useful information for defining criteria for a risk-informed inspection strategy [Gott, 2001], they are limited in providing the necessary damage vs. time information for predictive model development. This is illustrated in Figure 9-6a and b for the case of cracking in stainless steel piping in GE BWRs, where it is apparent that the scatter in data is due to an incomplete definition of the system (Figure 9-6a); in addition the wide range of predicted "time to failure" may be associated with aleatory uncertainties (Figure 9-6b). Such factors that make it hard to define with any certainty the desired life prediction algorithm from plant experience information alone.

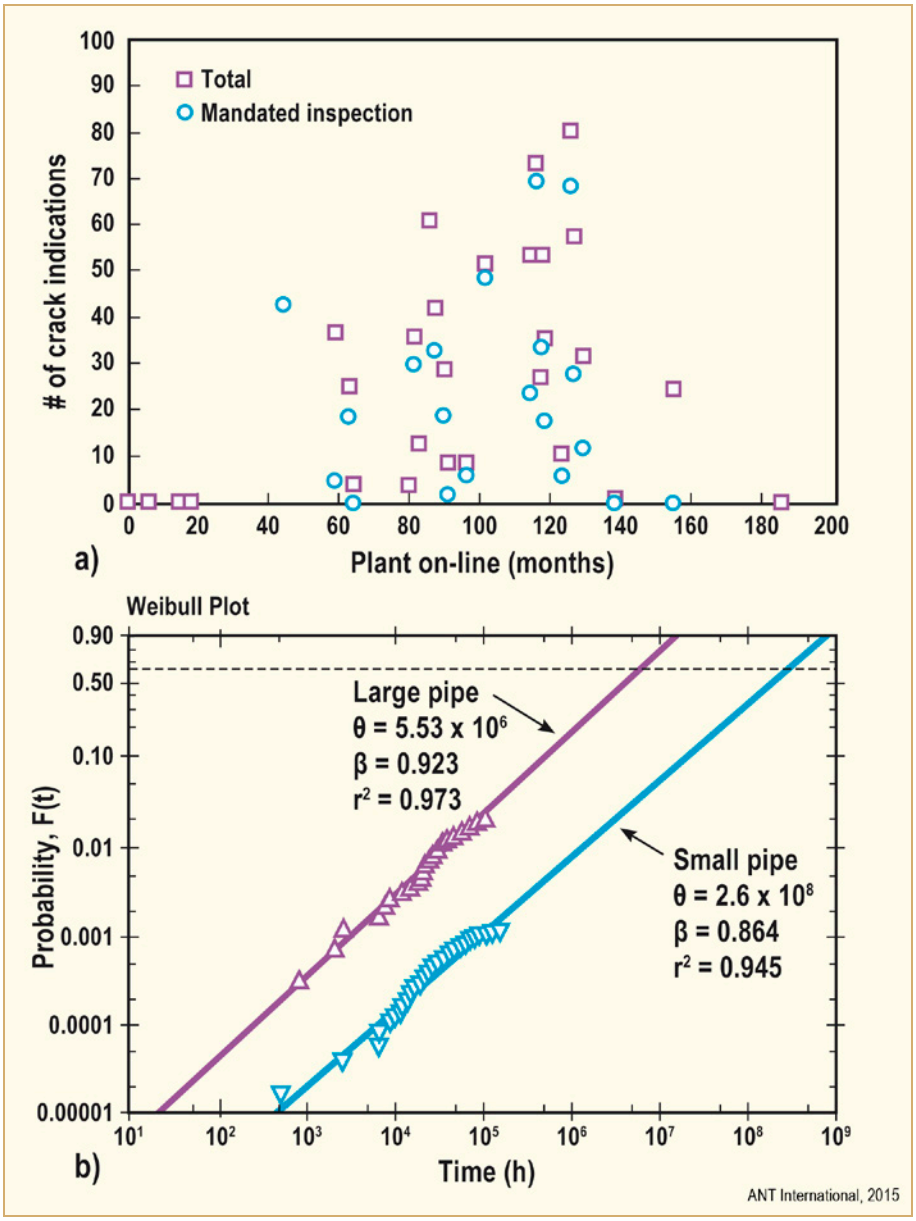

Figure 9-6: (a) Relationship between cracking incidents in BWR piping and operating time, after [Klepfer et al, 1975], (b) Probability of failure of Type 304 stainless steels in 2" and 4" diameter pipes in operating BWRs, after [Eason & Shusto, 1986].

9.3.2 The slip-oxidation mechanism of EAC propagation

As mentioned above, the reason for basing a life prediction methodology on a *mechanism* of crack *propagation* is to provide a theoretical base that might, (a) simplify the subsequent development for a multivariable life prediction system as well as well as, (b) form the basis for extrapolation outside the parametric ranges of available data (see Eq. 1-1 and Figure 9-3). Various mechanisms of crack propagation have been discussed in Section 4.6 and, in this Section, the slip-oxidation mechanism of crack propagation is chosen as the "working hypothesis" for EAC propagation of structural alloys in BWRs.

This emphasis on crack propagation was done for two reasons. First, there was an urgent need to develop justifiable propagation rate vs. stress intensity factor disposition relationships that provided an estimate of the crack advance that might occur before the next inspection. Second, from the viewpoint of predicting overall life, there was experimental evidence (Figure 9-7) that indicated that crack propagation of a single dominant crack could occur relatively quickly after loading, with "deep crack" rates being observed when the crack depth was only about 50 to 100 µm. In other words, the initial precursor, and microscopic crack initiation and coalescence periods, discussed Section 9.2 could be less significant than the propagation period in these BWR systems[30] for specific loading and environmental conditions.

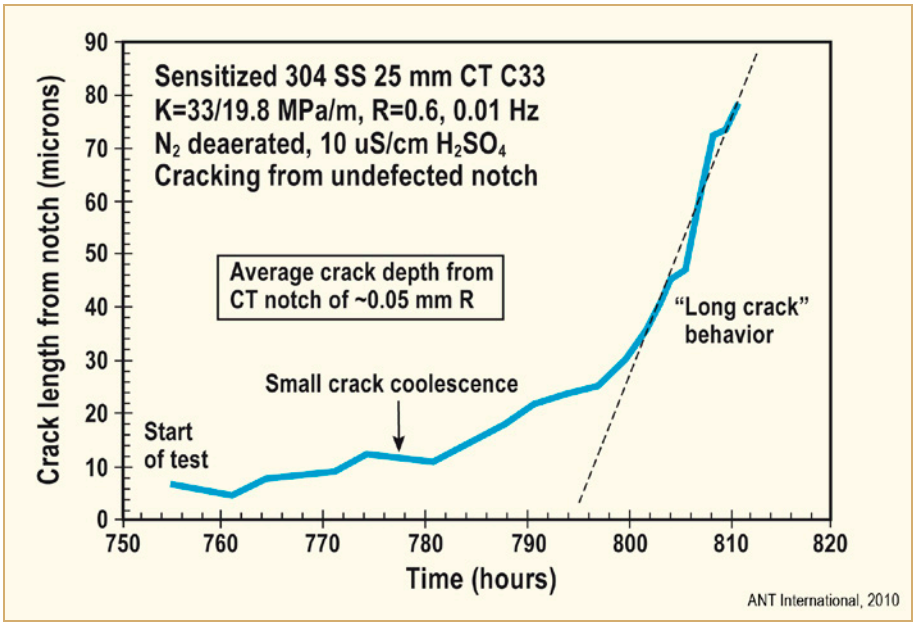

Figure 9-7: Crack depth-time relationship for intergranular cracks initiating, coalescing and propagating in a notched 1T CT specimen of sensitized stainless steel in 288°C water, after [Andresen et al, 1990].

The development of the slip –oxidation mechanism of crack propagation is briefly described below; more detailed descriptions are given elsewhere, e.g. [Ford et al, 2010].

Various crack advancement theories have been proposed to relate crack propagation to oxidation and the stress/strain conditions at the crack tip, and these assumptions have been supported by a correlation between the average oxidation current density on a straining surface and the crack propagation rate for a number of different alloy/environment systems [Parkins, 1979], [Ford, 1982a], [Ford, 1982b].

[30] Note that this statement is tempered by the fact that a crack of 50 µm depth is not resolvable by current commercial NDE techniques. For this reason, the word "microscopic" was inserted in this sentence. Obviously, if "initiation" is defined as an observable crack then the "engineering initiation time" may be considerable.

Quantitative predictions of the crack propagation rate via the slip-oxidation mechanism are based on the Faradaic relationship between the oxidation charge density on a surface and the amount of metal transformed from the metallic state to the oxidized state (e.g., MO or M^{z+}_{aq}). The change in oxidation charge density and current density with time following the rupture of a protective film at the crack tip is shown schematically in Figure 9-8a and b.

Once the protective oxide is ruptured, the crack will advance rapidly into the metal by oxidation (dissolution or solid state oxide formation) of the bare surface but will, within a matter of milliseconds, begin to slow down as the thermodynamically stable and protective oxide grows at the crack tip. Sustained crack advance depends, therefore, on maintaining a strain rate in the vicinity of the crack tip that will promote further rupture of the oxide film after a time period $[\varepsilon_f / (d\varepsilon/dt)_{ct}]$. Thus the average crack propagation rate, V, is governed, [Ford, 1988], [Ford, 1996] by the relationship:

Eq. 9-1: $$V = [MQ_f/z\rho F]\ (1/\varepsilon_f)\ (d\varepsilon/dt)_{ct}$$

If the passivation relationship, Eq. 9-2, is used:

Eq. 9-2: $$i = i_0\ [t/t_o]^{-n}$$

then Eq. 9-1 becomes:

Eq. 9-3: $$V = (M/zpF)\ (i_o t_o^{\,n}/(1-n)\ \varepsilon_f^{\,n})\ (d\varepsilon/dt)_{ct}^{\,n}$$

where:

M, p =Atomic weight and density of the crack tip metal;

F = Faraday's constant;

z = Number of electrons involved in the overall oxidation of an atom of metal;

i_o, t_o = Bare surface oxidation (dissolution) current density and its duration time;

ε_f = Fracture strain of the oxide at the crack tip;

$(d\varepsilon/dt)_{ct}$ = Crack tip strain rate;

Q_f = oxidation charge density following the rupture of the protective oxide at the crack tip.

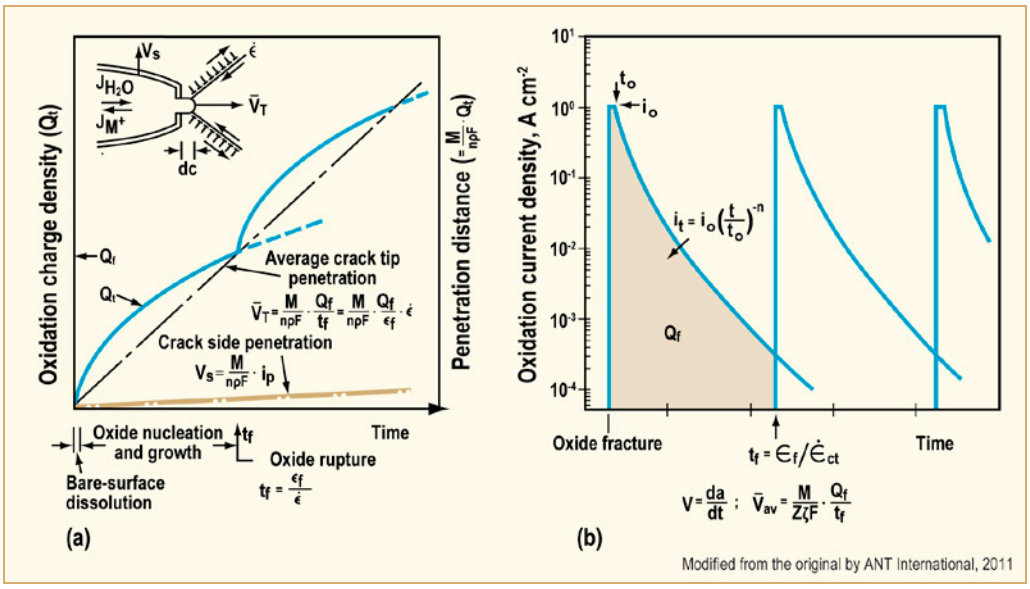

Figure 9-8: (a) Schematic oxidation charge density-time relationship for a strained crack tip and unstrained crack sides, after [Ford, 1982a] and [Ford, 1982b]. (b) Changes in oxidation current density following rupture of the oxide at a crack tip, after [Ford, 1988] and [Ford, 1996].

In order to transform the prediction algorithm (Eq. 9-3) according to the slip-oxidation model to practical usefulness, it is necessary to redefine that algorithm in terms of measurable engineering or operational parameters (Figure 9-9).

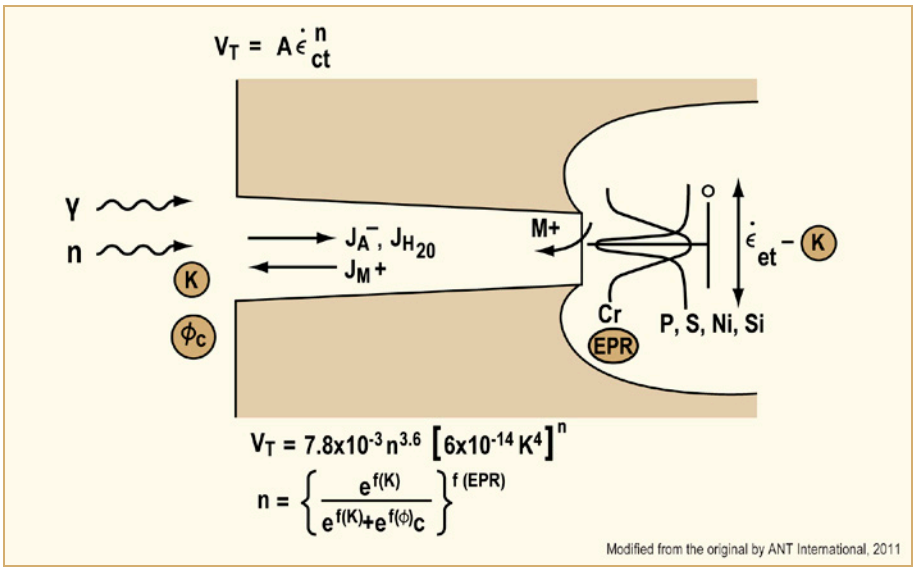

Figure 9-9: Schematic of the crack enclave and the relevant phenomena associated with the slip oxidation mechanism of crack propagation, after [Ford, 1988] and [Ford et al, 1987].

This involves:

a) Defining the crack tip alloy composition (primarily the grain boundary composition for an intergranular crack) in terms of the bulk alloy composition and fabrication heat treatment [Bruemmer, 1988]. An important parameter in this regard is the "electrochemical potential reactivation" (EPR) charge which is a non-destructive electrochemical measurement that correlates with the average chromium content at the crack tip.

b) Defining the crack tip environment in terms of the bulk anion concentration or conductivity, dissolved oxygen concentration or corrosion potential, etc.

c) Measuring the oxidation reaction rates (Figure 9-8b) for the simulated crack tip alloy/environment system.

d) Defining the crack tip strain rate in terms of continuum parameters such as stress, stress intensity factor, loading frequency, etc.

There has been extensive work conducted in these areas and, for brevity, this is not reviewed in any detail. In summary, however, the crack propagation rate for stainless steels in 288°C water is given by;

Eq. 9-4: $$V = 7.8 \times 10^{-3}\, n^{3.6}\, (d\varepsilon/dt)_{ct}^{n}$$

where da/dt is in units of cm/s.

The parameter 'n' varies between 0.33 and 1.0 (Figure 9-10) depending on the grain boundary chromium depletion (or EPR parameter), anionic impurity concentration (or conductivity), corrosion potential, and the crack tip strain rate in units of s^{-1}, as follows:

Eq. 9-5: $$n = \left\{ \frac{e^{f(\kappa)}}{e^{f(\kappa)} + e^{g(\phi_c)}} \right\}^{h(EPR)}$$

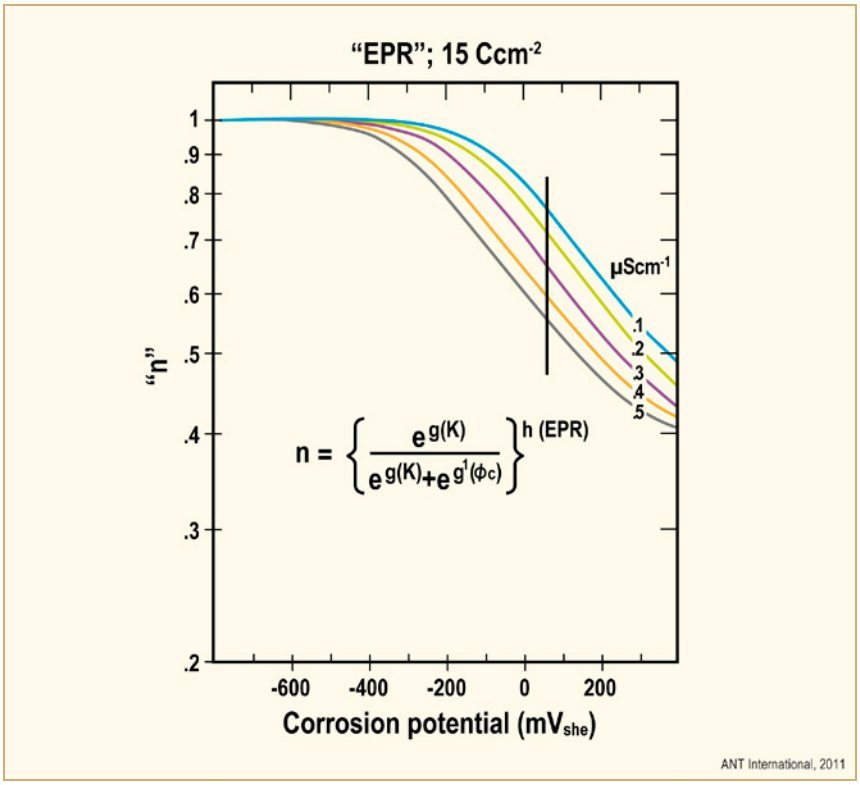

Figure 9-10: Relationships between "n" (in Eq. 9-2, Eq. 9-3 and Eq. 9-4) and the corrosion potential and bulk solution conductivity for a sensitized (EPR = 15 C/cm^2) Type 304 stainless steel in water at 288°C, after [Ford et al, 1987].

10 EAC in PWRs

10.1 Unirradiated austenitic stainless steels (Peter Scott)

Environmentally-assisted degradation of stainless steels in PWRs has been reviewed in detail in a previous ANT International publication where a detailed bibliography can be found [Ford et al, 2010] and updated in [Combrade et al, 2012]. A summary is presented here and updated as required by some key publications that have appeared since. A more recent review with a comprehensive bibliography and a discussion of perceived needs for long term guidance by the US nuclear power industry is also available in [Hosler et al, 2013].

Type 304L and 316L stainless steels (Table 3-4) are the main materials used for primary coolant piping and other components in PWRs (and BWRs). Cast Austenitic Stainless Steels (CASS) with similar compositions (designated CF-3, CF-3M and CF-8 – see Table 3-5) have also been widely used for large diameter primary piping, elbows, nozzles and valve and pump bodies in PWR primary circuits. Operating experience with respect to environmental degradation of all these low strength materials in PWRs since the mid-1960s has generally been excellent. The only major concerns that have been raised are with thermal ageing and embrittlement of some of the CASS products (see Section 3) and with the effects of irradiation on core support structures, as summarized here in Section 10.2.

SCC of low strength austenitic stainless steels has been comparatively rare in PWR primary service and when it has occurred in the absence of irradiation, in most cases the cause has been internal or external surface contamination by chlorides or out-of-specification chemistry in dead-legs or other occluded volumes. SCC involving external surface contamination or localised departures from the PWR primary water specification are summarized in Section 5. In a few cases it has been claimed that SCC may have occurred in normal quality PWR primary water but these cases concern austenitic stainless steels that have been significantly cold worked, as reviewed below.

10.1.1 Operating experience

Since the widespread problems that occurred with thermally sensitized weld HAZs of austenitic stainless steels in BWRs in the 1970's (see the preceding chapter), the normal fabrication practice has been to use low carbon grades of Types 304 and 316 stainless steels in both PWRs and BWRs. An alternative adopted in some countries has been to use niobium or titanium stabilized grades such as, respectively, Type 347 or Type 321, where the carbon is trapped as stable niobium or titanium carbides, which are very resistant to sensitization. Nevertheless, there is little doubt that in many older PWRs sensitized Type 304 and 316 stainless steels exist but practical experience shows that de-oxygenated, hydrogenated PWR primary water does not cause SCC, in contrast to BWR experience with oxygenated NWC coolant. The reason is clearly related to the presence of dissolved hydrogen in PWR primary circuits, which ensures that corrosion potentials are close to the hydrogen/water redox potential and well below the desired protection potential identified for thermally sensitized stainless steels in BWRs with HWC. The exceptions in PWRs primarily concern certain dead legs where air bubbles may be trapped during refuelling, as described in Section 5.

A comprehensive analysis of PWR operating experience of SCC in austenitic stainless steels has identified 137 confirmed cases, as shown in Figure 10-1 classified by plant age and whether or not there was any known departure from normal PWR primary water chemistry. The data in Figure 10-1 show that the total number of events is remarkably low given the size and age of the PWR fleet and that the frequency does not increase with time, which suggests that these events are not related to plant ageing. Moreover, 83% of the recorded SCC events were due to identifiable localised perturbations to primary water chemistry in occluded volumes while the remaining 17% appeared to show that intergranular or mixed intergranular/transgranular stress corrosion cracking (IGSCC/TGSCC) had occurred without any obvious departure from PWR primary water specifications. There also appeared to be a clear association between the incidence of cracking and hardness >300 HV but sensitization was clearly not a risk factor.

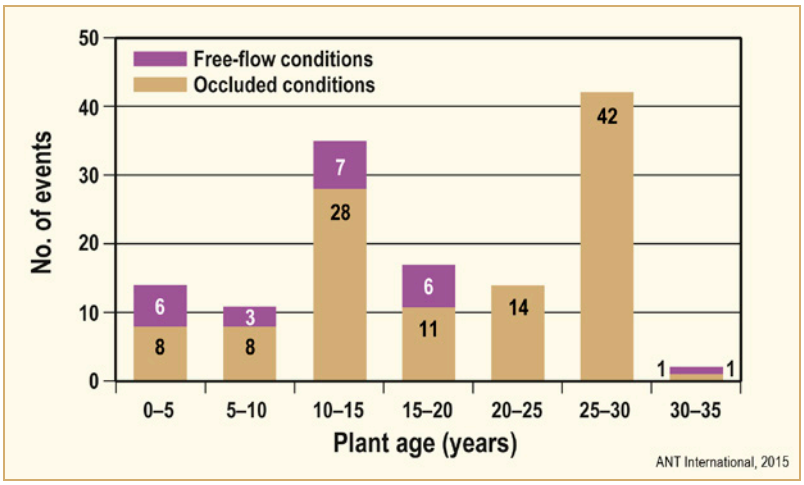

Figure 10-1: Summary of SCC of Austenitic SSs in PWR Primary Circuits, after [Ilevbare et al, 2010].

Concerning the 17% of SCC events that were concluded to have occurred in normal specification PWR primary water, there has been an unfortunate tendency in some of the published literature on this topic to call the cracking "PWSCC" that hitherto was a term used in the context of the generic IGSCC observed in Alloy 600 and similar nickel base alloys in PWR primary circuits. Given that there is no evidence of an aging related issue for austenitic stainless steels in obvious contrast to PWSCC of Alloy 600 and similar materials, and that the apparent trend with hardness indicates a specific issue related to localised cold work, use of the "PWSCC" label seems particularly inappropriate. Moreover, it should be noted that particularly in locations like the pressurizer, there has to be some doubt that the normal PWR primary water chemistry can be maintained at all times, particularly during power transients.

On the other hand, there are some SCC events in austenitic stainless steels that have indisputably occurred in flowing, normal quality, PWR primary water under some, albeit rare, circumstances. This is illustrated most convincingly by the discovery of shallow (2 mm deep), circumferential, intergranular cracking in the HAZ of a Type 316 safe end of a dissimilar metal weld between a (replacement) steam generator and the primary water inlet piping at Mihama 2 (during an intervention whose primary purpose was to apply a remedial surface treatment to the nickel-based Alloy 132 weld); see Figure 10-2. Circumferential cracking was also subsequently confirmed in the other weld HAZ of the safe end to primary piping connection. Additionally, very high surface hardness values due to grinding up to 450 HV were detected in the weld HAZs at both ends of the Type 316 safe end that reduced to between 200 and 300 HV in the bulk material at ~0.2 mm below the surface (still well above the hardness expected for wrought Type 316 stainless steel).

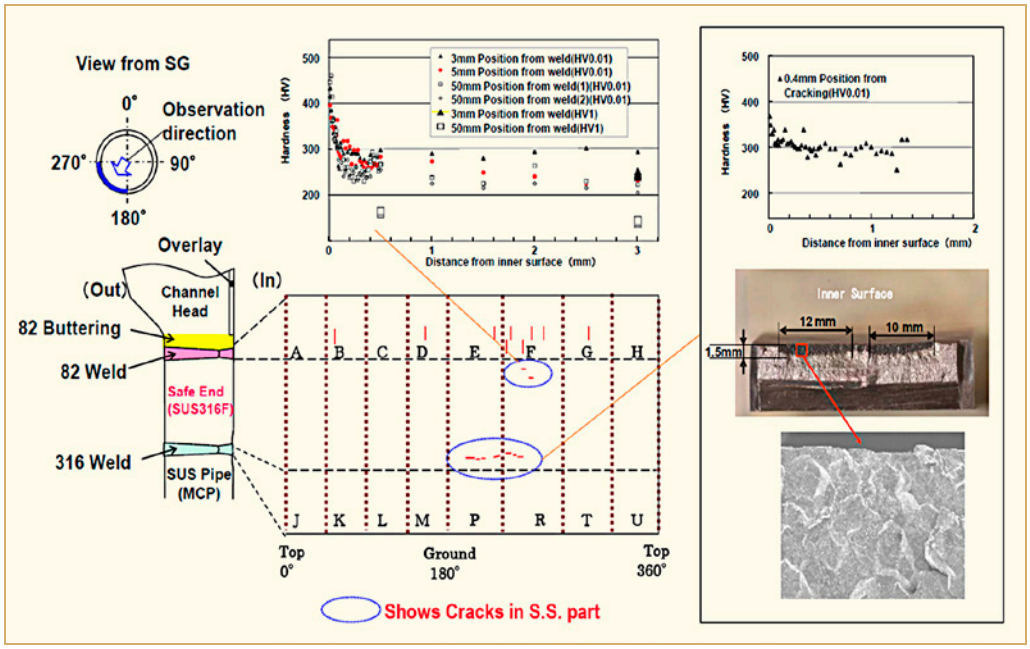

Figure 10-2: Steam generator hot leg safe end cracking at Mihama 2, after [Shoji et al, 2010].

Despite a growing body of experimental data summarized in the next Section 10.1.2 that clearly shows that austenitic stainless steels can crack in normal quality PWR primary water if they are sufficiently cold worked, the analysis of operating experience in relation to the 17% of events in normal PWR primary water omits, in the opinion of this author, some key information that points to other important parameters playing important roles, particularly in crack initiation.

Firstly, deliberately strain hardened austenitic stainless steels, mainly Type 316 and to a lesser extent niobium stabilized Type 347, have been used for many decades in PWRs for bolting and other purposes where moderate strength is required, and without apparent problems except when highly irradiated (see Section 10.2). However, a limit is imposed on the maximum yield strength of such deliberately strain hardened components of 90 ksi (or 625 MPa) [USNRC, 1999], which in practical terms for unstabilized austenitic steels with medium carbon content, corresponds to an upper limit on cold work of ~20% or a hardness of ~300 HV.

Secondly, there are other possibilities for coming into contact with out-of-specification primary water chemistry. For example, in heater/support plate crevices in pressurizers the occluded aqueous environment can become strongly alkaline at very low boric acid concentrations at the end of a fuel cycle and particularly during cycle stretch-out. Both pressurizers and CVCS heat exchangers are also vulnerable to air-saturated make-up water ingress due to a growing practice not to de-aerate the make-up water tanks of PWRs as the original vendors intended. This modification to operating practice now affects about half the operating PWR fleet and it is this make-up water that flows through the CVCS heat exchangers to a spray nozzle in the pressurizer (as well as to the shaft seals of the main circulating pumps and the CVCS nozzle in the primary circuit cold leg). Given the history of SCC of cold worked stainless steels in BWRs (see Section 9), this seems a likely contribution to SCC initiation.

A recent analysis of IGSCC affecting some Type 316Ti barrel bolts in KWU designed PWRs lends some support to the importance of local, transient oxidizing conditions in PWR primary circuits [Devrient et al, 2013], [Kilian et al, 2014]. The bolts were manufactured from cold worked Type 316 Ti austenitic stainless steel with a yield strength between 630 and 700 MPa, equivalent in this case to cold work of ~15%. The neutron dose to the barrel bolts with a star bolt design was well below the threshold for IASCC reported in literature. Maps of the bolt failures showed that they depended on their specific position in the core barrel according to their former level and to their angular position relative to the inlet nozzles. Cracking occurred where the local flow velocity in the downcomer between the core barrel and reactor pressure vessel was low. Analysis of oxide scales from barrel bolts after ~20 years of operation showed that the composition through the oxide thickness depended on bolt location and revealed the presence of localised, nominally oxidizing conditions during operation. Radiolysis calculations suggested inadequate access of hydrogen to the bolt shanks to suppress radiolysis and that fluid renewal rates at the bolt heads were very dependent on downcomer fluid velocity so that full suppression of radiolysis was difficult in some low flow locations, especially during plant start-up. It was concluded that localized oxidizing conditions combined with the cold work of the star bolts was responsible for the observed IGSCC. Dynamic loading was also suspected to play a role that may have its origin in periodic power transients associated with load following for the electrical distribution grid.

10.1.2 Laboratory tests

Interest in laboratory studies of SCC of cold worked austenitic stainless steels in PWR primary water has arisen mainly since 2000, firstly as a potential analogue of irradiated stainless steels without the testing problems associated with highly neutron activated materials, and secondly in direct support for the in-service incidents described in the previous sub-section. In addition, by analogy with BWR experience of IGSCC adjacent to the fusion lines of austenitic stainless steel welds due to strain hardening in non-sensitized HAZs (see Section 9), there are concerns that longer term problems could similarly arise in PWRs. Four main testing approaches have been used: the SSRT, also often called the CERT, constant load tests on notched tensile specimens, constant strain tests using a variety of classical fixed deformation SCC test specimens, and crack propagation rate measurements on fatigue pre-cracked fracture mechanics specimens. It has to be said that the SSRT does not seem to be well adapted to this problem because plastic strain introduced during testing will obviously change the amount of cold work in the material. Thus, only interrupted SSRTs, where the additional cold work introduced during the SSRT is small relative to the starting cold work condition, are likely to be very informative with regard to the dependence of the observables on prior cold work.

Many SSRT studies have shown that prior cold work of Type 304L or 316L stainless steels does lead to susceptibility to mixed IGSCC plus TGSCC in simulated PWR primary water. Susceptibility to SCC increases with increasing prior deformation ratio in tests usually conducted at strain rates around 10^{-7} s^{-1} on tensile specimens with prior cold work in the range 20 to 60%. The SSRT straining is usually in the same direction as the prior cold work and test temperatures are typically 340 to 360°C.

A variation on the SSRT test method, which seems particularly favourable for promoting IGSCC, is to use the so-called 'hump' specimen where a V-shape deformation is introduced into the gauge length of the specimen prior to the SSRT. In this case, the cold work condition in the hump is particularly high and complex. The effects of environmental chemistry of PWR water have been studied by SSRT using hump tensile specimens of Type 316 stainless steel revealing a small but monotonic increase in SCC susceptibility as a function of hydrogen concentration in the normal range for PWR primary water at 320°C. However, increasing boric acid was observed (surprisingly) to strongly suppress SCC susceptibility. An activation energy of ~90 kJ/mole was also measured in this work, while deliberately heat treating the material to form grain boundary carbides (i.e. sensitization) was observed to have a favourable influence on SCC susceptibility. The latter result was deduced to indicate that grain boundary sliding was involved in the mechanism and was seemingly supported by creep tests in air at 440 to 560°C.

Some considerable effort using the SSRT, constant strain and constant load testing has been put into studying the effect of different methods of introducing cold work into austenitic stainless steels. Cold working by shot peening, rolling, fatigue, pre-shearing, milling and tensile deformation have been studied and work has also been undertaken to elucidate the influence of the so-called 'strain path'. Two pre-conditions are necessary for SCC to initiate and propagate in Type 304L or 316L stainless steels in simulated PWR primary water (at 320 or 360°C); hardness >300 to 310 HV (i.e. an equivalent stress of ~700 MPa in L-grade materials) and dynamic straining. However, no significant creep occurs at 360°C (i.e. $<3 \times 10^{-12}$ s^{-1} for true stresses between 200 and 400 MPa). It is interesting to note that the hardness threshold observed by SSRT (~300 HV) is significantly lower than that deduced from in-service behaviour of high strength stainless steels (~350 HV) described here in Section 10.5. At hardness values >350 HV, hydrogen embrittlement susceptibility cannot be excluded, particularly at intermediate temperatures around 100 to 150°C.

Regarding the influence of strain path, plane tensile specimens have been tested either monotonically, i.e. in the same direction as the pre-straining, in the reverse direction to the pre-straining, and at right angles to the pre-straining. IGSCC is clearly favoured by the more complex strain paths such that the completely reversed strain path is the most severe. It is believed that oxidation is enhanced along pathways where strain is localized and, together with enhanced stress concentration ahead of crack tips due to strain hardening, enables cracks to grow by sequential brittle fracture of oxide penetrations ahead of the crack tip.

At literally constant load or strain, crack initiation leading to sustained propagation even in severely cold worked austenitic stainless steels (with hardness up to 450 HV) has proved to be very difficult despite small transgranular initiations up to 20 μm deep in notched tensile specimens, even after 17000 hours at 360°C [Raquet et al, 2005]. More recent testing has confirmed the difficulty in initiating and propagating cracks in heavily cold worked austenitic stainless steels at constant load or strain without either superimposed slow cyclic, high R, trapezoidal loading [Huguenin et al, 2013] or using the pressed hump geometry developed earlier for the SSRT and introduced into constant strain U-bends [Yonezawa et al, 2013], [Yonezawa et al, 2014]. With superimposed trapezoidal loading, the initiation time in notched tensile specimens depended on the ratio (stress/yield stress)$^{11.5}$ and the critical depth for sustained propagation was between 10 and 50 μm. In the second case, the hump shape was pressed into 15 to 30% cold rolled strips prior to forming U-bends and the resulting straining was so severe that ductile tears were observed, from which IGSCC initiated. In less severely stressed specimens no tearing and no cracking were observed. The authors concluded that the conditions for crack initiation were so extreme that it seemed unlikely that there was any generic issue for PWRs.

If the above results for constant load or strain testing in PWR primary water are compared to tests in oxygenated BWR NWC, IGSCC is easily reproduced in crevice bent beam specimens of cold worked austenitic stainless steels with a threshold hardness of ~270 HV for Type 304 and ~300 HV for Type 316L austenitic stainless steels (Figure 10-3). It is deduced therefore that structurally significant crack initiation is very difficult without exposure to oxygenated water and/or dynamic straining.

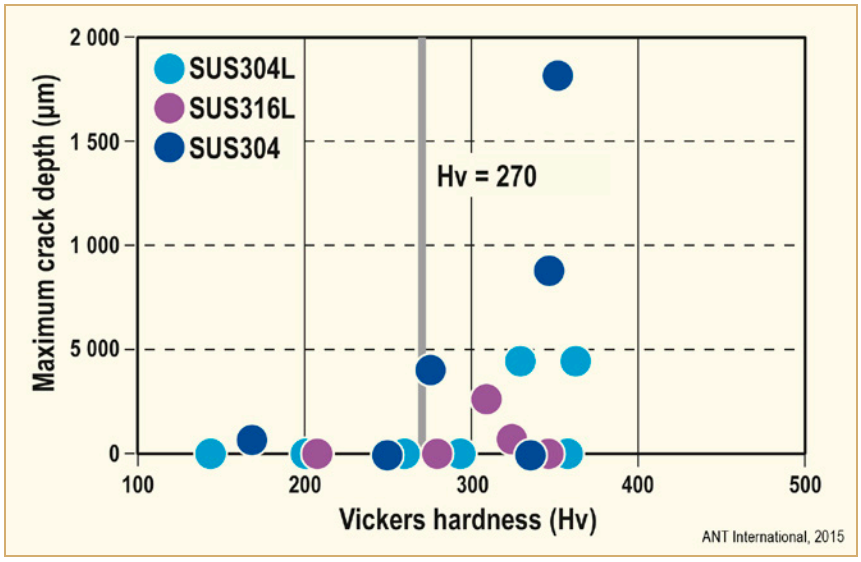

Figure 10-3: SCC of cold worked austenitic stainless steels as a function of hardness in BWR NWC at 288°C, after [Tsubota et al, 1995].

Another pertinent study of IGSCC of austenitic Type 304L and 316L stainless steels, this time in the thermally sensitized condition, was conducted in aerated pure water and boric acid solutions between 75 and 240°C representing the Safety Injection systems of PWRs [Tsuruta & Okamoto, 1992]. No cracking occurred at test temperatures of 150°C and below after exposure periods of 600 hours. The threshold stress for cracking coincided, as is often the case, with the yield point of the materials of ~200 MPa when tested in an un-creviced condition. However, no obvious stress threshold was observed when tested in a creviced condition. This is consistent with the conventional view of the effect of crevices where an aggressive, acidic, chemical environment containing impurity anions builds up in the crevice due to the action of an oxygen concentration cell between the exterior surface and the interior of the crevice. This aggressive crevice environment would also allow pitting to occur with consequent local concentration of stress, which could explain the failure to observe any applied stress threshold. Multiple specimen tests at ~350 MPa and 240°C revealed a distribution of cracking times that fitted a lognormal distribution, as shown in Figure 10-4. An interesting feature of these distributions is that there is clearly an offset for the start of the distribution on the time axis that corresponds to ~30 hours in aerated pure water and to ~80 hours in boric acid solution. These time offsets can be interpreted as incubation times for crack initiation during which oxide films stabilise and localised oxidation occurs prior to crack initiation. The longer incubation time in boric acid solution compared to pure water is consistent with the buffering effect of boric acid in high temperature water that reduces the aggressiveness of the crack tip environment. It will be seen that these crack incubation times are consistent with similar transients in cracking response observed during crack propagation testing, as summarized below.

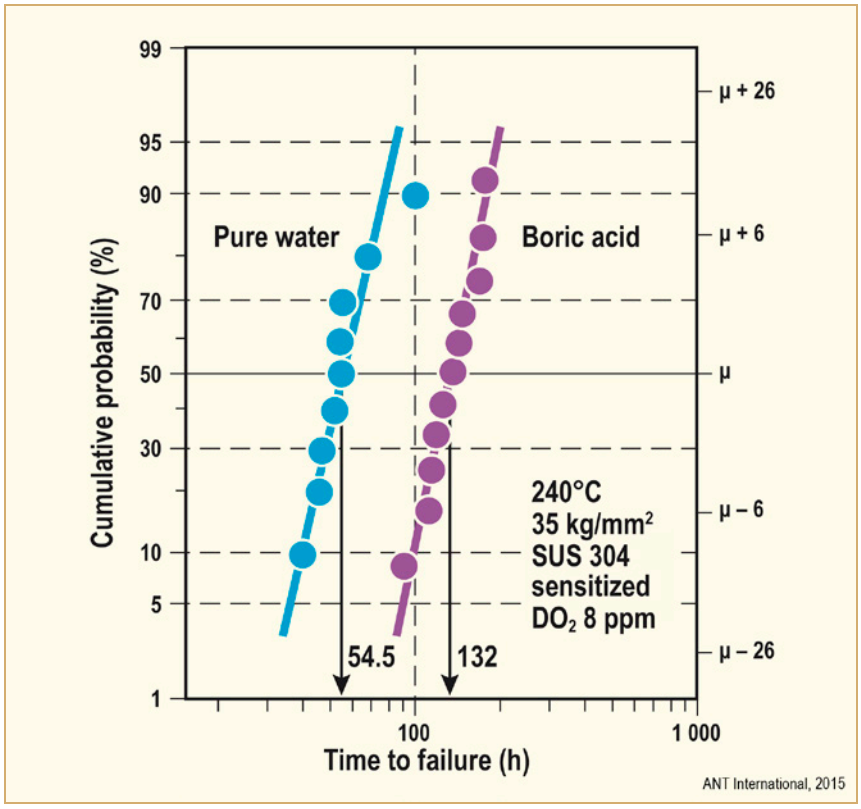

Figure 10-4: Comparison of times to failure in aerated high purity and borated water for sensitized Type 304 stainless steel at 350 MPa and 240°C, after [Tsuruta & Okamoto, 1992].

Most studies in the last decade or so of SCC in PWR primary water of austenitic stainless steels, typically Type 304L or 316L, have employed fracture mechanics, mainly CT specimens with fatigue pre-cracks. Since these specimens are normally machined from plates or bars, the usual method of cold working has been by rolling although some studies have also used tensile cold work or fatigue strain cycling. It is generally observed that cracks grow most easily and fastest in the plane of rolling but only after careful transitioning from a fatigue pre-crack to SCC has been achieved by superimposed trapezoidal loading. When other crack plane orientations are tested, cracks tend to deviate out of the intended crack growth plane and/or present an aspect with very uneven 'fingers' of crack growth. In these latter cases, crack growth rates are about order of magnitude lower than in the rolling plane and crack arrest is often observed. Mixed TGSCC and IGSCC are generally observed although prior tensile cold work appears to favour IGSCC.

Similar to results obtained by the SSRT, hardness or tensile strength has an important effect on propagation rates in simulated PWR water at 288 to 360°C. Most studies have succeeded in obtaining sustained crack propagation at constant load or stress intensity only when the hardness exceeds ~300 HV although there are some reports of measurable CGRs for harness values as low as 230 HV; see for example [Yonezawa et al, 2014]. If low frequency, trapezoidal, cyclic loading is used with an R ratio typically in the range 0.6 to 0.9, a continuous increase in growth rates with yield strength from 180 to 600 MPa (and hardness) is observed for a given value of (maximum) crack tip stress intensity. Recent evidence suggests that this effect may reach a growth rate plateau around 10^{-9} ms^{-1} (at 360°C) for high levels of cold work around 40% [Vaillant et al, 2013]. For high hardness values above the threshold required for crack growth at constant load/stress intensity, no enhancement of growth rates due to superimposed cyclic trapezoidal loading is observed, however.

Where Type 304L stainless steel has been studied, both cold and so-called 'warm working' have been employed in order to test for an effect of cold work induced martensite. In most cases, no significant effect of the presence of even large fractions of martensite on crack growth rates has been observed, although there are exceptions.

There have also been studies of the effect of alloy sulphur content that surprisingly revealed in one investigation that heats with higher sulphur contents were less susceptible to crack propagation in normal quality PWR primary water. However, a more recent study at the same laboratory of the effects of oxygen, chloride and sulphate impurities at 200 and 250°C, simulating possible fault or transient conditions in PHWR instrumentation lines, showed especially at 250°C that sustained crack propagation occurred at constant crack tip stress intensity following a period of crack propagation under cyclic loading, even in the absence of chloride or sulphate additions [Tice et al, 2013]. The propagation rate tended to decline with time at constant stress intensity and this result was interpreted to indicate that a local sulphur anion rich environment in the crack enclave resulting from dissolution of MnS inclusions intercepted by the crack tip was responsible for the high crack growth rates observed. A similar recent study of sensitized Type 304 stainless steel at temperatures between 77 and 327°C emphasized the importance of a high corrosion potential in the presence of oxygen for maintaining high impurity anion concentrations, especially chloride and sulphate, in crack enclaves as a precursor for high propagation rates [Morton, 2013].

Studies of the temperature dependence of crack growth in strain hardened austenitic stainless steels between 150 and 360°C have revealed rather variable apparent activation energies between 60 and 110 KJ/mole, comparable with those measured by SSRT. However, there is recent evidence that the effect of temperature may stabilize or may even decrease somewhat between 325 and 360°C with obvious implications for characterizing the temperature effect over broader ranges of temperature [Vaillant et al, 2013].

A study in support of the investigations into the Mihama 2 Type 316 stainless steel steam generator safe end HAZ cracking has revealed low crack propagation rates (equivalent to 0.13 mm per year) even at a hardness of 250 HV but no crack propagation was detected at 200 HV in normal quality PWR primary water (Figure 10-5). When PWR primary water is aerated, very high crack propagation rates (equivalent to 2.5 to 25 mm per year) are observed at all hardness levels studied between 200 and 300 HV. It should also be noted that in the low carbon Type 316L stainless steel studied, cold work ratios of 10 to 65% were required to generate hardness values between 200 and 300 HV.

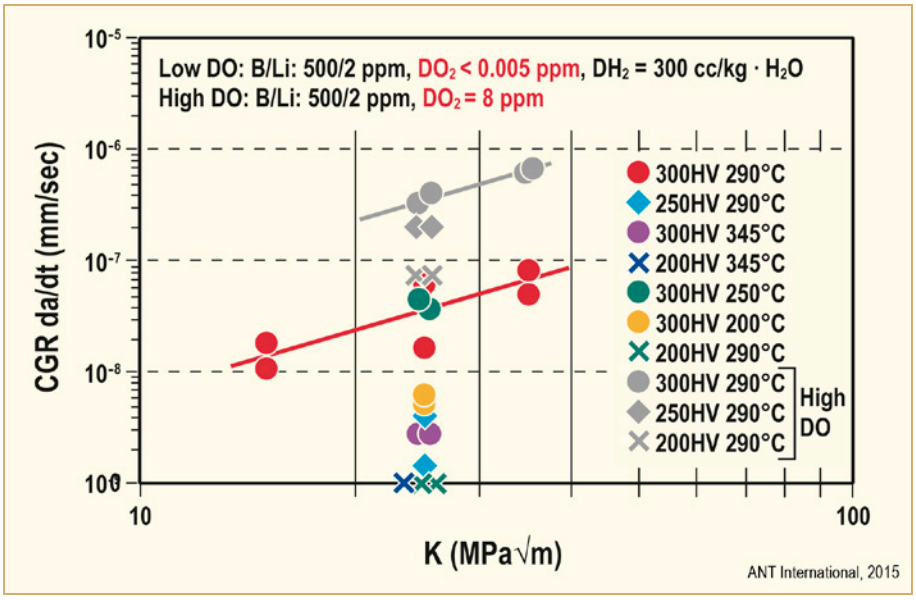

Figure 10-5: Comparison of SCC growth rates observed in cold worked Type 304 and 316L stainless steels in normal and aerated PWR primary water, after [Fujimoto et al, 2007].

Interestingly, intergranular cracks easily initiate from pre-fatigue cracks in cold worked Type 304 stainless steel when oxygen is added to the lithium hydroxide/boric acid mixture typical of PWR primary water. They then continue to grow without difficulty, albeit at a significantly lower rate, after the corrosion potential is restored to low values similar to that of the hydrogen redox reaction by the normal hydrogen partial pressure of PWR primary water. If oxygen is added to PWR primary water so that the potential rises to values more typical of BWR NWC, the SCC growth rate in sensitized material begins to accelerate by up to nearly two orders of magnitude to a rate equivalent to ~0.3 mm per day after ~20-50 hours exposure to the oxygen transient [Andresen & Morra, 2007].

It is important to note that the rate of crack growth follows the change of corrosion potential so that a high rate is only attained after the corrosion potential has reached its characteristic plateau value in oxygenated high temperature water. A similar crack growth transient observation from high to low crack growth rates is made when the potential changes from high to low as hydrogenated PWR primary water conditions are restored. As noted in Section 6, these changes in corrosion potential are governed by mass transport of hydrogen or oxygen to the corroding surface. However, it seems likely that the majority of the incubation period for crack initiation or changes in crack propagation rate is more likely to be due to stabilization of diffusion rates of ions across the inner protective oxide film once the corrosion potential has stabilized to the new environmental chemistry conditions.

As noted in connection with studies using SSRTs, crack growth studies comparing solution annealed and sensitized cold worked Type 316 stainless steel have shown that sensitization has no effect on crack growth rates in hydrogenated PWR primary water, unlike oxygenated environments such as BWR NWC. Indeed, the grain boundary chromium carbides from thermal sensitization appear to exert a favourable effect reducing crack growth rates in PWR primary water, whereas the associated grain boundary chromium depletion has no effect at low corrosion potential. Creep experiments in air (at >450°C) on 20% cold worked (non-sensitized) Type 316 stainless steel have shown that cold work accelerated creep with a similar activation energy to that observed for crack propagation in PWR primary water. It was suggested, based on ATEM observations of the crack tips showing nickel enriched zones, that diffusion of metal atoms and vacancies occurs before crack opening during both IGSCC and creep crack growth. On this basis, a strain induced grain boundary, vacancy diffusion model for crack propagation was proposed.

Very few studies of the stress corrosion susceptibility of cast austenitic stainless steels (CASS) in PWR primary water have been carried out, especially in the thermally aged condition. CASS with between 8 and 23% ferrite were studied using the SSRT method and at constant load (at two times the yield strength). Some susceptibility to SCC was revealed by SSRT even in the un-aged condition where TGSCC occurred primarily in the austenite phase. It was shown that SCC susceptibility increased with increasing ageing time in material containing 23% ferrite both by SSRT and at constant load, and appeared to be due to TGSCC in both the austenite and ferrite phases but mainly at the phase boundary interfaces.

Similarly, measurements of SCC propagation rates in Type 316 L weld metal and a 10% cold worked cast stainless steel (CF8M), both containing about 8% ferrite, have been tested before and after 40000 h ageing at 400°C. Crack propagation was observed in both materials in the presence of dissolved oxygen added to PWR primary water but after switching to normal hydrogenated conditions, cracks slowed down and eventually arrested. Crack propagation in the presence of dissolved oxygen was initially transgranular in the austenite phase and then intergranular, including ferrite/austenite boundaries. Type 308 weld metals, even after cold rolling to 20% reduction, have similarly been shown to resist SCC propagation in normal PWR primary water.

10.2 Irradiation effects on stainless steels (Peter Scott)

The practical background to this subject concerns the ageing and integrity of LWR core internals that support the fuel elements and ensure the required core geometry. Unlike the fuel elements that are discharged every three or four fuel cycles, core support structures are intended to remain in place for the entire design life of the plant. Consequently, the core support structure can receive considerable neutron doses, especially in PWRs where a layer of water only a few millimetres thick separates the core baffle plates from the peripheral fuel elements. In BWRs, the gap between the outer fuel elements and the core shroud is much larger and neutron doses to the nearest support structures are typically an order of magnitude smaller.

The precise values of neutron doses vary with the detailed design of the core internals, distances from nearest neighbour fuel elements and fuel loading as well as irradiation time. The dose rate falls off rapidly with axial distance from the core so that the upper and lower core support plates of PWRs may only receive neutron doses of a few dpa during the initial 40 year design life, whereas the most irradiated zones of core baffle plates may accumulate locally up to 80dpa. Another consequence of the proximity of the core baffle structures to the fuel elements in PWRs is the potential for considerable γ heating of thick sections. Any surfaces in contact with the primary coolant are cooled close to the same temperature as the fluid but considerable increases in internal metal temperature are possible, which in extreme cases may be up to ~100°C higher than the primary coolant.

IASCC is a term that defines EAC of core structural materials, mostly austenitic stainless steels, in which neutron and/or γ irradiation contributes directly to the initiation and propagation of cracks. By implication, in the absence of material damage by fast neutrons and/or modification of the environmental chemistry by ionizing radiations, EAC either does not occur or is significantly less severe.

IASCC of highly irradiated austenitic stainless steels has received considerable attention over the last 25 years following observations of intergranular cracking of core internal components of both BWRs and PWRs. The subject was reviewed in detail in a previous ANT International publication where a detailed bibliography can be found [Ford et al, 2010] and updated in [Combrade et al, 2012]. The neutron doses above which component cracking by IASCC has been observed in BWRs on NWC and in PWRs are respectively ~5×10^{20} and ~2×10^{21} n/cm^2 (E ≥1 MeV), equivalent to, respectively, ~0.7 and ~3 displacements per atom (dpa). The difference in these apparent IASCC threshold doses is attributed to the difference in corrosion potential established in the oxygenated NWC of BWRs and the hydrogenated primary water chemistry of PWRs (and BWRs on HWC).

An overview of these incidents together with the anticipated end-of-reactor-life doses and characteristic dose ranges for the irradiation induced physical processes that are likely to be important in IASCC are shown in Figure 10-6.

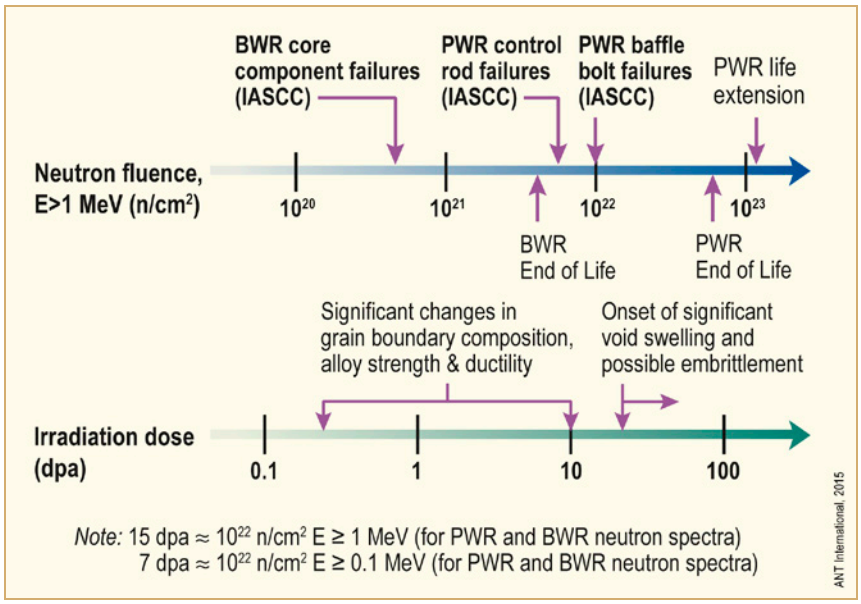

Figure 10-6: Summary of IASCC in light water reactors and associated metallurgical changes in austenitic stainless steels as a function of neutron irradiation in n/cm^2 (E ≥1 MeV) or displacements per atom (dpa), after [Bruemmer et al, 1999]. Note the logarithmic scale for neutron dose.

Before describing the current understanding of IASCC in PWRs (the phenomenon in BWRs is reviewed in Section 9), the main consequences of neutron irradiation on the microstructure and mechanical properties of austenitic stainless steels are summarized in the next sub-section. A recent review summarizing irradiation induced degradation mechanisms of austenitic stainless steels and possible ways forward for producing more radiation resistant alloys is also available [Nelson et al, 2013]. Radiolysis of water and its consequences for corrosion potentials of stainless steels, with or without deliberate hydrogen additions to the primary coolants of PWRs and BWRs, are described in Section 6.

10.2.1 Neutron irradiation damage in austenitic stainless steels

Irradiation of all materials by high-energy particles such as neutrons, α particles and other heavy ions, and electrons causes atom displacements from their equilibrium crystallographic locations thereby creating atomic scale point defects, i.e. vacancies and interstitials. Each displaced atom generates one vacancy and one self-interstitial atom known as a Frenkel pair. The displacement of atoms during irradiation causes changes in microstructure, microchemistry and mechanical properties and consequently the preferred fundamental unit for measuring the irradiation response of a material is displacements per atom (dpa). A useful approximation to convert between dpa and neutron doses in n/cm^2 that is suitable for the neutron spectra of both PWRs and BWRs close to the core periphery is 1 dpa ≅ 7 × 10^{20} n/cm^2 (E ≥1 MeV). Note that this conversion factor is not universal since the neutron energy spectrum will vary with distance from the core and with the density of materials through which the neutrons pass.

The type of particle and its energy determine the rate of point defect production and distribution of point defects. Charged particles typically penetrate a few tens of microns into metals because of Coulombic interactions whereas fast neutrons can penetrate many centimetres. Neutrons generate large cascades of point defects as the energy transfer to the displaced atoms is large so that the displaced atoms in turn continue and cause knock-on collisions and even more atom displacements. Although many of the vacancies and interstitials initially created recombine, sufficient numbers survive to agglomerate into clusters, dislocation loops and cavities, or diffuse to traps to cause significant changes in microstructure, microchemistry and mechanical properties.

Irradiation damage of materials is affected not only by the neutron dose (fluence), dose rate (flux) and type of incident energetic particle and their energy but also by the initial composition, microstructure, extent of cold work, and temperature of the substrate undergoing irradiation. In addition, neutron capture reactions induce transmutation reactions and hence changes in chemical composition together with the production of helium and hydrogen gases.

In recent years, quite a lot of attention has been given to characterizing stainless steels irradiated at typical light water reactor (LWR) operating temperatures, whereas much of the basic knowledge in the field was gained several decades ago in the context of fast reactor development and, consequently, at significantly higher temperatures. Most of these recent studies have been focused on Type 316 and Type 304L stainless steels, the former often in a cold worked (typically 10 to 20%) starting condition; see for example [Pathania et al, 2007] and [Edwards et al, 2009]. The main trends observed show that most of the knowledge obtained from fast reactor irradiations is relevant to the mixed (thermal plus fast) neutron energy spectra of PWRs and BWRs. The only parameter that changes significantly is a large increase in helium and hydrogen production from transmutation reactions in mixed neutron spectrum reactors.

Irradiations with ions accelerated to high energies have a long history of use in metallurgical studies of irradiated materials. One successful strategy that has been deployed to study the metallurgical characteristics (and IASCC susceptibility) of irradiated austenitic stainless steels has been the use of proton irradiations. Proton irradiated stainless steels, typically using a proton energy of 3.2 MeV, have the advantage that activation is very much less than with neutrons so that subsequent experimentation is greatly facilitated. The main disadvantages are that the maximum practicable dose that can be achieved economically is about 5 to 10 dpa in a few hundred hours and that the depth of material affected by irradiation damage is only a few tens of microns.

10.2.1.1 Mechanical properties of irradiated stainless steels

The first and most obvious microstructural change that occurs in irradiated austenitic stainless steels at low to moderate temperatures up to those typical of water cooled reactors is the formation of many very small point defect clusters and faulted dislocation loops (Frank loops) of nanometre dimensions. These irradiation-induced features are often generically called “black dot damage” after their appearance in bright field images taken in transmission electron microscopes (TEM). Their density is relatively independent of irradiation temperature in the low to moderate range <350°C. The number density and size are observed to saturate with neutron dose in solution annealed and cold worked stainless steels at between ~2 to 10 dpa.

Frank loops and/or black dot damage act as barriers to dislocation motion and are responsible for radiation hardening, loss of ductility and reduced fracture toughness. Examples of hardening and loss of ductility of a solution annealed Type 304 stainless steel after irradiation to relatively low doses of a few dpa at 330°C are shown in Figure 10-7. Substantial loss of ductility and work hardening is already apparent with a clear yield point appearing after ~2 dpa.

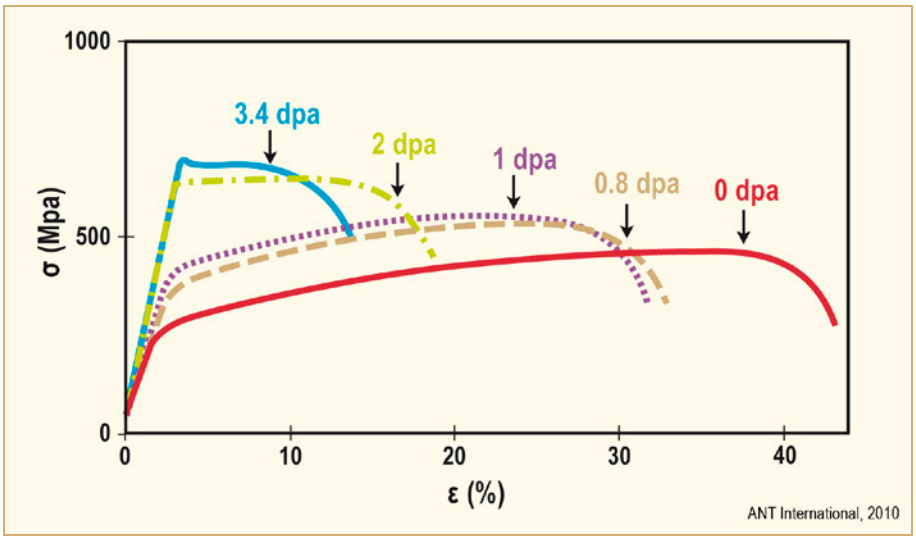

Figure 10-7: Stress-strain curves at 330°C for Type 304 stainless steel after different irradiation doses up to 3.4 dpa, after [Pokor et al, 2004].

A saturation in yield stress with neutron dose is observed at fluences between 5 and 10 dpa, as illustrated in Figure 10-8 for both solution annealed Type 304L and initially cold worked Type 316 stainless steels. The neutron spectrum and helium/dpa ratio appear to have little influence on these mechanical properties as a function of irradiation fluence in dpa. However, some recent evidence has suggested that higher dose rates may enhance the increase in yield stress, at least at doses well below saturation [Kondo et al, 2013]. For a given fluence, the yield and ultimate tensile strengths increase only slowly with irradiation temperature from room temperature to ~350°C but the reduction in strain hardening is most severe for irradiation temperatures between ~250 and 350°C.

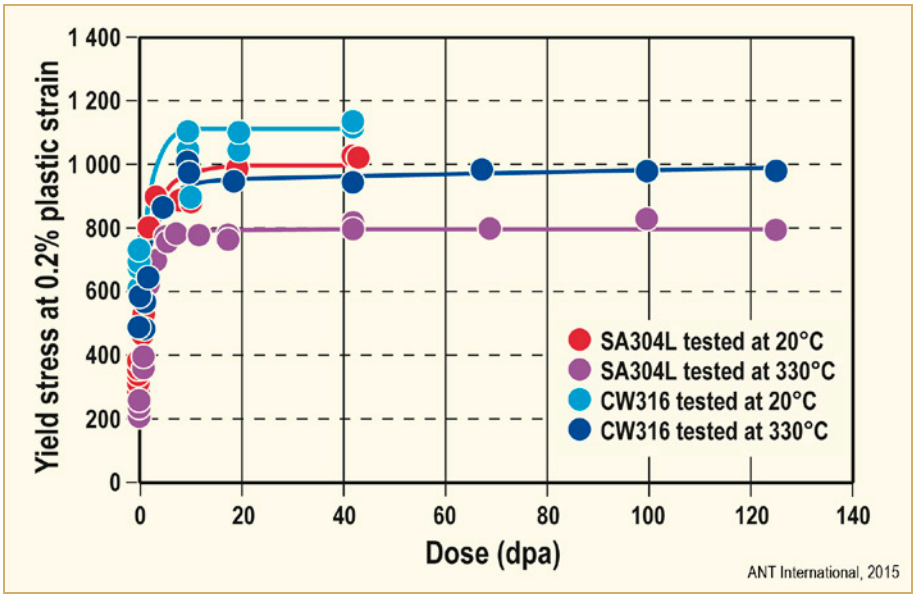

Figure 10-8: Compilation of tensile test data at 20 and 330°C for austenitic stainless steels irradiated at 330°C, after [Garnier et al, 2007].

Transgranular ductile failure is observed in all tensile tests of austenitic stainless steels at the doses tested up to 125 dpa and in the temperature range up to ~350°C. As the dose increases, homogenous deformation observed at low doses shifts to heterogeneous deformation at higher doses where saturation of the mechanical properties is observed. Plasticity is then localized to channels that are created when a dislocation clears a slip plane of radiation damage. This then provides an easier path for subsequent dislocation motion and slip becomes confined to narrow bands of slip planes called 'dislocation channels', which causes intense localized necking and the observed sharp reduction in uniform elongation. Uniform elongations of <1% are typically observed at ~300°C once the tensile strength has stabilized with increasing neutron dose but total elongations remain significant at around 5 to 10%.

The loss of ductility of irradiated austenitic stainless steels with increasing dose is accompanied by a dramatic reduction in fracture toughness from several hundred MPa√m to ~50 MPa√m at 10 dpa with an accompanying severe drop in tearing modulus. It has been recommended that a LEFM analysis be performed for neutron doses between 5 and 15 dpa with a limiting value of 55 MPa√m; correlations between toughness, tearing modulus and lower neutron doses have also been proposed [Carter & Gamble, 2002]. In the case of higher doses above 15 dpa relevant to PWRs, compilations of data from both fast reactor and LWR irradiations suggest a slightly lower limiting value of fracture toughness of 38 MPa√m, as shown in Figure 10-9.

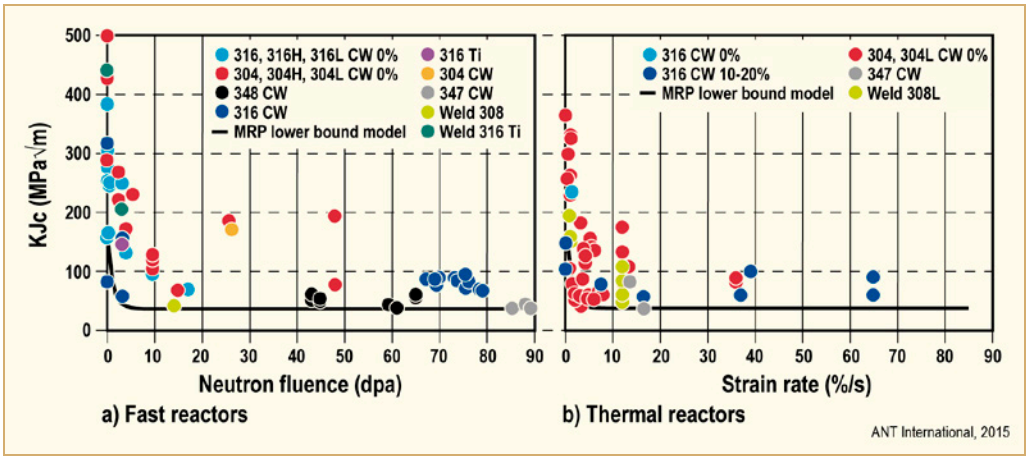

Figure 10-9: The effect of neutron fluence on fracture toughness comparing fast reactor and LWR irradiated stainless steels, after [Fyfitch et al, 2009a].

In some designs of PWR internals, cast austenitic stainless steels (CASS) components are used just below the core where they receive doses estimated at a few dpa over the initial 40 year design life. In addition, some designs of PWR internals are welded so that there is an interest in the effects on irradiation on the toughness of stainless steel weld metals such as Type 308 as well as CASS that contain significant fractions of ferrite. Concerns have been expressed that a combination of thermal ageing of the ferrite phase at the reactor coolant temperature and low levels of neutron irradiation could have a synergistic detrimental effect on fracture toughness. Somewhat conflicting conclusions can be drawn as to whether there is any significant synergistic interaction between thermal ageing and irradiation embrittlement from available results at low doses of a few tenths of a dpa. Lower bound toughness can be estimated from well-known thermal ageing models. At higher neutron doses the fracture toughness lower bound for fully austenitic stainless steels is also an adequate lower bound for CASS and weld metals.

11 Fatigue and corrosion fatigue (Claude Amzallag)

11.1 Introduction

Fatigue is an important degradation mechanism with direct consequences for safety, availability, maintenance programmes and Plant Life Management. This section presents a review of key factors involved in Environmental Assisted Fatigue (EAF) of Reactor Materials in LWR Coolant Environments.

Available laboratory data show that the fatigue life of reactor materials may be significantly reduced in the low-cycle fatigue domain under certain conditions of strain rate, temperature and oxygen concentration in the aqueous environment.

However, up to now service experience has been good in the low-cycle fatigue domain and fatigue cracking has only concerned the high-cycle fatigue domain (caused by fluid mixing zones, vibrations, etc.) rather than the low-cycle fatigue domain.

The transferability of laboratory data to components in service is therefore a question for debate.

Issues to be addressed concern crack initiation in both the low-cycle and high-cycle fatigue domains and include: the effect of temperature, environment, loadings (variable amplitude and multi axial loadings, cumulative damage), and thresholds.

11.2 Background

11.2.1 Fatigue analysis of pressure vessels

Cyclic loadings on a reactor pressure boundary component occur because of changes in mechanical and thermal loadings as the system goes from one operating condition (e.g., pressure, temperature, moment, and force loading) to another. The number of such cycles applied during the design life of the component seldom exceeds 10^5 and is typically less than a few thousand (i.e., low–cycle fatigue).

The main difference between high–cycle and low–cycle fatigue is that the former involves little or no plastic strain, whereas the latter involves strains in excess of the yield strain. Therefore, design curves for low–cycle fatigue are based on tests in which strain rather than stress is the controlled variable although the results may be presented in the form of pseudo Stress Amplitude, S_a, versus the number of applied strain cycles where S_a is equal to the applied Strain Amplitude multiplied by the elastic modulus.

Thermal loading due to flow stratification or mixing of fluids at different temperatures was not included in the original design basis analyses.

Section III, Subsection NB, of the ASME Boiler and Pressure Vessel Code contains rules for the design of Class 1 components of nuclear power plants [ASME, 2007].

The mandatory Appendix I to Section III of the ASME Boiler and Pressure Vessel Code specifies fatigue design curves that define the allowable number of cycles as a function of applied stress amplitude, for different Classes of materials:

- Carbon, Low Alloy, High Tensile Steels,
- Austenitic Steels, Nickel-Chromium-Iron Alloy, Nickel-Iron-Chromium Alloy and Nickel-Copper Alloy, Nickel Base Alloys,
- Wrought 70 – Copper 30 Nickel Alloy,

- High Strength Steel Bolting,
- Nickel-Iron-Chromium-Molybdenum Alloys: Super Alloys of the Hastelloy type,
- Grade 9 Titanium.

Figure 11-1 shows the Design Fatigue Curves for Carbon, Low Alloy and High Tensile Steels.

Two curves are presented depending on the level of Ultimate Tensile Strength.

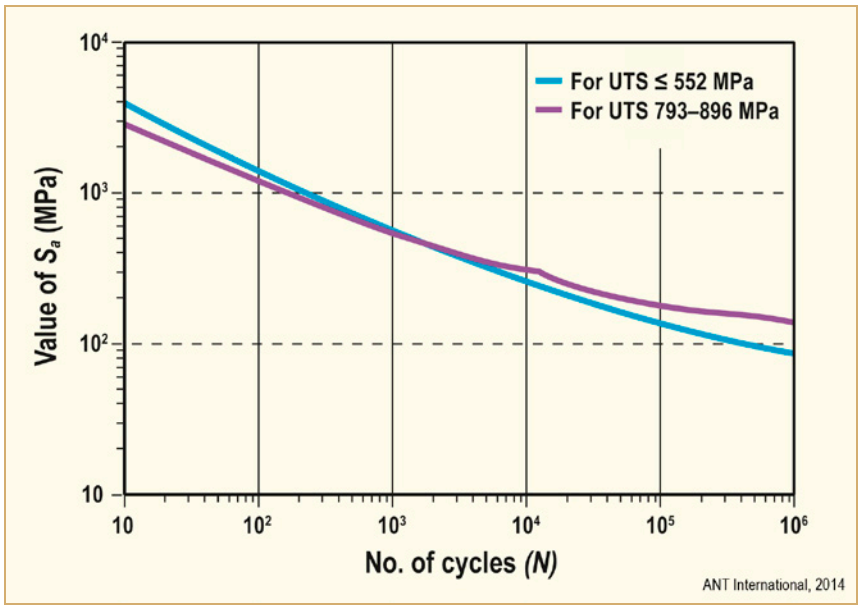

Figure 11-1: Design fatigue curves for carbon, low alloy, and high tensile steels for metal temperatures not exceeding 370°C, after [ASME, 2007].

Figure 11-2 shows the Design Fatigue Curves for Austenitic Steels.

As in the previously cited case, the data are presented in terms of Stress Amplitude, S_a, as a function on number of cycles N.

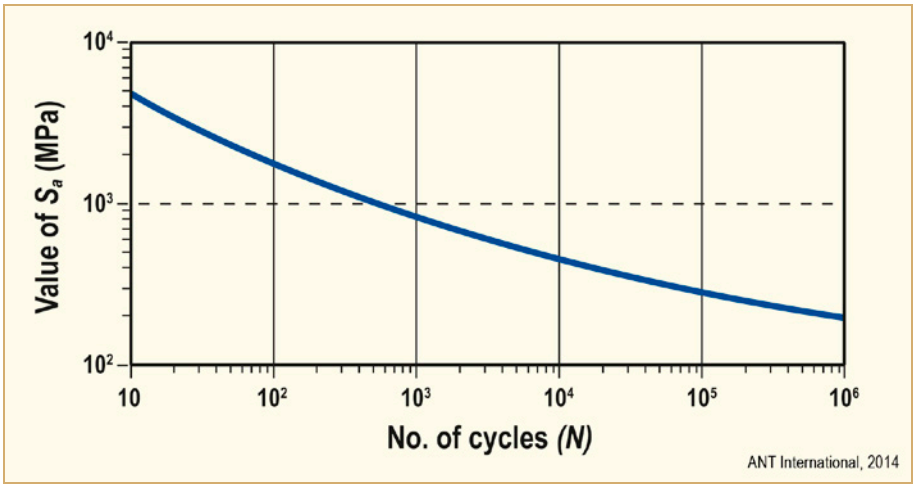

Figure 11-2: Design fatigue curve for austenitic steels, nickel-chromium-iron alloy, nickel-iron-chromium alloy, and nickel-copper alloy for S_a >194 MPa and temperatures not exceeding 425°C, after [ASME, 2007].

The ASME Code presents two sets of curves for Stainless Steels:

- one for a number of cycles below 10^6 cycles (Figure 11-2),
- one for a number of cycles greater than 10^6 cycles (Figure 11-3).

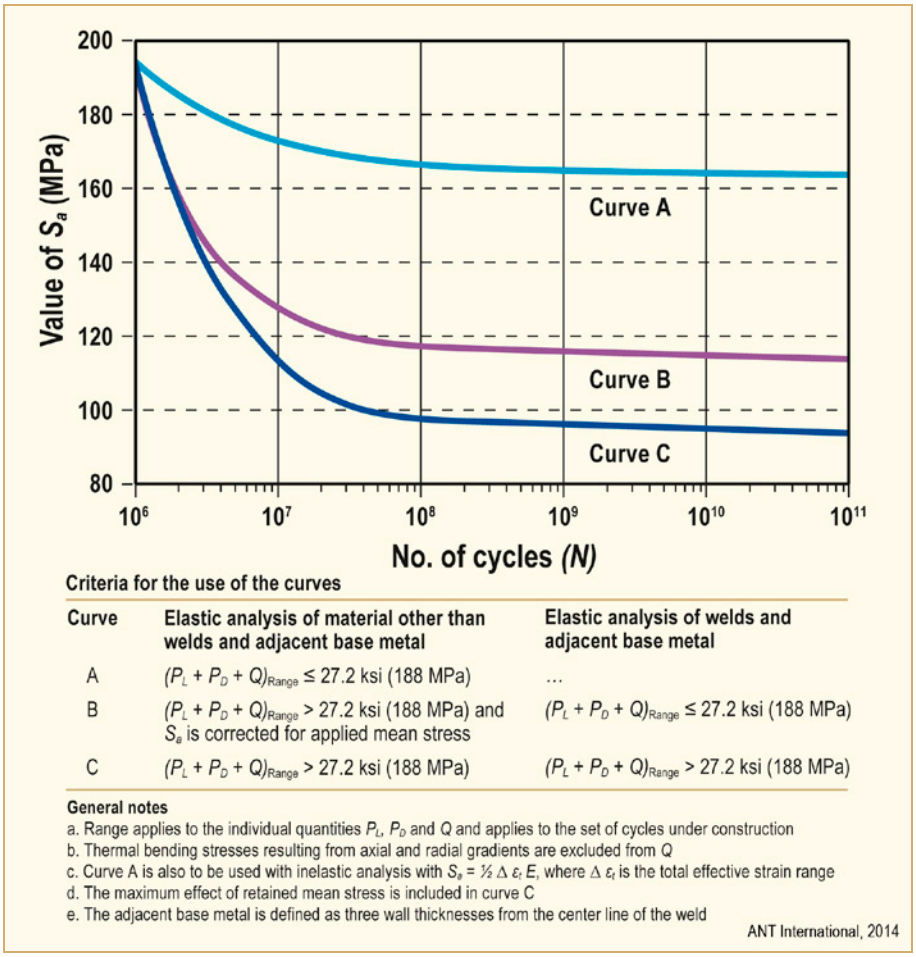

Figure 11-3: Design fatigue curve for austenitic steels, nickel-chromium-iron alloy, nickel-iron-chromium alloy, and nickel-copper alloy for $S_a \leq 194$ MPa and temperatures not exceeding 425°C, after [ASME, 2007].

For a number of cycles greater than 10^6 cycles, there are three options: A, B and C.

The choice of curve A, B or C is based on the configuration and on the level of mean stress, stress range and presence of weld material, as described in the figure.

Curve A is an extrapolation of the previous curve presented in Figure 11-2.

Curve C corresponds to a maximum mean stress Goodman correction.

11.2.2 Origin and use of ASME design fatigue curves

The ASME design fatigue curves were developed in the late 1960s and early 1970s [ASME, 1969]. They are based on strain-controlled fatigue tests performed on small polished uniaxial specimens, conducted at room temperature in laboratory air environments.

Similar curves are applied also in other design codes, e.g., the German KTA [KTA, 1996] and French RCC-M [RCC-M, 2007].

The data used to develop the ASME mean curve were obtained on specimens that were tested to complete failure.

In this approach, the failure of small specimens corresponds to crack initiation in large components (Figure 11-4).

The basic premise of the local stress-strain approach is that the local fatigue response of the material at the critical point of a stress concentration, i.e. the site of crack initiation, is analogous to the fatigue response of a smooth specimen subjected to the same cyclic strains and stresses.

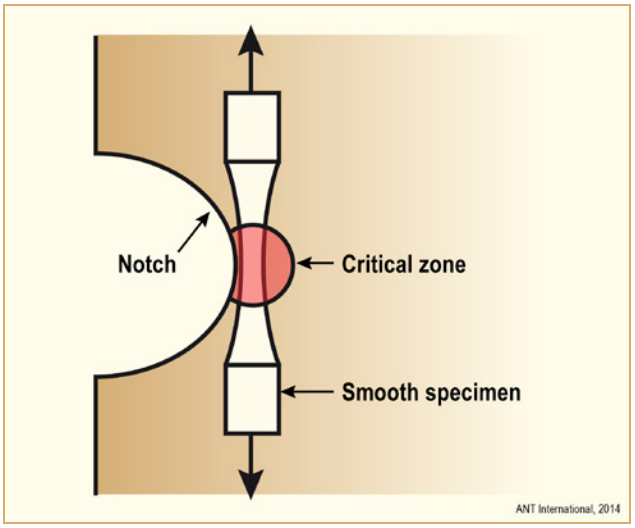

Figure 11-4: Smooth specimen analogue of material at a critical stress concentration point in the structure.

The failure of small specimens corresponds to a crack of engineering significance, i.e. about 3 mm deep.

The Design Fatigue Curves were obtained from Mean Fatigue Curves. Figure 11-5 presents the Mean Fatigue Data Curve (Langer Curve) and the Design Fatigue Curve for Austenitic Stainless Steels [ASME, 1969].

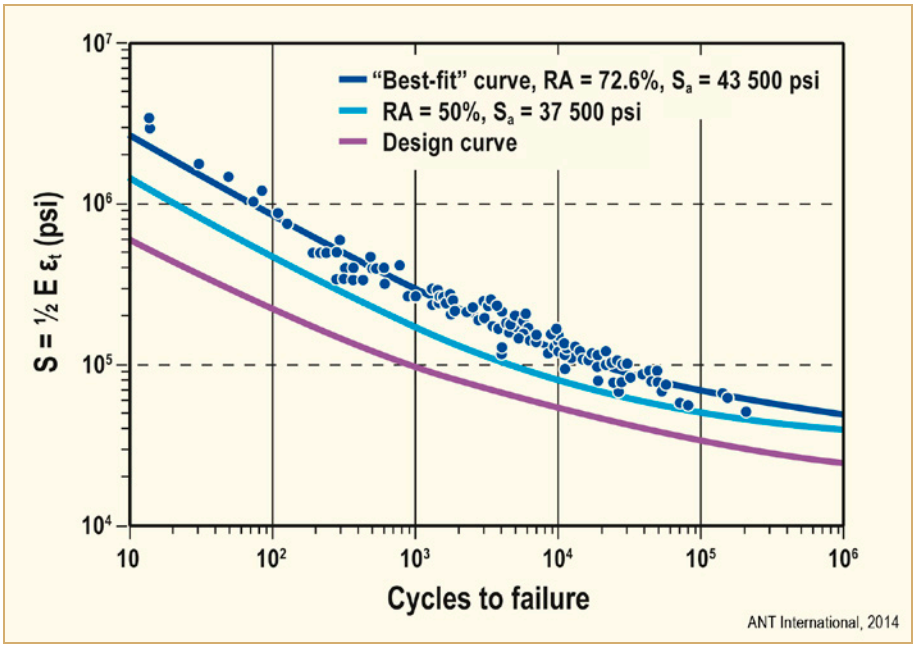

Figure 11-5: Mean fatigue data curve (Langer curve) and design curve for austenitic stainless steels, after [ASME, 1969].

The Design Fatigue Curves were then obtained by reducing the fatigue life at each point on the adjusted Mean Curve by a factor of 2 on strain (or stress) amplitude or 20 on cycles, whichever is more conservative.

The factors of 2 and 20 are not safety margins but rather adjustment factors that should be applied to small-specimen data to obtain reasonable estimates of the lives of actual reactor components.

The factors were intended to cover effects such as environment, size effect and scatter in the data [RCC-M, 2007].

Detailed justifications for the factor of 20 were not formally published, but are based on three sub factors [Chopra & Shack, 2007]:

- 2.0: scatter in the data,
- 2.5: size effect,
- 4.0: surface finish, and environment.

Other breakdowns of the factor 20 have been derived and reported in the literature.

Although the Section III criteria document states that these factors were intended to cover such effects as environment, the term "atmosphere" was intended to reflect the effects of an industrial atmosphere in comparison with an air-conditioned laboratory, not the effects of a specific reactor coolant environment. Subsection NB-3121 of Section III of the Code explicitly notes that the data used to develop the fatigue design curves (Figs. I-9.1 through I-9.6 of Appendix I to Section III) did not include tests in the presence of corrosive environments that might accelerate fatigue failure. Article B-2131 in Appendix B to Section III states that the owner's design specifications should provide information about any reduction to fatigue design curves that is necessitated by environmental conditions.

The Data and Design Fatigue Curves are plotted in terms of pseudo-stress amplitude $S_a = E \times \varepsilon_a$, where E is the Modulus of Elasticity of the material (Figure 11-6).

This convention is selected to be consistent with the elastic stress analysis method commonly used to design components. At plastic strain concentrations, a linear stress $S_a = E \times \varepsilon_a$ is clearly not the actual plastic stress in the metal, but the method of derivation explains the large apparent values of stress on the S-N curve.

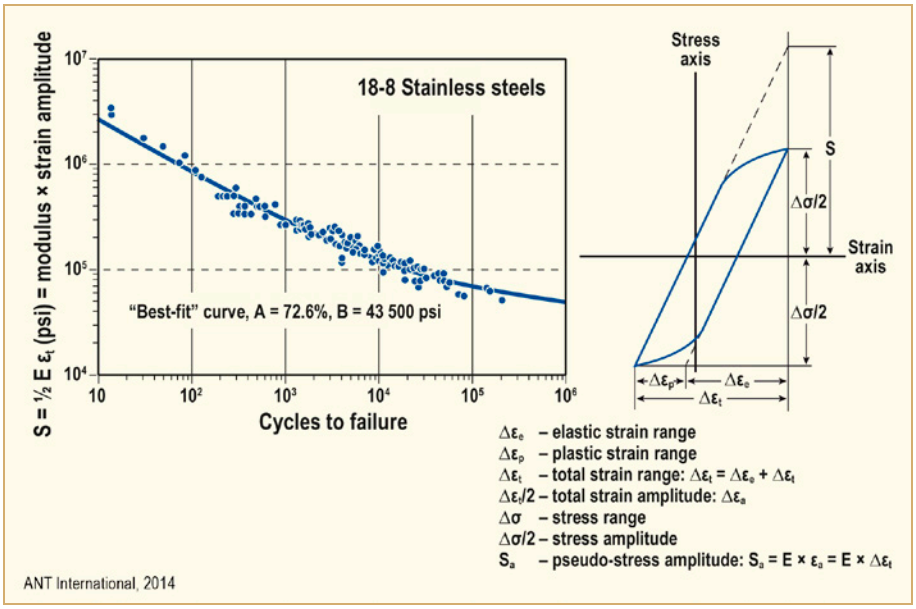

Figure 11-6: Stress and strain range and amplitude.

The transferability of test specimen data to component behavior has been the subject of an ongoing debate. Recent developments to modify the design fatigue curves and adjustment factors are intended both to reduce perceived conservatisms and to account for the effects of aqueous reactor coolant environments.

11.3 Fatigue damage

For variable amplitude loading, Miner's rule of linear damage summation is used.

For each stress cycle or load set pair of a particular magnitude (i.e. transient type), an individual fatigue usage factor is determined by the ratio of the number of cycles anticipated during the lifetime of the component to the number of allowable cycles.

The cumulative usage factor (CUF) is the sum of the individual usage factors for all transient types, and ASME Code Section III requires that at each location the CUF, calculated on the basis of Miner's rule, must not exceed 1.

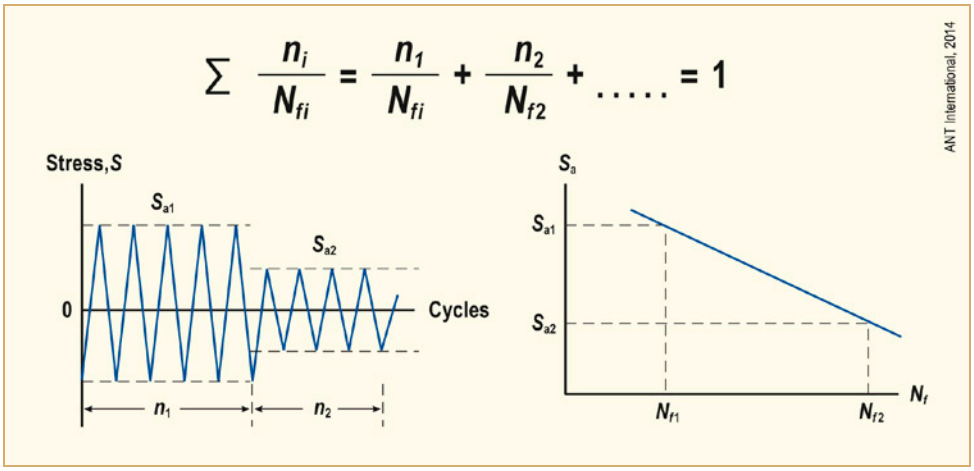

Figure 11-7: Fatigue Damage Summation using Miner's Rule.

11.4 Environmental assisted fatigue of reactor materials in LWR coolant environments

Laboratory fatigue data indicate significant effects of LWR environments on fatigue lives, especially in the low cycle domain.

Fatigue ε-N (S-N) data have been evaluated to:

- identify key environmental parameters that influence fatigue life,
- define ranges for these parameters where environmental effects are significant, i.e., establish threshold and saturation values.

If these conditions exist during reactor operation, environmental effects will be significant and must be addressed.

The effects of key parameters on the fatigue resistance of Carbon and Low Alloy Steels, Austenitic Steels and Ni-Cr-Fe Alloys and Welds are summarized in the paragraphs below.

11.4.1 Carbon and low alloy steels

The fatigue lives of both carbon and low-alloy steels are decreased in LWR environments predominantly in the low cycle domain (Figure 11-8) [Chopra, 2007] and [Majumdar & Natesan, 2011].

The reduction depends on temperature, strain rate, dissolved oxygen (DO) concentration in the water, and the Sulphur content of the steel.

LWR coolant environments have no effect on the fatigue lives at strain amplitudes below a threshold value.

12 Degradation management

12.1 Corrosion testing and quality control (Peter Scott)

The practical objectives of corrosion testing either to support the construction of new plant or resolve corrosion problems encountered in operating plant are to:

- Aid the design of industrial components;
- Choose the most appropriate materials;
- Optimize their installation;
- Verify adequate corrosion resistance during the design life of the component or predict the safe working life;
- Explain in-service failures and define solutions;
- Manage the kinetics of any identified or potential degradation;
- Slow down the kinetics of known degradation;
- Propose improved replacement materials.

The testing techniques associated with fulfilling the above objectives are outlined below. A particular difficulty that has come to the fore in recent times concerns the qualification of highly EAC resistant materials in LWR environments. In particular, the extent to which stress/strain, environmental chemistry and temperature can be exaggerated in order to have results on an accelerated timescale compared to the hoped for lifetime in service have become an issue.

The requirements of corrosion testing in aqueous solutions are influenced by the expected timescale of the application. For typical lifetimes of industrial installations these may be, for example, several years for engines, several tens of years for chemical and oil processing plant, 30 to 80 years for nuclear power reactors, about 100 years for buildings and major civil works, and finally thousands of years or even 10^4 to 10^5 years for deep underground storage of radioactive waste. Clearly, for periods beyond a few years, prototypic lifetime testing is not practical and the qualification data required must be based on threshold measurements, kinetic measurements and predictive models.

Examples of routine codified tests for corrosion resistance that would normally be the first step for any new industrial application include:

- Intergranular corrosion tests (ASTM A262, Practice C) for austenitic stainless alloys, most of which detect chromium depletion (sensitization) at grain boundaries:
  - the “Huey” test (65% nitric acid), which also detects the presence of carbides and phosphorus segregation;
  - the acidified copper sulphate “Strauss” test (ASTM A262 Practice E) for sensitization;
- The ferric chloride test for localized corrosion such as pitting and crevice corrosion;
- The boiling $MgCl_2$ test for chloride-induced stress corrosion cracking of stainless steels.

Such standard corrosion tests do not give any direct information on the in-service resistance of materials. They can sometimes be correlated with in-service behaviour via experimental correlations such as, for example, the $FeCl_3$ test for the resistance of corrosion resistant alloys in seawater. They can also be used as quality control tests, or to characterize the surface condition of a product, or to verify that a SS part is not sensitized by, for example, a new welding or heat treatment process. The boiling $MgCl_2$ test for stainless steels cannot, however, predict cracking of stainless steels in neutral, dilute chloride solutions since it is a very severe test due to its acidity and the fact that the cathodic reaction is proton reduction. Occasionally, it may not be severe enough. For example, silicon SSs do not crack in boiling $MgCl_2$ solution but do crack in the same way as 18/10 type SSs in dilute, aerated, chloride solutions. Acceptable uses of the boiling $MgCl_2$ test are detection of residual stresses above a known threshold for example for the development of stress relief procedures, and development of fabrication methods to minimize residual stresses; such as procedures for SG tube expansion into tube sheets.

In the case of corrosion processes that normally proceed at a constant rate, such as active general corrosion, erosion-corrosion, and wear-corrosion, there is no requirement in principle for 'accelerated' corrosion testing. It is sufficient to determine the kinetics of the corrosion process, e.g. uniform general corrosion rates. However, the feasible environmental and/or metallurgical conditions under which the corrosion degradation mechanism could change should be identified. Examples include abrupt changes in corrosion kinetics due to breakaway corrosion, initiation of localized corrosion such as pitting corrosion, crevice corrosion, and initiation of cracking by SCC or corrosion fatigue.

Prototypic experiments under the same conditions (mechanical loading, environment chemistry and temperature, test times equivalent to service lifetimes) as those anticipated in service yield data that are directly applicable. Short-term experiments under conditions representative of those in service but with shorter exposure times compared to the anticipated component lifetime obviously necessitate extrapolation of the data as a function of time. 'Accelerated' experiments under conditions that are assumed to produce damage representative of that occurring in service but in much shorter times due to experimental conditions that are more severe compared to those in service require acceleration factors to be determined in order to relate the test results to service conditions. Measurements of certain critical parameters can allow predictions to be made from knowledge of service conditions such as, for example, no localized corrosion is possible if $E_{corr.} < E_p$, no SCC if $\sigma < \sigma_{th}$ or, for pre-existing cracks, if $K_I < K_{Iscc}$, and no corrosion fatigue cracking if the cyclic stress is below the endurance limit in the operating environment. Other examples of prototypic experiments include simulations of service conditions using standard test SCC specimens such as tensile bars, C-rings, U-bends, CT specimens etc., mockups of specific component details, pilot plant, and industrial plant equipped with suitable measuring equipment.

Measurements of critical threshold potentials for localized corrosion processes such as the pitting potential (E_p) should take into account the stochastic character of the pitting process, which may change with time. A similar comment can be made for determination of the repassivation potential (E_{rp}) and there are concerns in any case that this parameter may not be an intrinsic material property but dependent on the precise measurement conditions. Identification of critical threshold potentials or bands of potential for SCC based on polarization curves can provide useful indications of susceptible conditions that should be avoided. For example initiation of hydrogen embrittlement can only occur if the corrosion potential is below the hydrogen evolution potential while many other SCC mechanisms are clearly associated with passive film breakdown over specific bands of potential. Nevertheless, caution is required that the test conditions are genuinely prototypic, particularly in situations where the structure of passive oxide films takes thousands of hours to fully stabilize.

Considerable attention is needed when testing prototypic conditions to identify possible hidden parameters and to identify local chemical perturbations. For laboratory environmental simulations, it can be difficult to identify all the species likely to be present and the local evolution of complex chemical 'soups' due to electrochemical concentration processes in pits, crevices and especially in super-heated cavities due to boiler water impurity hideout. It is also necessary to correctly identify likely surface temperatures due to the effects of boiling and evaporation, γ heating, hydrodynamic factors, high fluid velocities and associated phenomena such as erosion, abrasion and cavitation. The degree of surface aeration/de-aeration may also depend on the flowrate, the presence of dead-legs, and the formation of deposits.

Potential problems with short-term and accelerated testing include extrapolation beyond the domain of the tested experimental parameters, particularly in the absence of any knowledge of the underlying corrosion mechanism and, above all, the rate limiting processes. There are several types of experimental problems that require particular vigilance including the risk that the degradation process can change during short-term experiments and accelerated experiments such as statistical uncertainties in measured data and rate constants and unidentified influencing parameters. The investigator also has to be aware of possible variations in service conditions due to in-service transients, plant shutdown and maintenance procedures, changes in operating parameters, and operational accidents. The likely vital role of surface condition, including the as-fabricated initial state and possible changes in service, must also be taken into account.

Accelerated testing techniques include increasing the test temperature, modifying the environment chemistry, e.g. by aeration and/or solute concentration, changing pH, use of additives. Mechanical loads may be increased for SCC tests to higher stresses than those applicable in service. Other mechanical loading options are dynamic loading or straining that may be cyclic or trapezoidal but sometimes continuously increasing at controlled strain rates. In the case of SCC testing, because the phenomena generally occur over limited ranges of corrosion potential, the tendency is to test at potentials where susceptibility is maximized, which may or may not be representative of service conditions. Temperature also affects critical corrosion potentials as well as reaction kinetics and generally there is no physical basis for predicting how critical potentials change with temperature. The results of reducing crack initiation times by increasing stress can be affected by the definition adopted for crack initiation since time to failure can depend on specimen size. In general, the problems of extrapolation are all the more critical when the accelerated test conditions do not overlap the likely domain of service conditions.

Use of the slow strain rate test (SSRT) for determining SCC susceptibility is often favoured as an accelerated test method but one which, in the authors' opinion, the results should be regarded with considerable caution. The fundamental justification is based on the passive film rupture mechanism of SCC which may or may not be relevant in LWR service; there are other cracking mechanisms for which dynamic straining is not a necessary condition. Cracking is usually observed only over a restricted range of applied strain rates which may or may not be industrially pertinent. SCC susceptibility is also often announced on the basis on very little non-ductile cracking and after very large amounts of plastic deformation that are not practically relevant.

There are also cases known where the critical conditions for cracking are significantly different under dynamic loading compared to static loading: e.g. Alloy 600 in hydrogenated, high temperature water. For nickel base alloys in general in PWR primary water, and for Alloy 690 in particular, it is necessary to work at the lower end of the accessible strain rate range between 10^{-7} and 2×10^{-8} s^{-1}, which severely exacerbates problems caused by (typically) low test system stiffness and largely eliminates the testing time advantage. A high density of grain boundary carbides can give rise to an increased frequency of mechanically induced grain boundary separations at high strains, and is a particular problem in the case of carburized or nitrided surface layers. Observed cracks in Alloy 690 after SSRT are short (<120 μm deep) and gaping, implying that they formed (and arrested) at unrealistically high plastic strains. A similar problem is observed in sensitized austenitic stainless steels at low corrosion potential. In the authors' opinion, industrially significant cases of SCC should be characterized in SSRTs by the presence of a few, deep, tight cracks on the gauge length that develop at low plastic strains (e.g. <5 to 10% depending on the applied strain rate.

The problems of selecting the most appropriate SCC test are greatly amplified when investigating highly resistant materials such as Alloy 690 and austenitic stainless steels in PWR primary water or BWR HWC. In order to demonstrate that a corrosion cracking problem will not occur over a very long projected lifetime of many tens of years requires very long test times (albeit shorter than that of the plant itself otherwise laboratory testing serves no purpose), a demonstration that crack propagation is not possible, and ideally an understanding of the mechanism allowing a well-founded predictive model to be established.

Recent work on CW austenitic stainless steels and CW Alloy 690 at low corrosion potentials in simulated hydrogenated, high temperature, aqueous coolants have often demonstrated cracking either during crack growth tests in the plane of cold rolling, or by SSRTs, or recently in smooth specimens of CW Alloy 690 with incrementally increased 'constant loads'. It now seems clear that dynamic strain seems to be key to crack initiation in all cases. Creep cavities ahead of crack tips have also been observed in several cases as well as severe permanent sets in CT specimens. This prompts a question: is it right that SCC resistance in service should be questioned on this basis, especially of materials with such evidently excellent records in operational service as austenitic stainless steels and Alloy 690 with a maximum of only modest levels of CW?

Firstly, it should be noted that the ASME Section III code expressly forbids the sum of primary membrane and bending stresses to exceed two thirds of the yield stress. The purpose is to prevent plastic deformation and collapse, in which respect these rules have been eminently successful in practice. SCC is, nevertheless, usually initiated where local stresses have plainly been above the nominal yield stress for the reason that secondary stresses developed by constraint of displacements caused by thermal expansion or movement of external restraints have caused local secondary stresses to reach the yield stress, which is permitted by the ASME Section III code. The problem is compounded by the fact that the yield stress itself has often increased very significantly due to strain cycles imposed during fabrication, see Figure 10-33. Most practical cases of stress corrosion cracking are in fact caused by residual (secondary) fabrication stresses. The conclusion is that it is not cold work per se that is dangerous for crack initiation but cold work combined with strain reversal that gives rise to excessively high surface, mainly secondary, tensile stresses where continuous dynamic deformation cannot occur because secondary stresses are fully balanced by stresses of opposite sign through the thickness. It is no accident therefore, that successful laboratory testing (of Alloy 600 for example) has primarily used bend-type specimens where this strain reversal can be simulated.

Secondly, the issue of primary creep of highly loaded tensile specimens is, in the authors' opinion, a particular concern for testing Alloy 690 and its associated weld metals in PWR primary water. All the evidence to date from recent experiments points to creep being very important to the initiation of PWSCC even in highly cold worked Alloy 690. In fact, the recent observations confirm some results of several earlier studies of Alloy 690 using the SSRT. Although much of the observed cracking by SSRT concerned some experimental SG tube heats with unacceptable microstructures, including highly carburized internal surface layers, it was clear that some cracking, albeit quite short compared to equivalent tests on Alloy 600, had also occurred in good quality Alloy 690 tube heats with acceptable microstructures. However, no crack initiation occurred in any other specimen geometry, including SG tube capsules with the most severe roll expansion anomalies tested for 100 000 hours at 360°C. It seems clear from these comparisons that crack initiation in Alloy 690 can only occur during dynamic straining. It is therefore absolutely necessary to clearly distinguish test methods where dynamic straining can occur and those where it does not (except transiently at the beginning of a test). Many investigators will doubtless argue that transient straining is a fact of life for field components but this is a fallacious argument. First, it is evident that no long term distortion occurs in LWRs (unless radiation creep is active) and second, tests conducted years ago to qualify austenitic bolted joints and springs for use in high temperature water clearly show that any primary creep is exhausted within ~100 hours after loading.

Thus, testing methods that lead to prolonged primary creep should be avoided because it is a disallowed situation by design principle. On the other hand, because it is known that extremely high stresses are required even for cracking of susceptible Alloy 600 and similar Ni-base alloys in PWR primary water service, successful test methods have always depended on achieving very high secondary stresses, not primary stresses that would cause continuing plastic deformation and eventually plastic collapse. The usual technique to achieve the necessary very high secondary stresses is to deform the test section first in compression and then into tension (see Figure 10-33). Successful testing should therefore be based on specimens with high (secondary) bending stresses and not on uniaxial, highly loaded, tensile test methods. Some recommended specimen geometries for testing highly SCC resistant materials are shown in Figure 12-1 and Figure 12-2.

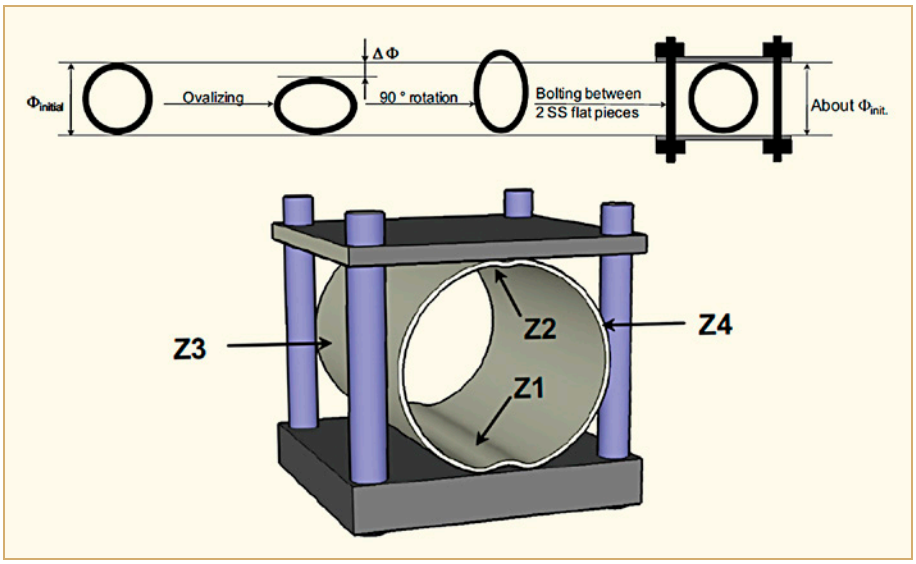

Figure 12-1: Loading procedure for ovalized tubes and expected cracking zones Z1 to Z4 (deformed zones exaggerated), after [Calonne et al, 2011].

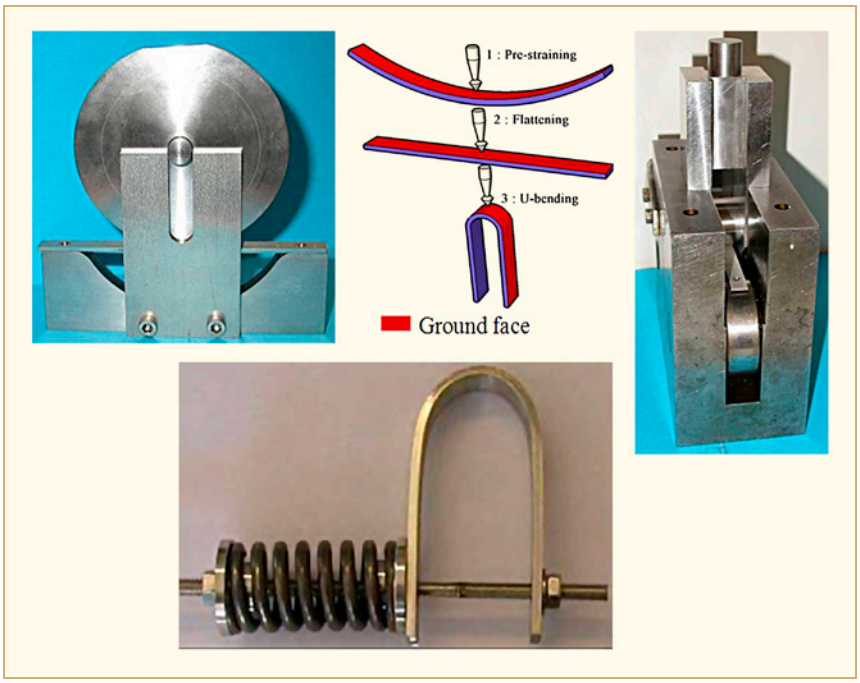

Figure 12-2: Loading procedure for spring loaded U-bends made from rectangular strips with a cold worked surface layer [Calonne et al, 2010].

12.2 EAC mitigation in BWRs (Peter Ford)

EAC mitigation in BWRs is discussed below in terms of the role of various materials, stress and environment conditions.

12.2.1 Materials solutions

Material solutions for mitigating IGSCC in BWR piping consist primarily of: (a) replacing susceptible Type 304 and 316 stainless steels and 182/600 nickel-base alloys with more sensitization-resistant materials, such as the low carbon (L- and NG-grades) versions of these alloys and/or utilizing the stabilized grades such a Type 321 and 347 stainless steels or high N-bar nickel-base alloys; (b) re-dissolving the chromium carbides by solution heat treatment; and (c) cladding with crack-resistant weld metal.

12.2.1.1 Nuclear grade stainless steels and nickel-base alloys

The replacement of structural alloys with materials more resistant to grain boundary sensitization is a straight-forward approach to mitigating IGSCC in stainless steels and nickel-base alloys. This resistance may be accomplished by attention to the alloy composition and the fabrication details (as was discussed in Section 3.2.2). From the alloy composition standpoint it is well documented that decreasing the carbon content of stainless steel, for instance, will delay $Cr_{23}C_6$ nucleation and growth (Figure 3-16) and hence the accompanying chromium depletion in grain boundaries (Figure 3-15). Thus, the 0.08% C maximum specification for "standard" Type 304 and 316 stainless steels is lowered to 0.03% maximum for the L-Grade versions, and a further decrease to 0.02% maximum is specified for Nuclear Grade (NG) steels (Table 3-4). The second important composition characteristic of Type 304NG and Type 316 NG stainless steels is the specification of 0.060 to 0.10% N in order to offset the decrease in alloy strength due to the reduction of the carbon content; this change also permits design allowable stresses similar to those of Type 304 stainless steel without a costly redesign of the piping system.

Control of the composition of nickel-base alloys may also increase the SCC resistance as discussed in Section 9.4.2.2 via the Nb, Ti and C content in "High N bar alloys" and of further additions of Ta and Cr in the increased Stress Corrosion Resistance Index (SCRI) alloys.

Full-size 102 mm (4") diameter pipe tests utilizing Nuclear Grade materials have shown that factors of improvement in extending the operating life over Type 304 stainless steel performance can be expected to be at least 50 to 100 under BWR NWC operation [Alexander, 1980] and [Alexander, 1982]. Type 316L stainless steel is also now routinely used for core internals, whereas Type 316NG stainless steel is used for replacement piping in the United States and Japan.

Another successful approach that has been used in Germany is to use low-carbon, niobium-stabilized (with Nb/C >13) Type 347NG stainless steel (DIN Type 1.4550) for core internals. This approach has also been successful for Type 321 stainless steel piping provided there is no excessive surface cold work [Kilian et al, 1995] and [Hoffmann et al, 2007].

12.2.1.2 Solution Heat Treatment (SHT)

Immunity against IGSCC of Type 304 stainless steel can be provided by eliminating weld-sensitized regions by solution heat treatment that re-dissolves the chromium carbides and eliminates chromium depletion at previously sensitized grain boundaries. In addition, solution heat treatment also reduces the effects of detrimental cold work and weld residual stress in the pipe weld. For this purpose, the entire pipe segment is solution annealed after butt-welding at 1040 to 1150°C (1900 to 2100°F) for 15 min per 25 mm (1.0 in.) of thickness, but not less than 15 min or more than 1 h regardless of thickness. The pipe segment is then quenched in circulating water to a temperature below 205°C (400°F). Solution heat treatment is generally limited to those weld joints made in the workshop where heat treatment facilities are available and because of dimensional tolerance considerations, size constraints of the vendor facilities (furnace and quench tank), and cooling rate requirements (dead end legs). Note that approximately half of the welds in, for instance, a recirculation line are shop welded and can therefore be solution annealed; the remainder are field welds which cannot be rendered SCC resistant by this approach.

12.2.1.3 Corrosion-resistant cladding (CRC)

The corrosion-resistant cladding remedy increases resistance to intergranular SCC by using the IGSCC resistance of duplex, austenitic-ferritic weld metals that is associated with the Cr healing process that takes place at the $M_{23}C_6$/ferrite interfaces [Alexander, 1982]. Thus, although the carbide precipitation observed in the HAZ on the inside surface is also present in the weld metal, the duplex structure of the weld metal provides resistance to IGSCC in BWR coolants provided the ferrite content is >7%. As with Type 304 stainless steel, reducing the carbon level is also beneficial as in the L-grade steels.

For the corrosion-resistant cladding technique, Type 308L weld metal is applied to the inside surface at the ends of the pipe before making the final field weld. The duplex weld metal therefore covers the region of wrought stainless steel that will become sensitized during the final welding process, thus providing IGSCC resistance by maintaining low carbon and sufficient ferrite on the inner surface of region that would normally be sensitized.

12.2.1.4 Weld overlay repair (WOL)

The weld overlay repair (or “back-lay”) [Pickett, 1986] is similar to the preceding corrosion-resistant cladding process in that it uses layers of IGSCC resistant, duplex Type 308Lweld metal (Figure 12-3). The most significant difference between the WOL and CRC processes is that the layer of weld metal in the WOL process is placed on the outside surface of the pipe while the pipe is being cooled internally with water. This procedure minimizes the degree of sensitization on the internal surface of the pipe and also produces a favourable (compressive) axial and circumferential residual stress pattern in the original pipe, the extent of which depends on the length of the overlay and the thickness of the pipe wall. The weld overlay is also applied as a structural reinforcement to restore the original piping safety margins should the latter be cracked. The development of the weld overlay repair technique has been reviewed by Mehta [Mehta, 2006].

The weld overlay technique has the potential for being the most cost-effective repair method compared to other repair techniques (pipe replacement, solution heat treatment, corrosion-resistant cladding), which require draining of the system. This process has been applied to several BWR piping systems in the USA as well as Spain, Switzerland and Taiwan. In the USA, these weld overlays are considered as a long term repair.

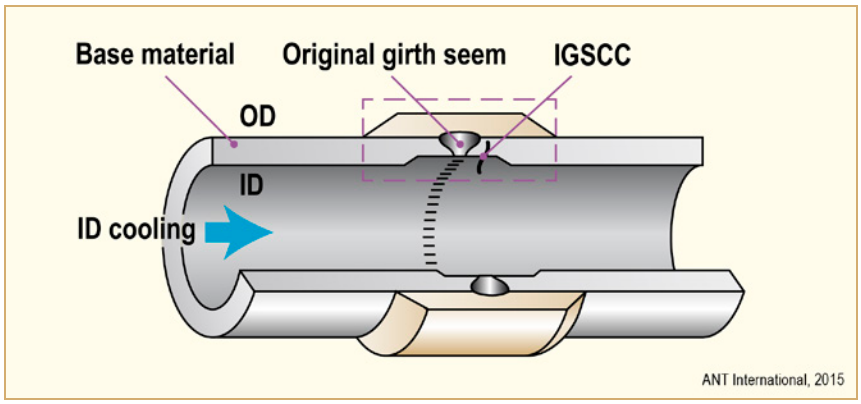

Figure 12-3: Weld overlay intergranular SCC mitigation technique.

12.2.2 Stress solutions

Stress solutions primarily affect the weld residual stress profile by placing the inner surface weld residual stress in compression. These solutions discussed below include surface peening, heat sink welding, induction heating stress improvement, and last pass heat sink welding.

12.2.2.1 Surface peening

Surface deformation to produce a compressive stress on the inner pipe surface has long been applied to engineering structures that are subject to degradation due to the presence of a pre-existing tensile residual stress. Peening via shot blasting, laser-peening, or by cavitation jet peening [Soyama, 2004] have been effective. There are concerns about this peening approach, however, associated with: (a) the effect of the associated balancing tensile stress component deeper beneath the surface, especially if the component has a pre-existing crack that is deeper than the thickness of the compressive surface layer; and (b) relaxation of the compressive stress due to a subsequently applied tensile or compressive stress cycle.

12.2.2.2 The ReNew™ surface improvement process

General Electric has developed a surface treatment process [Offer et al, 2006] using a flexible abrasive wheel to remove cold worked surface layers that may be introduced during manufacture (e.g. by machining, welding, or grinding). The process, as indicated in Figure 12-4, also introduces a surface compressive stress up to a depth of 50 μm, thereby countering the considerable tensile stress that that may exist on an abusively ground surface. The examples of residual stress measurements shown in Figure 12-4 are for the radial and hoop directions in the J-weld of a mockup of an in-core monitor housing. Very similar results are obtained on nickel base Alloys 600, 182 and 132 and Type 304 and 316L stainless steels in various configurations, including plates, weld cladding and mockups of PWR and BWR bottom-head penetrations containing partial-penetration groove and fillet welds.

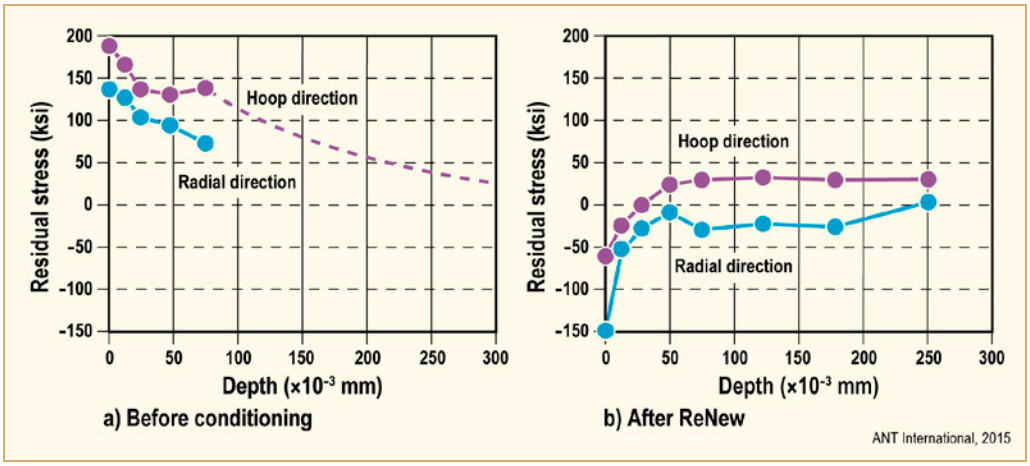

Figure 12-4: Residual stress/depth profiles in the hoop and radial directions before and after the application of the Renew™ process. In this case, the residual stress profiles were obtained on the Alloy 132 J-weld of a Type 304 stainless steel in-core monitor housing mockup.

12.2.2.3 Heat sink welding (HSW)

The heat sink welding procedure reduces both the sensitization produced on the inside surface of a welded pipe and also changes the state of the internal surface residual welding stresses from tension to compression. This approach can be used for workshop or field applications. Heat sink welding involves water cooling the inside surface of the pipe during all weld passes subsequent to the root pass or first two weld deposit layers. Water cooling can be provided by either flowing or turbulent water, by spray cooling through a sparger placed inside the pipe, or, in a vertical run, by still water.

12.2.2.4 Induction heating stress improvement (IHSI)

This technique changes the normally high tensile residual stress present on the pipe inside surface of weld HAZs into a beneficial compressive stress [Offer, 1983]. The process involves induction heating the outer pipe surface of completed girth welds to approximately 400°C (750°F) while simultaneously cooling the inside pipe surface, preferably with flowing water (Figure 12-3). Thermal expansion caused by the induction heating plastically yields the outer surface into compression, while the cool inside surface plastically yields in tension. After cool down, contraction of the pipe outside surface causes the stress state to reverse, leaving the inner surface in compression and the outer surface in tension. This process has been applied in Japan and the USA to Type 304 stainless steel pipes where care has to be taken to limit the temperature on the outside surface of the pipe to 400°C so as to minimize sensitization on the inside surface. Because of this maximum temperature specification, the inside surface may be under slight tensile stress after application of IHSI, albeit less than before. In order to overcome this limitation, the process has been modified in Japan for use on Type 316NG piping where full compressive stresses may be achieved by increasing the temperature on the outside surface to 650°C without sensitizing the material on the inside surface.

13 References

Abe H. and Watanabe Y., *Stress Corrosion Cracking Behaviour near the Fusion Line of Dissimilar Weld Joint with Alloy 182-A533B Low Alloy Steel,* Proceedings of Fifteenth International Conference on Environmental Degradation in Nuclear Power Systems-Water Reactors, Eds. J. Busby, G. Ilevbare and P. Andresen. Pub. The Metallurgical Society, Colorado Springs, August 7-11th, pp. 791-802, 2011.

Adler J., Marks C. and Gorman J., *Materials Handbook for Nuclear Plant Pressure Boundary Applications*, EPRI Report 1022344, 2010.

Ahonen M., Ehrnstén U. and Hänninen H., *Low temperature crack propagation of nickel-based weld metals in hydrogenated PWR primary water,* Proceedings of Fontevraud 7, 2010.

Ahonen M., Ehrnstén U., Saukkonen T., Todoshchenko O. and Hänninen H., *The effect of microstructure on Low Temperature Crack Propagation (LTCP) susceptibility of nickel-base Alloy 182, 152 and 52 weld metals in PWR primary water*, Proceedings of Fontevraud 8, Avignon, 2014.

Akashi M. et al, *Photochemical Protection of Stainless Steels from Stress Corrosion Cracking in BWR Primary Coolant*, Proceedings of Seventh International Symposium on Environmental Degradation in Nuclear Power Systems–Water Reactors, Breckenridge, Eds. R. Gold, A. McIlree, National Association of Corrosion Engineers August 7-10, pp. 621, 1995.

Akashi M and Nakayama G., *Effect of acceleration factors on the probability distribution of SCC initiation life of Alloys 600, 182 and 82 in high temperature and high purity water environments*, in Proceedings of 9th Conference on Degradation of materials in Nuclear Power systems Newport Beach CA 1999.

Alexander J. E., *Alternate Piping Alloy Qualification,* EPRI Report WS-79-174 Vol.1 May 1980.

Alexander J. E., *Alternative Alloys for BWR Pipe Applications*, EPRI NP-2671-LD, Electric Power Research Institute, October 1982.

Alley D. and Dunn D., *Current NRC perspectives concerning primary water stress corrosion cracking*, Proceedings of 15th International Conference on Environmental Degradation in Nuclear Power Systems–Water Reactors, Colorado Springs, pp. 14-27, Eds. Busby and Ilevbare, Pub. TMS. August 2011.

Amberge K. J. and Demma A., *Aging management of PWR reactor internals in U.S. plants,* Proceedings of Fontevraud 8, Avignon, 2014.

Amzallag C., Flavenot J. F., Leroux J. C. and Peyra C., *Influence de l'état de surface sur la résistance à la fatigue de l'acier inoxydable austénitique 304L*, 22èmes Journées de Printemps, 2003.

Amzallag C., *Fatigue Behavior of a 304L Stainless Steel in Air and PWR Water at 150°C and 300°C,* Proc. 3rd International Symposium on Mechanical Science Based on Nanotechnology, Sendai, Japan, 2005.

Amzallag C., *Effect of PWR Environment on the Fatigue Behavior of a 304L Stainless Steel,* International Symposium Fontevraud VI, 2006.

Ando M. and Nakata K, *Crack Growth Rate Behaviour of Low Carbon Stainless steels of Hardened Heat Affected Zone in PLR Piping Weld Joints*, Proc. 13th Int. Symp. on Environmental Degradation of Materials in Nuclear Power Systems – Water Reactors, Whistler BC, August, 2007.

Andresen P. L. and Duquette D. J., *The Effect of Chloride Ion Concentration and Applied Potential on the SCC Behaviour of Type 304 Stainless Steel in Deaerated High Temperature Water*, Corrosion, 36, 2, 85, 1980.

Andresen P. L., *The Effects of Aqueous Impurities on Intergranular Stress Corrosion Cracking of Sensitized 304 Stainless Steel* EPRI Report NP-3384, November 1983.

Andresen P. L., Ford F. P., Murphy S. M., and Perks J. M., *State of Knowledge of Irradiation Effects on EAC in LWR Core Materials,* in Proceedings of Fourth International Symposium on Environmental Degradation in Nuclear Power Systems - Water Reactors. Jekyll Island, August 6-10, 1989. Eds. D. Cubicciotti, E. Simonen. Published by National Association of Corrosion Engineers. ISBN 1-877914-04-5 pp. 1.83-1.121, 1989.

Andresen P. L., Vasatis I. P. and Ford F. P., *Behavior of Short Cracks in Stainless Steel at 288°C, Paper 495,* NACE Conference, Las Vegas, 1990.

Andresen P. L., *Effects of Specific Anionic Impurities on Environmental Cracking of Austenitic Materials in 288°C Water,* in Proceedings of Fifth International Symposium on Environmental Degradation in Nuclear Power Systems - Water Reactors. Monterey August 25-29, 1991 Eds. D. Cubicciotti, E. Simonen. Published, by American Nuclear Society. ISBN 0-89448-173-8, pp. 209-218, 1991.

Andresen P. L. and Diaz T. P., *Effects of Zinc Additions on the Crack Growth Rate of Sensitized Steel and Alloys 600 and 182 in 288°C Water*, Water Chemistry of Nuclear Reactor Systems 6, Vol. 1, BNES, London, October 1992.

Andresen P. L., *Effect of Temperature on Crack Growth Rate in Sensitized Type 304 Stainless Steel and Alloy 600*, Paper 89 NACE Corrosion 92, Nashville, April 1992.

Andresen P. L. *Specific Anion and Corrosion Potential Effects on Environmentally Assisted Cracking in 288°C Water*, GE-CRD Report 93CRD215, December 1993.

Andresen P. L. and Ford F. P., *Modelling and Prediction of Irradiation Assisted Cracking,* Proceedings of Seventh International Symposium on Environmental Degradation in Nuclear Power Systems - Water Reactors. Breckenridge, Eds. R. Gold, A. McIlree. Published by National Association of Corrosion Engineers. ISBN 0-877914-95-9, pp. 893-908, August 7-10, 1995.

Andresen P. L., Ford F. P., Higgins J. P., Suzuki I., Koyama, M., Akiyama M. Okubo Y., Mishima Y., Hattori S., Anzai H., Chujo H., and Kanazawa Y., *Life Prediction Of Boiling Water Reactor Internals*, Proc., ICONE-4 Conference, ASME, 1996.

Andresen P. L. *Effects of Flow Rate on SCC Growth Behaviour in BWR Water,* Proceedings of Eighth International Symposium on Environmental Degradation in Nuclear Power Reactors, Amelia Island Eds A. Mcllree and S. Bruemmer, American Nuclear Society, pp. 603-614, August 10-14 , 1997.

Andresen P. L., Ford. F. P., Angeliu T. M. Solomon H. D. and Cowan R. L., *Prediction of Environmentally- Assisted Cracking and its Relevance to Life Management in BWRs*, in Proceedings of Ninth International Symposium on Environmental Degradation in Nuclear Power Systems – Water Reactors, EdsS. Bruemmer, F.P.Ford. Published by The Metallurgical Society. ISBN 0-87339-475-5, pp. 423-433, Newport Beach August 1-5, 1999.

Andresen P. L., *Stress Corrosion Cracking Testing and Quality Considerations* in Proceedings of 9th International Symposium on Environmental Degradation in Nuclear Power Systems – Water Reactors, Eds. S. Bruemmer, F. P. Ford. Published by The Metallurgical Society. ISBN 0-87339-475-5, pp. 411-421, Newport Beach August 1-5, 1999.

Andresen P. L., Angeliu T. M., Emigh P. W. and Horn R. M., *Crack growth rate behaviour of nickel-alloys,* Corrosion/2000, Paper 00202, NACE, 2000.

Andresen P. L., Emigh P. E. and Young L. M., *Mechanistic and Kinetic Role of Yield Strength / Cold Work / Martensite, H_2, Temperature, and Composition on SCC of Stainless Steels*, Proc. Int. Symp. on Mechanisms of Material Degradation in Non-Destructive Evaluation in Light Water Reactors, Osaka, Japan, May published by Inst. of Nuclear Safety System, pp. 215-239, Japan, 2002.

Andresen P. L., *Similarity of Cold Work and Radiation Hardening in Enhancing Yield Strength and SCC Growth of Stainless Steel in Hot Water,* Corrosion/02, Paper 02509, NACE, 2002.

Andresen P. L., Emigh P. W., Morra M. M. and Horn R. M., *Effects of Yield Strength, Corrosion Potential, Stress Intensity Factor, Silicon and Grain Boundary Character on the SCC of Stainless Steels*, Proc. of 11th Int. Symp. on Environmental Degradation of Materials in Nuclear Power Systems – Water Reactors, ANS, pp. 816-831, 2003.

Andresen P. L., Emigh P. W., Morra M. M. and Horn R. M., *SCC of high strength Ni-base alloys in high temperature water*, Corrosion/2004 Annual Conference and Exhibition, New Orleans, Louisiana, 28 March - 1 April, 2004.

Andresen P. L. and Morra M. M., *Effects of Si on SCC of Irradiated and Unirradiated Stainless Steels and Nickel Alloys,* in Proc. 12th Int. Symp. on Environmental Degradation of Materials in Nuclear Power Systems - Water Reactors, TMS, Snowbird, pp. 87-108, 2005.

Andresen P. L. and Morra M. M., *Emerging Issues in Environmental Cracking in Hot Water*, in Proceedings of 13th International Conference on Environmental Degradation of Materials in Nuclear Power Systems, Whistler, British Columbia, August 19-23, Sponsored by Canadian Nuclear Society, 2007.

Andresen P. L., Hickling J., Ahluwalia K. S. and Wilson J. A., *Effects of PWR primary chemistry on PWSCC of nickel alloys,* Proceedings of 13th International Conference on Environmental Degradation of Materials in Nuclear Power Systems, Whistler, British Columbia, Canadian Nuclear Society 2007.

Andresen P. L., *Challenges in Quantitative, Fundamental Understanding and Prediction of SCC Initation,* Workshop on Detection, Advance, Mechanisms, Modeling and Prediction of Stress Corrosion Cracking Initiation in Water-Cooled Nuclear Plants, 2009.

Andresen, P. L., Private communication, 2011.

Andresen P. L and Chou P. *Effects of Hydrogen on SCC Growth Rate of Ni Alloys in BWR Water*, Proceedings of Fifteenth International Conference on Environmental Degradation in Nuclear Power Systems–Water Reactors, Eds. J. Busby, G. Ilevbare, P. Andresen. Pub. The Metallurgical Society, Colorado Springs, August 7-11th, pp. 2039-2059, 2011.

Andresen P. L., Morra M. M. and Ahluwalia K., *Effect of deformation temperature, orientations and carbides on SCC of Alloy 690,* Proceedings of 16th International Conference on Environmental Degradation of Materials in Nuclear Power Systems - Water Reactors, Asheville, USA, August 11-15, 2013a.

Andresen P. L., Morra M. M. and Ahluwalia K., *SCC of Alloy 152/52/52i weld metals in PWR primary water,* Proceedings of 16th International Conference on Environmental Degradation of Materials in Nuclear Power Systems - Water Reactors, Asheville, USA, August 11-15, 2013b.

Angeliu T. M. and Was G. S., *Behaviour of Grain Boundary Chemistry and Precipitates upon Thermal Treatment of Controlled Purity Alloy 690*, Met Trans. A, Vol. 21A, pp. 2097-2107, 1990.

Angeliu T. M., Sung J. K. and Was G. S., *The Role of Carbon and Chromium on the Mechanical and Oxidation Behavior of Nickel-base Alloys in High Temperature Water,* Proceedings of 5th Symposium on Degradation of Materials in Nuclear Power Systems, Monterey, CA, 1992.

Angeliu T. M., Andresen P. L., Sutliffe J. A. and Horn R. M., *Intergranular Stress Corrosion Cracking of Unsensitized Stainless Steels in BWR Environments*, in Proceedings of Ninth International Symposium on Environmental Degradation in Nuclear Power Systems–Water Reactors, Newport Beach, Eds. S. Bruemmer, F. P. Ford, The Metallurgical Society, pp. 311-318, August 1-5, 1999.

ANL-01/09, *Environmentally Assisted Cracking in Light Water Reactors*, Semiannual Report July 2000 -December 2000. Washington, DC, U.S. Nuclear Regulatory Commission Office of Nuclear Regulatory Research, NUREG/CR-4667, Vol. 31, 2000.

Aria T. et al., Paper 140 NACE Corrosion Conference, 1998.

Arioka K., Yamada T., Terachi T. and Miyamoto T., *Dependence of Stress Corrosion Cracking for Cold-Worked Stainless Steel on Temperature and Potential, and Role of Diffusion of Vacancies at Crack Tips*, Corrosion 64, pp. 691, 2008.

Asano K., Fukuya K., Nagata K. and Kodama M., *Changes in Grain Boundary Composition Induced by Neutron Irradiation on Austenitic Stainless Steels,* Proceedings of Fifth International Symposium on Environmental Degradation in Nuclear Power Systems-Water Reactors, Monterey, Eds. D. Cubicciotti and E. Simonen, American Nuclear Society, pp. 838-846, August 25-29, 1991.

ASM, *Stainless Steels*, ASM Publication 1994.

ASM, *Weld Integrity and Performance*, Pub. ASM International, 1997.

ASME, *Boiler and Pressure Vessel Code for Design by Analysis in Sections III and VII Division 2*, 1969.

ASME, *Boiler & Pressure Vessel Code. Section III, Division 1 - Subsection NB: Class 1 Components, Rules for Construction of Nuclear Power Plant Components*, 2007.

ASME, *Fatigue Evaluations Including Environmental Effects, Section III, Division 1*, American Society of Mechanical Engineers. Code Case N-792, 2010.

ASME, *Design Fatigue Curves. Section III, Mandatory Appendix 1*, 2013.

Audouard J. P., Désestret A., Catelin D. and Soulignac P., *Special Stainless Steels for Use in Sea Water*. Corrosion'88, paper #413, 1988.

Avery R. E., *Pay Attention to Dissimilar Metal Welds – Guidelines for Welding Dissimilar Metals*, Chemical Engineering Progress May 1991 and Nickel Development Institute Series No 14-018, 1991.

Baelecken E. et al., *Investigations Concerning the Transformation Behavior, the Notched Impact Toughness and the Susceptibility to Intergranular of Iron-Chromium Alloys with Chromium Contents to 30%*, Stahl und Eisen 81, (12), p. 768, 1961.

Bajaj R., Mills W. J., Lebo M. R., Hyatt B. Z. and Burke M. G., *Irradiation-assisted stress corrosion cracking of HTH Alloy X-750 and Alloy 625*, Proceedings of 7th Int. Conference on Environmental Degradation of Materials in Nuclear Power Systems - Water Reactors, American Nuclear Society, pp. 1093-1105, Breckenridge, 1995.

Bamford W. H., Rao G. V. and Houtman J. L., *Investigation of service-induced degradation of steam generator shell materials,* Proceedings of 5th International Symposium on Environmental Degradation of Materials in Nuclear Power Systems - Water Reactors, Monterey, pp. 588-595, 1992.

Nomenclature

AISI	American Iron and Steel Institute
ANL	Argonne National Laboratory
ANS	American Nuclear Society
ANT	Advanced Nuclear Technology
ANTI	Advanced Nuclear Technology International
AOA	Axial Offset Anomaly
ASME	American Society of Mechanical Engineers
ASTM	American Society for Testing Materials
ATEM	Analytical Transmission Electron Microscopy
AVT	All Volatile Treatments
BAC	Boric Acid Corrosion
Bcc	Body Centred Cubic
Bct	Body Centred Tetragonal
BMI	Bottom Mounted Instrumentation
BPV	Boiler & Pressure Vessel
BWR	Boiling Water Reactors
BWROG	BWR Owners Group
BWRVIP	BWR Vessel and Internals Project
C&LAS	Carbon & Low Alloy Steels
CANDU	Canadian Deuterium Uranium
CASS	Cast Austenitic Stainless Steels
CCT	Continuous-Cooling-Transformation
CCW	Closed Coolant Water
CEPM	Corrosion Enhanced Plasticity Model
CERT	Constant Extension Rate Test
CF	Corrosion Fatigue
CGR	Crack Growth Rates
CIB	Core Internals Basic
CIOA	Core Internals Overaged
CIST	Core Internals Spring Temper
CNS	Canadian Nuclear Society
CPY	Contrat Programme
CRC	Corrosion-Resistant Cladding
CRDH	Control Rod Housing
CRDM	Control Rod Drive Mechanism
CUF	Cumulative Usage Factor
CUI	Corrosion Under Insulation
CVCS	Chemical Volume Control System
CW	Cold Work
CZR	Central Zone Remelting
DDC	Ductility Dip Cracking
DO	Dissolved Oxygen
DSA	Dynamic Strain Ageing
EAC	Environmentally-Assisted Cracking
EAF	Environmental Assisted Fatigue
ECCS	Emergency Core Cooling System
ECP	Electrochemical Corrosion Potential
EDF	Electricite de France
EDM	Electro-Discharged Machining
EDTA	Ethylene Diamine Tetra Acidic Acid
EDX	Energy Dispersive X-Ray
EFPY	Effective Full Power Year
EPFM	Elastic-Plastic Fracture Mechanics
EPR	Electrochemical Potential Reactivation
EPRI	Electric Power Research Institute
ESHT	Electroslag Hot Topping

ESR	Electroslag Remelting
ETA	Ethanolamine
FAC	Flow Accelerated Corrosion
FCAW	Flux-Cored Arc Welding
Fcc	Face-Centred Cubic
FIB	Focused Ion Beam
FM	Fracture Mechanics
GALL	Generic Aging Lessons Learned
GE	General Electric
GL	Guidance Letters
GTA	Gas Tungsten Arc
GTAW	Gas Tungsten Arc Welding
HAZ	Heat Affected Zone
HCF	High Cycle Fatigue
Hcp	Hexagonal Close Packed
HFT	Hot Functional Tests
HSW	Heat Sink Welding
HV	Hardness Vickers
HWC	Hydrogen Water Chemistry
IASCC	Irradiation-Assisted Stress Corrosion Cracking
ID	Inner Diameter
IG	InterGranular
IGA	InterGranular Attack
IGA-IGSCC	Intergranular Attack-Intergranular Stress Corrosion Cracking
IGC	Intergranular General Corrosion
IGSCC	Intergranular Stress Corrosion Cracking
IHP	Inner Helmoltz Plane
IHSI	Induction Heating Stress Improvement
ISI	In-Service Inspection
ISO	International Standardization Organization
KKL	KernKraftwerk Leibstadt
KKM	KernKraftwerk Mühleberg
KWU	KraftwerkUnion
LAS	Low Alloy Steel
LCC	LWR Coolant Chemistry
LCF	Low Cycle Fatigue
LEFM	Linear Elastic Fracture Mechanics
LET	Linear Energy Transfer Rate
LP	Low Pressure
LPCI	Low Pressure Coolant Injection
LR	License Renewal
LTCP	Low Temperature Crack Propagation
LWR	Light Water Reactor
MA	Mill Annealed
MGB	Migrated Grain Boundaries
MHWC	Medium Hydrogen Water Chemistry
MIC	Microbially Induced Corrosion
MIG	Metal Inert Gas
MMA	Manual Metal Arc
MOMOS	Manganese Oxidizing Microorganisms
MPa	Mega Pascal
MSIP	Mechanical Stress Improvement Process
NACE	National Association of Corrosion Engineers
NDE	Non-Destructive Examination
NG	Nuclear Grade
NISA	Nuclear and Industry Safety Agency
NMCA	Noble Metal Chemical Addition
NMT	Noble Metal Technology

Unit conversion

TEMPERATURE		
°C + 273.15 = K	°C × 1.8 + 32 = °F	
T(K)	T(°C)	T(°F)
273	**0**	32
289	16	61
298	25	77
373	**100**	212
473	**200**	392
573	**300**	572
633	360	680
673	**400**	752
773	**500**	932
783	510	950
793	520	968
823	550	1022
833	560	1040
873	**600**	1112
878	605	1121
893	620	1148
923	650	1202
973	**700**	1292
1023	750	1382
1053	780	1436
1073	**800**	1472
1136	863	1585
1143	870	1598
1173	**900**	1652
1273	**1000**	1832
1343	1070	1958
1478	1204	**2200**

Radioactivity	
1 Sv	= 100 Rem
1 Ci	= 3.7×10^{10} Bq = 37 GBq
1 Bq	= 1 s^{-1}

MASS	
kg	lbs
0.454	**1**
1	2.20

DISTANCE	
x (µm)	x (mils)
0.6	0.02
1	0.04
5	0.20
10	0.39
20	0.79
25	0.98
25.4	**1.00**
100	3.94

PRESSURE		
bar	MPa	psi
1	0.1	14
10	**1**	142
70	7	995
70.4	7.04	**1000**
100	10	1421
130	13	1847
155	15.5	2203
704	70.4	**10000**
1000	100	14211

STRESS INTENSITY FACTOR	
MPa√m	ksi√inch
0.91	**1**
1	1.10